HARMONIC VOLTAGE PROFILE CALCULATIONS
OF
ELECTRIC POWER TRANSMISSION SYSTEMS

A Thesis

Submitted to the College of Graduate Studies and Research

in Partial Fulfillment of the Requirements

for the Degree of

Doctor of Philosophy

in the

Department of Electrical Engineering

University of Saskatchewan

By

Vinay K Sharma

Saskatoon, Saskatchewan

September 1989

COPYRIGHT

ACKNOWLEDGEMENTS

The author wishes to express his thanks and appreciation to Dr. R.J. Fleming for his helpful guidance and assistance during the course of this study. His advice in the preparation of this thesis is thankfully acknowledged. He would take this opportunity to thank members of advisory committee for their help in guidance and editing of the thesis. Thanks also to Dr. El-serafi, Dr. M.S. Sachdev, and Dr. S.P. Verma for their consultation and help in reviewing the work.

Thanks and appreciation to Saskatchewan Power Corporation for financial assistance in the form of Postgraduate Scholarship; Ian MacPhedran for his assistance with the VAX/VMS computer system; Ms. Edna Wilson and the staff of Engineering Library; and Ms. Mridula Sharma, Mr. Anant Jalnapurkar, and Mr. T.L. Reddy for help in proofreading the thesis.

UNIVERSITY OF SASKATCHEWAN

Electrical Engineering Abstract 89A311

HARMONIC VOLTAGE PROFILE CALCULATIONS OF ELECTRIC POWER TRANSMISSION SYSTEMS

Student: Vinay K Sharma Supervisor: Dr. R.J. Fleming

Ph.D. Thesis presented to the College of Graduate Studies and Research

September 1989

ABSTRACT

Rapid developments in the semiconductor industry have made possible a revolutionary improvement in the power handling capabilities of the rectifying devices. This has led to increased number and size of solid state power conditioning equipment installed on power system networks. The direct consequence of this is the increase in the stationary harmonic frequency voltages and currents on power system networks causing distortion of the sinusoidal waveforms. The renewed interest in the harmonics and a need to study the impact of such harmonics is the basis for the work reported in this thesis.

Studies reported in this thesis are concerned with the harmonic voltage profile calculation of an electric power transmission network. The transmission lines due to their long lengths, tend to exhibit standing wave patterns comprising nodes and antinodes at harmonic frequencies. The studies are directed specifically towards the determination of the harmonic voltage profile of transmission lines. The effect of various parameters of the transmission system on the harmonic character of the transmission line voltage and current is studied. An iterative algorithm based on non-linear frequency domain analysis is presented in this thesis.

An important factor in this effort is the accurate modelling of various equipment of the power system including sources of harmonics. A dynamic model of a six pulse ac/dc converter is presented and the effect of the impedance of the converter transformer on the commutation delay is included to accurately determine the harmonic spectrum of the line current of the converter. The phase shifting behaviour of the transformer is preserved in the equivalent admittance matrix model of a transformer for the harmonic frequency analysis. The cascaded equivalent pi model of the transmission line is used in order to minimise the errors. Also, a cascaded pi model lends itself to obtaining the harmonic voltage profile. The skin effect, due to increased harmonic frequency, is also taken care of in modelling the transmission system. An iterative approach is proposed for the overall algorithm based upon the criterion of mismatch of active and non-active power.

Five example applications of the algorithm are presented ranging from a power system comprised long transmission lines to an industrial power system. The algorithm is general and can be used for any kind of balanced power system to study the harmonic bus voltages, harmonic line currents, harmonic voltage profiles of transmission lines etc. due to the harmonic loads, and resonance and filtering effects of VAR compensation. Other information available from the program is the distortion factor and bus impedance versus frequency table.

The approach taken is general and well suited for the analysis of balanced power system networks with ac/dc converters of various sizes.

Table of Contents

List of Figures

List of Tables

LIST OF PRINCIPAL SYMBOLS

$A_{11}, A_{12}...$	Miscellaneous constant.
A, B, C	Phase sequence of a polyphase system.
D	The differential operator $\frac{d}{dt}$.
D_r	The distortion volt ampere.
f	Frequency in hertz.
f_{a1}, f_{a2}, f_{c1}	Miscellaneous functions
E	Back EMF of the active dc load.
E_p, E_q	RMS ac voltages
i	Instantaneous current.
i_d	Instantaneous dc current.
I	Average or rms current.
k, M, N ...	Integers.
L_e	Inductance of the transmission line due to the external flux distribution.
L_i	Inductance of the transmission line due to the internal flux distribution.
L_d	Inductance of the converter dc load.
L_n	Inductance of the converter transformer.
L_N	Negative sequence inductance of the synchronous generator.
L_d''	Direct axis subtransient inductance of a synchronous generator.
L_q''	Quadrature axis subtransient inductance of a synchronous generator.
P	Real power.
Q	Reactive power.

QD	Non-active power.
R_d	Resistance of the converter dc load.
R_{dc}	Dc resistance of the transmission line.
R_k	Ac resistance of the transmission line for kth harmonic order.
R_n	Resistance of the converter transformer.
s	Length of the transmission line and the slip of the induction motor.
t	Time.
v	Instantaneous voltage.
V_L	Line to line voltage of the polyphase power system.
y, Y	Complex admittance.
Y_π, Y_{SH}	Shunt admittance of the equivalent pi model.
z,Z	Complex impedance.
Z_π, Z_{se}	Series admittance of the equivalent pi model.
Z_{nk}, Z_{11k}, Z_{12k}, Z_{Tk}, Z_{22k}	Miscellaneous impedances
α	Delay(Firing) angle of the converter.
δ_k	Harmonic sequence indicator.
ϕ	Phase angle in radians.
λ	Wavelenth of the ac signal.
μ	Commutation delay angle of the converter.
μ_r	Permeability of the media.
θ	Angular displacement in radians.
ρ	Propagation constant.
τ_{12}, τ_n, τ_{22}	Miscellaneous time constants
ω	Fundamental angular frequency of the power system.

1. INTRODUCTION

1.1. Introduction

Electrical power systems are subjected to transient and harmonic disturbances due to switching, lightning, load changes, and equipment failures. Previously, these disturbances were not significant because of their limited magnitude and duration; however during the past decade, there has been tremendous change in the types of loads on the ac power system. Present trends are towards the use of static power converters, induction motor switching, and electronic devices which require dc voltages and currents.

Several different types of power conditioning equipment are in use ranging from uncontrolled rectifiers and fully controlled rectifiers to complex cascaded rectifier configurations. The application of power converters is widespread. Their applications range from use in power supplies for digital computers and other electronic devices to ac and dc motor control. The increased interest in power converter equipment is due to lower cost, smaller size, and less maintenance compared to other techniques. It is the widespread use of power converters that has increased the incidences of harmonic voltages and currents in power systems several fold.

Another area of concern is the integration of variable speed power generation to the fixed frequency grid. Brown Boveri and others have installed variable frequency windmill generators whose output is rectified and inverted back to the constant frequency network[1]. This technology, if used, will further increase the power system harmonic levels.

The potential for detrimental effects of harmonic current and voltage levels on the protection and the metering equipment are serious concerns to utility

engineers[2,3,4,5]. There are many cases of revenue loss due to negative torque on energy meters caused by the negative sequence nature of some harmonics. There is also a likelihood of malfunction of relaying equipment[6], and cases of insulation failure due to self resonance and transfer resonance.

There is a renewed interest in obtaining better understanding of the harmonic signal levels (voltages, currents, and power flows), and in methods of minimising the effects of harmonics on power system equipment. The recent volume of research publications on this subject matter and activities of international committees illustrate this concern.

1.2. Purpose and Objective

The phenomenon of waveform distortion of the power system voltage is mainly of two kinds; transient waveform distortion, and stationary waveform distortion. The transient waveform distortion can be caused by a fault and the post fault conditions, sudden switching of the load, the lightning effect, and the loss of generation. The stationary waveform distortion is caused by the steady injection of harmonic current from non-linear loads. Such non-linear loads include ac/dc converters, switching power supplies, dc/ac inverters integrated to the power grid, ac phase control circuits, and cycloconverters.

The stationary power system waveform distortion is addressed in this thesis. The term Harmonic Signal, from now on, refers to the harmonic signals which are responsible for the stationary waveform distortion in the power system.

The range of harmonic signals is broad. There has been considerable discussion and research on radio and television interference due to high frequencies, whereas little or no attention has been given to the effects of frequencies in the lower band.

The most damaging frequencies to power devices and machines appear to be the lower frequency range (below 5 kHz) while higher frequencies interfere with communication systems. The existence of lower frequencies in the power system has been recognised for a long time, but the magnitudes and sources of these harmonics were very limited. The increase in power system losses from harmonics has so far been small and ignored due to inexpensive energy cost.

The harmonic voltage levels which exist as a result of harmonic sources are affected by the transmission and the distribution system characteristics. The power system network response to the harmonic sources is determined by the interaction of capacitances and inductances of the system, and by the damping(absorption) provided by the system loads and losses. The power system response may vary from a simple waveform distortion to near harmonic resonance or a full resonance condition. The resonance condition may be categorised into series and parallel cases. Further, these conditions can be classified into 'self resonance' and 'transfer resonance'. The term self-resonance is used to denote a voltage maximum at a bus where the shunt compensation, which causes the resonance, is applied. The transfer-resonance means the occurrence of a voltage maximum at a different place than the bus where the shunt compensation is applied.

The objective of the studies reported in this thesis was to develop an algorithm for the calculation of the harmonic voltage profile of a transmission line due to the injection of harmonic currents from harmonic sources. In light of the foregoing discussion, it is imperative to calculate the harmonic voltage profile on each transmission line of the network. Such a calculation can be used to detect the possibility of a resonance condition which might result in a standing wave formation on a transmission line. Voltage profile calculations will also help identify the points of voltage maxima and minima in the transmission network. Reliable system response calculation requires careful modelling of

the power system components and the knowledge of the harmonic injection from non-linear loads.

The topics presented in this thesis are divided into the following sections:

1. Chapter 1 contains the introduction to the project and thesis. Historical background material and a literature summary are also presented in the first chapter.

2. Definition of the harmonic power flow problem is included in Chapter 2. Various sources of harmonic injections are identified and discussed. The comparative study of various harmonic sources is presented in order to single out the main sources of harmonic injection. The conventional power flow problem is reviewed and its limitations at the harmonic frequencies are discussed.

3. The modelling of elements of the power system transmission network is carried out in Chapter 3. The ac/dc converters are identified as the main sources of harmonic injection. The complete modelling of a six pulse bridge converter is developed by including the effect of inductance and resistance of the converter transformer. The modelling of transformer, transmission line and electrical loads is discussed. The reasons for models chosen for ac motors, filters, and static VAR compensators are also included. The system equations for harmonic energy flow are formulated. The justification for the independent treatment of each harmonic frequency is given; also a complete algorithm for the calculation of the harmonic voltage profile is included.

4. The new definitions of the energy flow in a system where the source of single frequency and non-linear loads give rise to coexistence of fundamental and harmonic frequencies are presented in Chapter 4. The algorithm given in Chapter 3 based on the non-linear frequency domain analysis is modified to include the new definitions. The overall convergence criterion of the modified algorithm is discussed. An example of a two bus system is used to illustrate step by step execution of the algorithm

   Chapter 4 also includes a brief description of the sparse methods used in solving the system equations arising from the harmonic power flow algorithm. The minimum degree algorithm is discussed and its implementation using graph theory is illustrated. The methodology due to George and Liu[7] is extended to the example of the power system harmonic analysis. A dynamic

data structure is proposed for the implementation of the algorithm. Finally Sato and Tinney's[8] algorithm is discussed for the final solution of the system equations.

5. The application of the algorithm for calculating the harmonic voltage profile is given in Chapter 5. Four example systems are presented and the analysis results are discussed. The resonance condition and filtering effects are illustrated for various example systems. The effect of various system parameter variations on the harmonic voltage profile is studied. The relevant data are presented in graphical and tabular form.

6. The conclusions and recommendations are included in Chapter 6. Main contributions of the project are discussed. Some general and specific contributions of the work are given. Recommendations for further work pertaining to the harmonic flow problem are also included.

1.3. History and Literature Summary

Power system waveform distortion is not a new phenomenon. Historically, with reference to power system harmonics, it was in Germany during the 1920s and 1930s when the subject of waveform distortion was first brought to the attention of power system engineers. In North America, earlier investigations pertained to the nonlinearity of transformers and the use of wye and delta connections to eliminate some of these harmonics. A paper by Clinker[9] published in AIEE transaction in 1914 discussed the transformer harmonics. Later in 1915, the California railroads were electrified and rectifier loads were first discussed in a committee report[10]. The harmonic voltage induction in a parallel circuit was first experienced at an experimental 22 kV voltage system in 1914. The discussion of harmonic was mainly qualitative, and Fourier analysis was not yet common. A technique similar to the Fourier analysis in this area was first reported by Peters[11] in 1915.

In 1914, Langmuir(USA) introduced controlled mercury arc rectifiers. By the mid thirties, mercury arc rectifiers reached a climax and were extensively used in electric tramways, railways, and electrolytic plants. The first paper that dealt with the harmonic generation by static converters was presented in 1945 by Read[12]. As the mercury arc rectifier technology matured, the semiconductor technology grew from the infancy state to a well developed state. In 1948, the transistor effect in a germanium crystal was discovered and silicon and germanium contact diodes were developed. Also, after the Second World War, the mercury arc rectifiers were employed extensively in DC motor drives. In the late fifties and early sixties, semiconductor converters started replacing mercury arc rectifiers[13]. During this period, a number of papers were presented on harmonic generation which are summarised in a book by Kimbark[14]. The book by Kimbark is devoted to HVDC transmission and covers in detail the generation of harmonics, filter design, and the harmonic reduction.

Throughout the early representative work on the power system harmonics, emphasis has been on reducing the harmonics by transformer connection, isolation, and separation of circuits. The mathematical tools, such as Fourier analysis were not applied due to the lack of mathematical models of the power system components. The concept of the equivalent circuit of a transformer at harmonic frequencies was first introduced by Osborne[15] in 1915 and later by Morgan[16] in 1933.

In recent years, there has been a tremendous increase in the industrial processes that rely on controlled rectification for their operation, and therefore generate current harmonics. The design of rectifiying equipment assumes the existence of a voltage source free of harmonics, a situation which can only occur if the power system supplying the equipment had a very low source impedance. Consequently the smaller industrial users of electricity are being subjected to increasing difficulties caused by the interaction of their own power conditioning equipment with the power supply.

An extensive bibliography produced by the IEEE Power System Harmonics Working Group[17, 18] is a rich source of literature concerning harmonics in the power system. Most of the modern literature on the subject of power system harmonics is of the nature of case histories in which difficulties are documented and alleviated. Canadian Electric Association Research Report 415 U 474[19] gives an assessment of the modern problems associated with power system harmonics. An IEEE Guide[20] contains definitions of important terms associated with the operation of ac/dc converters. It also describes the technique for measuring harmonic currents and voltages. The effect of harmonics on various power system equipment is well covered. The impact of harmonics on protective equipment is documented in an IEEE Power System Relaying Committee Report[6]. It also contains a bibliography of related work. Papers by Fuchs[4, 5] et al. presented at the 1985 IEEE Winter Power Meeting describe a comprehensive work on the impact of harmonics on household appliances.

A large amount of research reported is on the application of ac/dc converters and dc/ac inverters. These devices are employed extensively in HVDC transmission, the processing industry, the mining industry and the steel industry. The line commutated converters constitute the major source of harmonics in the power system due to their widespread applications. Halley's thesis[21] describes a general method of calculating ac harmonics generated by the line commutated converter, however, the method presented is limited to the resistive rectifier loads. A paper by Emanuel[22] presented at the Second International Conference on Harmonics in Power Systems gives a good description of the mechanism of generation of harmonics from ac/dc converters. The theory presented by Emanuel is general and can be extended to the application of phase control circuits as well. Dewan[23] developed an analytical technique for calculating of the line current harmonics due to a cycloconverter. One of the foremost papers on an analytical method of calculating the harmonics of a pulse width modulated inverter (PWM

inverter) is presented by Barton[24]. The method suggested by Barton is based on the Bessel function approach.

The modelling of the transmission line for harmonic frequency analysis has been presented very well by Arrillaga, Bradley, and Bodger[25]. The skin effect is included since the X/R ratio decreases, or at least stays constant, with increasing frequency. The nominal PI model of the transmission line is usually used, but it is important to consider the electrical length of the line as related to the wavelength of the harmonic of interest. Mahmoud[26] suggested the use of the equivalent PI model of the transmission line. However, in order to obtain a profile of voltage on the transmission line, it is essential that a number of PI sections be considered.

Load modelling plays an important role in harmonic propagation, particularly in the case of resonance where an equivalent shunt resistance can add damping. EPRI report EL-1627[27] presents some sensitivity studies for a single bus system with various load models. The accepted harmonic model is a lumped resistance in parallel with a lumped reactance. Mahmoud[26] suggests a reactance model for the induction motor load. At higher frequencies, the slip of an induction motor increases and the rotor resistance and the stator resistance become smaller relative to the reactance. The reactance, on the other hand, increases linearly with the frequency.

The first network analysis algorithm for determining ac impedance at the HVDC converter site was developed by Hingorani[28]. EPRI report EL-1627 extended Hingorani's method to include the load effect as well. Stratford[29] suggested a similar method for calculating impedance at the node of interest for each harmonic frequency. A paper by Ortmeyer[30] gives a comparison of the non-linear time domain and the non-linear frequency domain harmonic analysis of the power system. The time domain analysis pertains to determining the solution by integrating the system equations over time for the

set of given initial conditions. The approach is limited to a small system as the cost of the solution increases rapidly for larger systems[31].

The frequency domain analysis comprises two methods; the first pertains to the extension of the load flow method to harmonic power flow. The formulation and solution of the harmonic power flow problem was first presented by Heydt, Xia and Grady[32, 33, 34]. The discussion by Heydt et al. also introduces the definition of distortion volt ampere due to the commutation need of the converter. The second non-linear frequency domain analysis pertains to the solution of the problem by iterative solution of the admittance matrix. Pillegi et al. used this method to predict the harmonic voltages in a distribution system[35]. This method, also referred to as the "extended current injection method", is adopted for the calculation of the harmonic voltage profile on the transmission lines. Both frequency domain methods require that the harmonic content of the sources be known beforehand. The multiple harmonic sources can also be included conveniently.

The text books by Stevenson[36] and Anderson[37] give detailed studies of the basic power system principles. A textbook by Arrillaga[25] et al. gives basic principles of analysis of the Fourier method and modelling of power system equipment at the harmonic frequencies. A book by Shepherd and Zand[38] is a good source of definitions associated with the non sinusoidal power flow. Finally textbooks on semiconductor technology by Rashid[39], Hoft[40], Dewan[41], Finney[42], Kloss[13], Pelly[43], Dubey[44], and Williams[45] are good sources of information on the working principles of converters and inverters.

1.4. Summary

It is clear from the foregoing discussion that the subject of power system harmonics is not new. The evolution of the subject has taken place from heuristic analysis, and experimental analysis to the application of Fourier analysis.

Due to a substantial increase in non-linear loads, the overall levels of harmonics in power systems are increasing. There is need to determine the behaviour of the power system network at different harmonic frequencies with a high degree of accuracy. Due to transfer resonance, the pattern of the standing wave may also exist in the power system. Therefore it is also essential to determine the harmonic voltage profile of the transmission lines, particularly the long transmission lines.

2. HARMONIC POWER FLOW

2.1. Introduction

Chapter 2 describes various sources of harmonic injection into the power system. The relative magnitudes of harmonic current and voltage injections from various harmonic sources are reviewed. It is shown that the static ac/dc power conditioning equipment is the main source of harmonic distortion. A brief review of the conventional load flow problem is given. The limitations of the conventional load flow in the presence of harmonic signals are described. The concept of the harmonic power flow is illustrated by assuming the converter load as the source of the harmonic power.

2.2. Harmonic Sources

A power system network includes generation, transmission and distribution elements. The equipment used in all three parts of the power system is likely to generate harmonic signals(voltage or current). The generation of harmonic signals can be categorised as either due to the supply of harmonic voltages from generators or due to the demand of harmonic current from the power system load. The supply of harmonic voltages results from generators due to the non-sinusoidal mmf created in the air gap, and the demand for harmonic currents results from the non-linear loads, such as transformers, saturable core reactors, arc furnaces, and electronic control and power conversion equipment. The injection of harmonic signals may be due to the generation of harmonic voltages or due to the demand of harmonic current, both cause pollution of frequency in the power system. The harmonic signals generated by conventional equipment such as transformers, motors have been limited in the past. Particularly, the magnitudes of harmonic voltages generated by the synchronous generator are very small. It is the wide spread use of electronic switching control of electric power that has increased the level of harmonics in power systems. The electronic switching control of electric power produces harmonics by imposing cyclic changes of impedance in the power system supply circuit.

The following sections present a brief review of non-linear types of loads which play a major role in generating harmonics in the power transmission system.

2.3. Non-linear Industrial Loads

There are several examples of non-linear loads in use in the industry; static power converters, phase control circuits, equipment with hysteresis such as transformers, induction motors, and arc furnaces. The static power converters are used in processing industry, mining industry, the steel industry, for the purpose of traction, and HVDC transmission. Due to a large level of constant harmonic current injection, static power converters have become a major concern of pollution of frequency in electric power systems.

2.3.1. Static power converter

The era of semiconductor electronics dawned in the sixties and has since continued to grow in all areas of electro-technology. Semiconductor devices are now used for a wide range of applications ranging from simple rectification to complex control applications. The impact of harmonics generated from converters is dependent on its power rating, principle of operation, and the circuit configuration. Figure 2.1 illustrates the role of converters[13] in energy conversion and control. Static converters lie in the path of energy flow from sources at the top to the loads at the bottom of the diagram. The components and the classification of converters are given on the left and right sides of the converter diagram, respectively. The harmonic power injected back into the ac system is shown as reactive power, since it does not result in useful power.

There are two main categories based on the principle of operation of converters: (i) line commutated converters; (ii) forced or self commutated converters. Converters can also be divided into three broad categories based on the power rating: (i)

large power converters used in HVDC transmission, and the metal reduction industry; (ii) medium size converters such as those used for motor control and railway traction; (iii) low power converters used in power supplies for communications and computers. Finally, converters can also be classified on the basis of circuit configuration used, such as: (i) single way or half way converters; (ii) six-pulse converters; and (iii) twelve-pulse converters. Although the aforementioned categories appear to have ill defined boundaries, it is convenient to study the harmonic behaviour of converters according to the classification by circuit configuration.

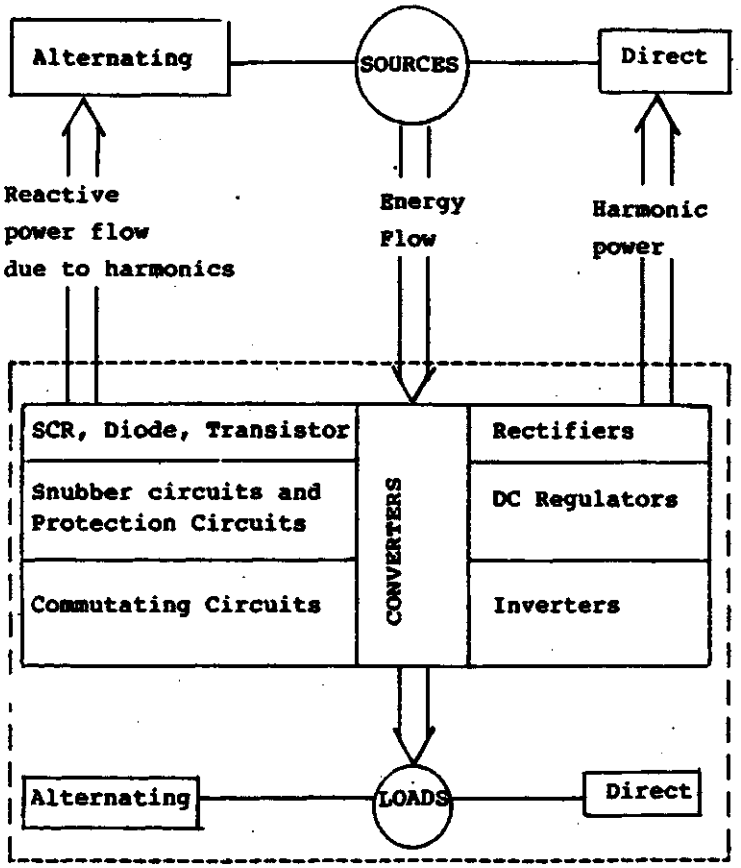

Figure 2.1: Role of converters.

2.3.1.1. Six-pulse bridge converter

A six-pulse bridge configuration is the most popular configuration of the converter circuit in use. This configuration can be obtained by combining two three phase single way converters as shown in Figure 2.2. The upper single way circuit provides the positive voltage and the lower single way circuit provides the negative voltage to the load. Thus a pair of SCR's (one in each single way circuit) ideally conducts for exactly 120 electrical degrees of the ac cycle. If the firing of the SCR's occurs at the same instant as the SCR becomes forward biased then the circuits act the same as an uncontrolled rectifier. Usually it is operated in the controlled range i.e. firing angle is delayed(from the natural state). Firing signals are applied simultaneously to the pair of on-coming SCR's. The detailed mathematical analysis of the six-pulse converter circuit is given in Chapter 3. If the smoothing reactor on the dc side is assumed to be large, and commutation overlap neglected then the operation is ideal and the current waveforms on the ac side are essentially square as shown in Figure 2.3. In this case the Fourier series for the ac current in line A is given by (2.1).

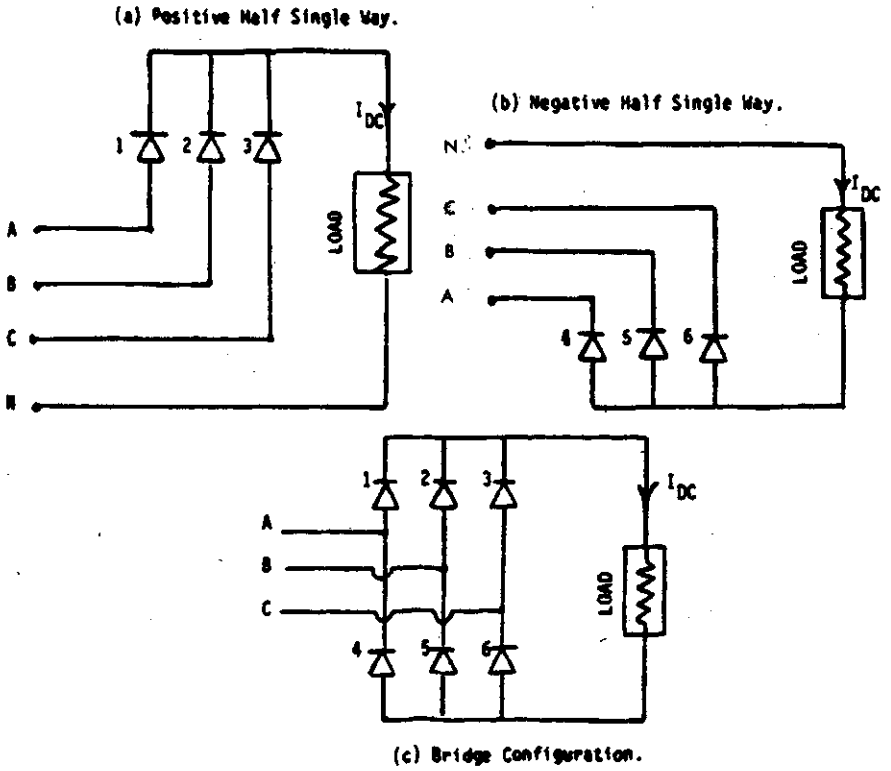

Figure 2.2: Six-pulse bridge converter.

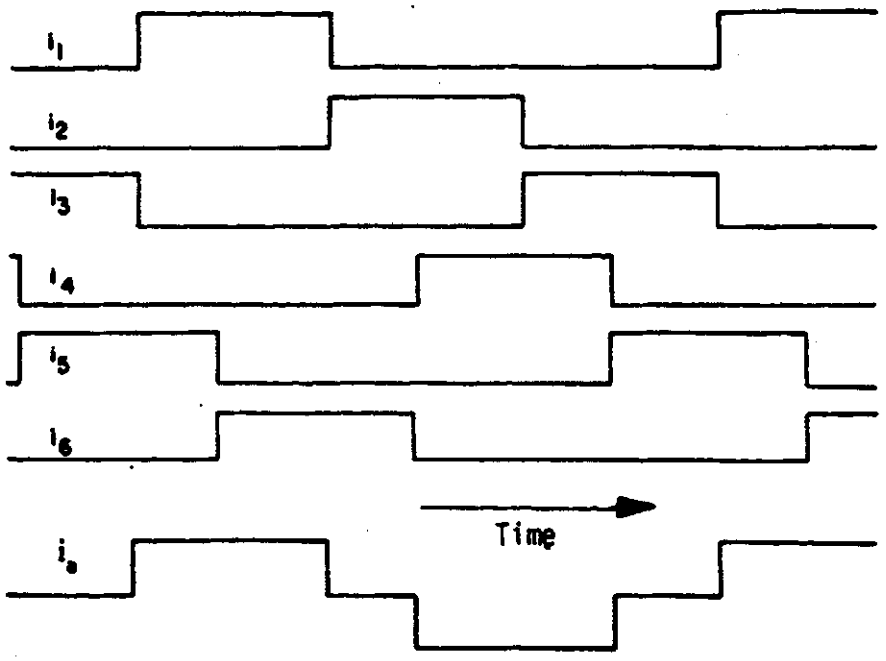

Figure 2.3: Line current waveforms of a converter.

$$i_A = K[cos(\theta) - \frac{1}{5}cos(5\theta) + \frac{1}{7}cos(7\theta) - \frac{1}{11}cos(11\theta) + \frac{1}{13}cos(13\theta)...]. \quad (2.1)$$

Clearly the order of the harmonics of line current is given by $n = kM \pm 1$, where M is the pulse number, and k is an integer 1,2,3,.... These harmonics are known as characteristic harmonics of the ac line current of an M-pulse converter. Assuming the 100% value for current at the fundamental frequency, the values of characteristic current harmonics of a square current waveform varies from about 20% for the 5th harmonic to 4% for the 25th harmonic. In Figure 2.4, the theoretical values obtained by assuming the square waveform are compared with the typical values that exist in actual operation of the converter.

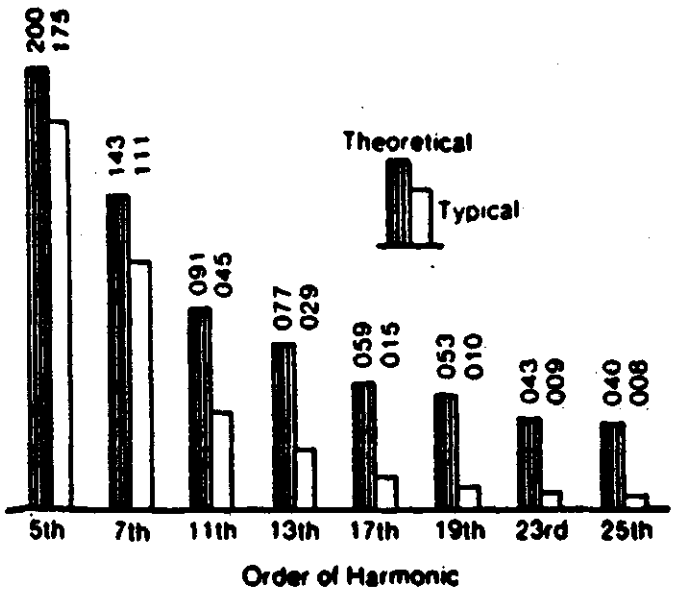

Figure 2.4: Typical values of harmonic currents for a six-pulse converter.

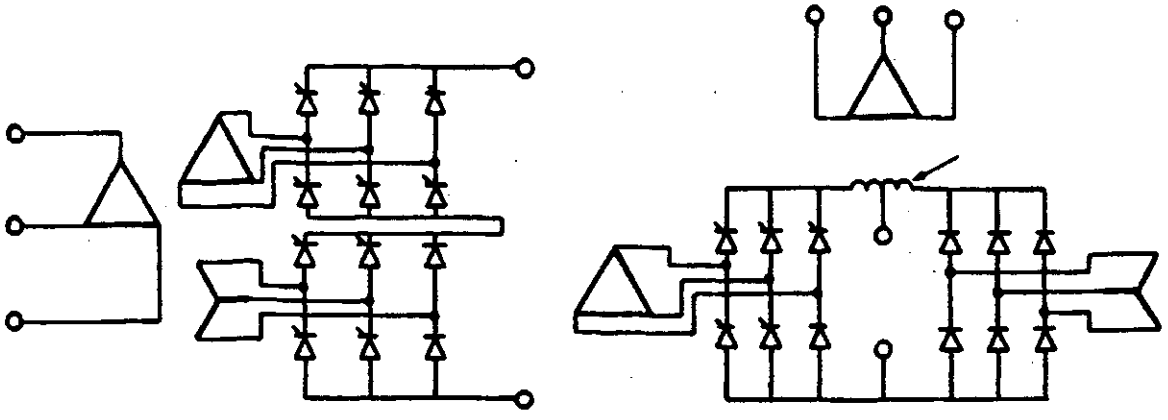

Figure 2.5: Twelve-pulse bridge converter.

2.3.1.2. Twelve-pulse converter

The usual configuration of the converter used for a HVDC converter station is a twelve-pulse configuration. The twelve-pulse converter can be derived by connecting two six-pulse converters as shown in Figure 2.5. One group of the bridge configuration is fed by a Δ-Δ connected converter transformer and the other group of bridge configuration is fed from a Δ-Y connected transformer. Two six-pulse converters can either be connected in parallel or series on dc side to meet the current or the voltage requirement. The line current harmonics of the group fed by Δ-Δ connected transformer is the same as that given by equation (2.1). The line current harmonics for the second group fed by Δ-Y connected transformer can be obtained from equation (2.1) by incorporating the phase shifts of 30 electrical degrees introduced by the Δ-Y connection. Equation (2.2) gives the line current harmonics of the second group of converter. The Fourier series of the total ac line current on the primary side of the converter transformer of a twelve-pulse converter can be then obtained by the addition of i_A and $i_A^{'}$ and is given by the equation (2.3).

$$i_A^{'} = K[\cos(\theta) + \frac{1}{5}\cos(5\theta) - \frac{1}{7}\cos(7\theta) - \frac{1}{11}\cos(11\theta) + \frac{1}{13}\cos(13\theta)...]. \quad (2.2)$$

$$i_A+i_A^{'} = 2K[\cos(\theta) - \frac{1}{11}\cos(11\theta) + \frac{1}{13}\cos(13\theta) - \frac{1}{23}\cos(23\theta) + \frac{1}{25}\cos(25\theta)...]. \quad (2.3)$$

Again, it is clear that the order of harmonics can be obtained by $n = kM \pm 1$, where M now equals 12. In equations (2.1), (2.2), and (2.3), K is the fundamental rms current and can be obtained from the direct current of the converter.

2.3.1.3. Higher-pulse converter

It is obvious from equations (2.1) and (2.3) that for a six-pulse converter, the first dominant harmonic is the 5th, while for the twelve-pulse converter the first dominant harmonic is the 11th. Therefore by increasing the number of phases, the dominant harmonic can be further extended into the higher frequency region. For example, a 24-pulse converter can be obtained by means of four transformers with 15 electrical degrees phase shifts. Such a configuration will result in first dominant harmonic of 23rd order. However, there is added cost of equipment which may not be justifiable. Similar economic problems discourage the use of a 48-pulse converter configuration, which will have the first dominant harmonic of the order of 47. The pulse number above 48 is not possible practically, due to the fact that the small level of waveform distortion can have much influence on the voltage zero crossings and hence cause misfiring of the converter devices.

In the foregoing discussion, the converter is assumed to be ideal, i.e. the commutation overlap is assumed to be zero and dc current is assumed to be ripple free. However, in reality, the commutation of current (transfer of current from off-going SCR to on-coming SCR) does not take place instantaneously. The finite amount of delay is called commutation overlap. In a practical situation, when commutation is included in the analysis, the order of characteristic harmonics remains the same as that of the ideal converter, but the magnitudes are greatly affected. The magnitudes of current harmonics obtained from an ideal converter model are limiting cases. Figures 2.6, 2.7, and 2.8 show the effect of commutation angle on the magnitude of the 5th, 7th, and 11th harmonic currents respectively. The plots are obtained for various firing angles. The detailed calculation of the ac current harmonics of a six-pulse converter is given in Chapter 3. The exact calculation is carried out by taking into account the resistance and inductance of the converter transformer. The ripple in the dc load current is taken care of. Also, the

harmonic voltages of the power system affect the operation of the converters. This effect is taken care of by an iterative process of calculating the harmonic current demand of the converter as described in Chapter 3 and Chapter 4.

As shown in the foregoing section, a stationary current harmonic spectrum injected by the converter operation is appreciably large (approximate 20% for fifth harmonic order) and cannot be ignored. The wide spread use of the converter technology further aggravates the situation, since the amount of harmonic current injected into the power system network increases substantially.

2.3.1.4. Power inverter

One method of integrating the alternate sources of energy, such as wind power, to the existing grid is variable speed generation. For example, a windmill can be used to generate a variable frequency power supply. The variable frequency power supply is then rectified and inverted back to the fixed frequency[1] in synchronism with the power grid frequency. This has not been used widely, due to the inefficient and expensive method of harnessing alternate energy sources; however, there is a greater potential in future implementations of such systems.

The harmonic spectrum of the inverter output voltage is broad and depending upon the methodology, significant low order harmonic frequencies may be generated. Figures 2.9 and 2.10 show typical harmonic voltages produced from a square wave inverter and a pulse width modulated inverter respectively. Results for the pulse width modulated inverter are shown for an ideal case, in an actual case, there may be some uncharacteristic harmonic components as well. While the spectrum for square pulse inverter comprises odd harmonics, the spectrum for the PWM inverter system contains a band of harmonic components near the integer multiples of the modulating frequency. If the modulating index is higher, the significant harmonic voltages exist in the high

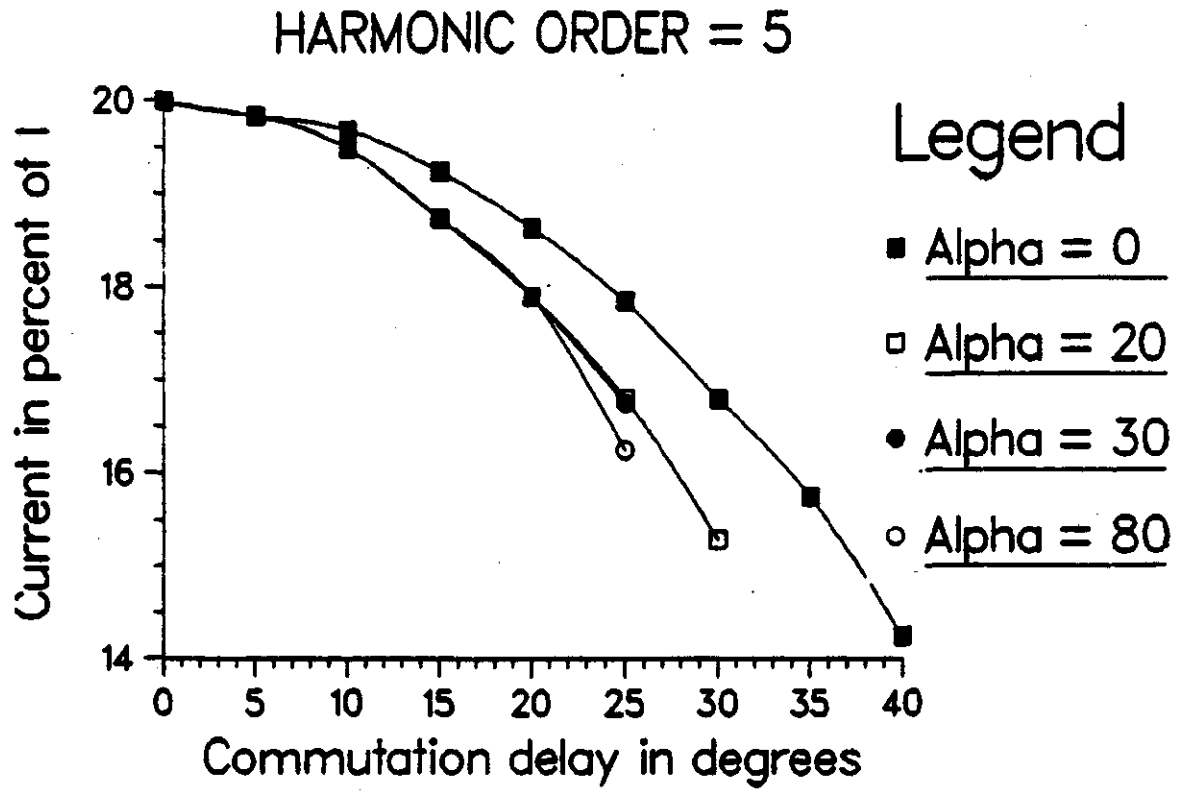

Figure 2.6: 5th harmonic current of a six-pulse converter.

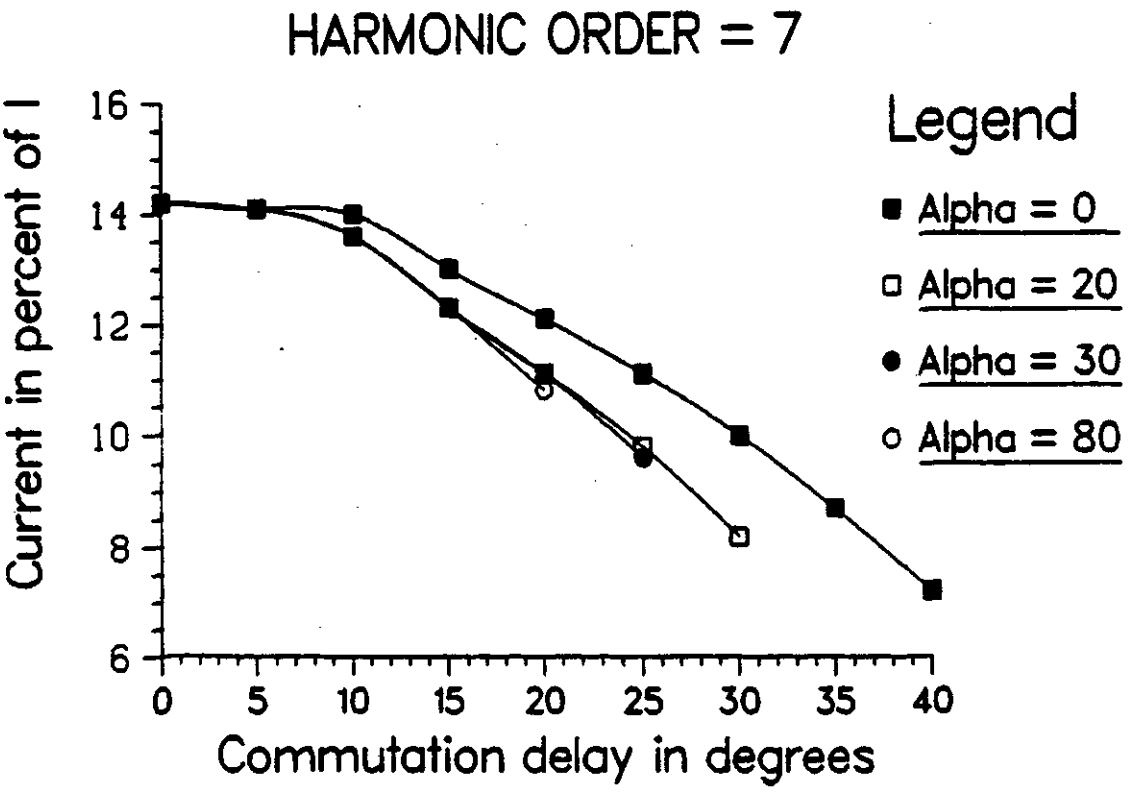

Figure 2.7: 7th harmonic current of a six-pulse converter.

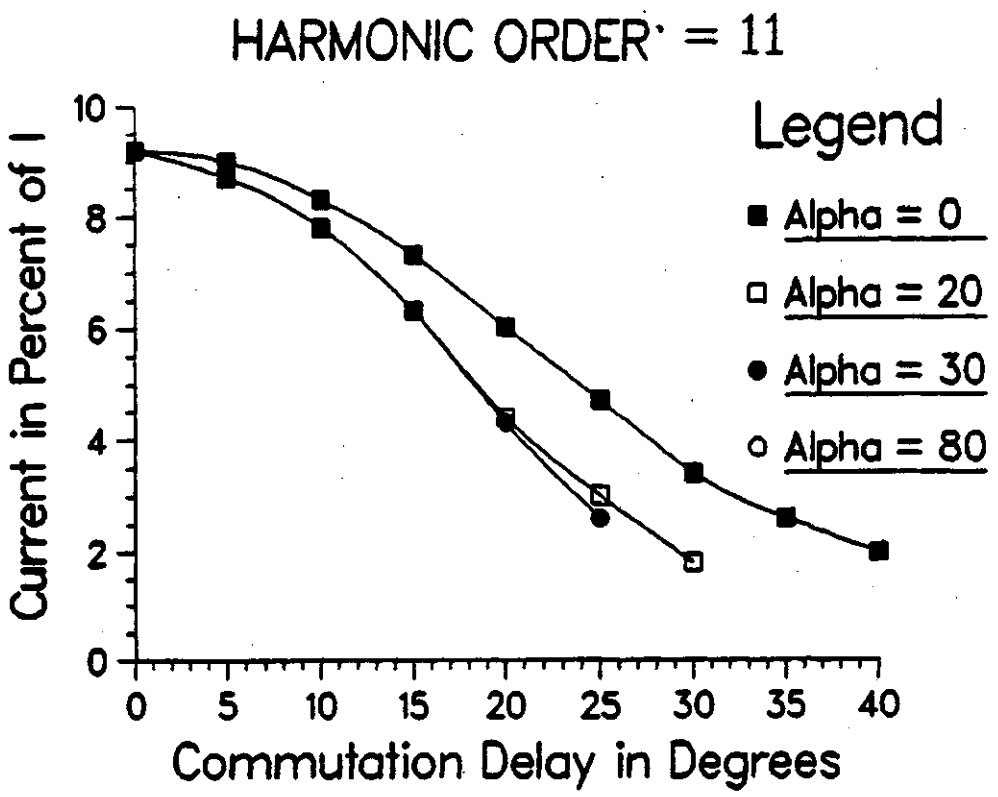

Figure 2.8: 11th harmonic current of a six-pulse converter.

frequency region. In Figure 2.9, the modulating ratio of 6 is used, as a result there are strong harmonic components in the lower region.

Power inverters are also used for speed control of ac motors. However the front end of such systems is a an ac/dc converter. Thus the harmonic interaction between the ac speed drives and the power system can be studied by considering an ac/dc converter with an active dc side load. The power inverter systems are not considered further in this thesis due to their limited use.

2.3.2. Transformers

Clinker's paper[9] on harmonic voltages and currents in transformer windings first brought the subject of harmonic generation from the excitation of the transformer to the attention of engineers. The excitation current waveform necessary to produce the sinusoidal flux wave contains harmonics, which are produced by hysteresis and by the

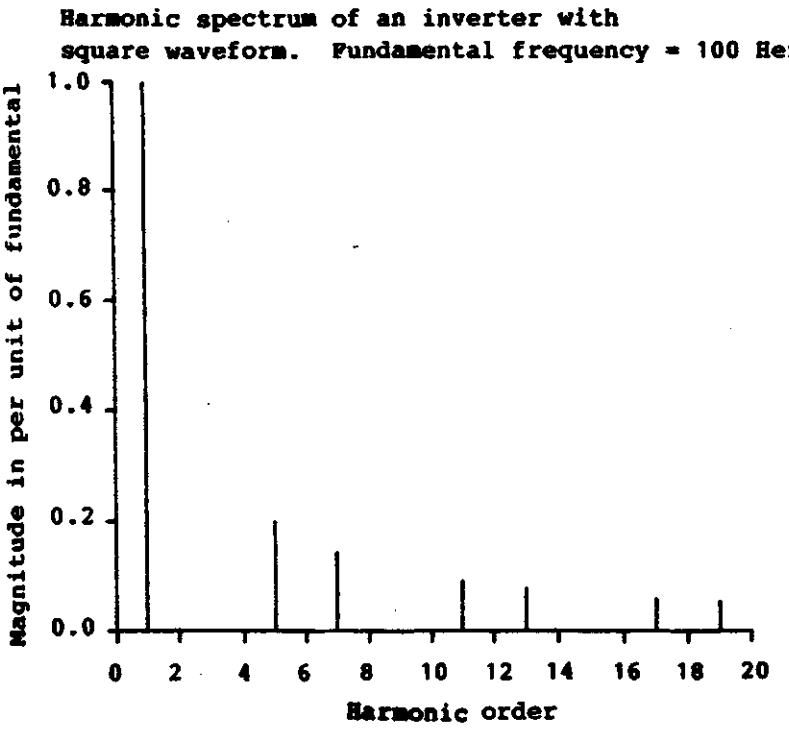

Figure 2.9: Harmonic spectrum of voltage of an inverter with square waveform.

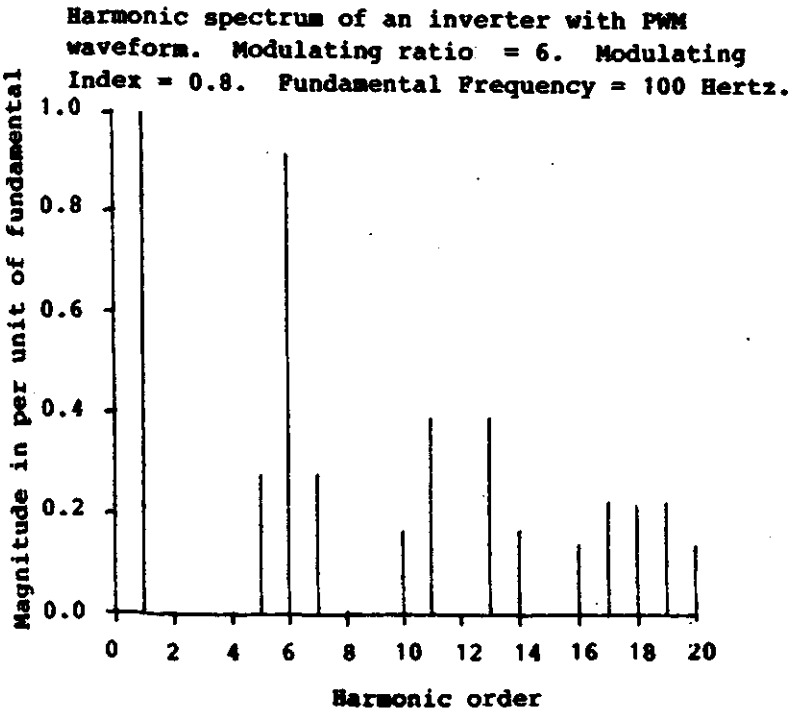

Figure 2.10: Harmonic spectrum of voltage of an inverter with PWM waveform.

variation of permeability of the iron. The amount of harmonics produced is substantial if the transformer core is saturated. Figure 2.11 shows the generation of harmonics due to the hysteresis of the core. The magnetising current waveform is not sinusoidal, and the distorted waveform is rich in harmonics. The most noticeable harmonics are the third, fifth, and seventh. These harmonic currents flow in the supply lines. The triplen harmonics are usually eliminated from the supply lines by the use of delta connected windings.

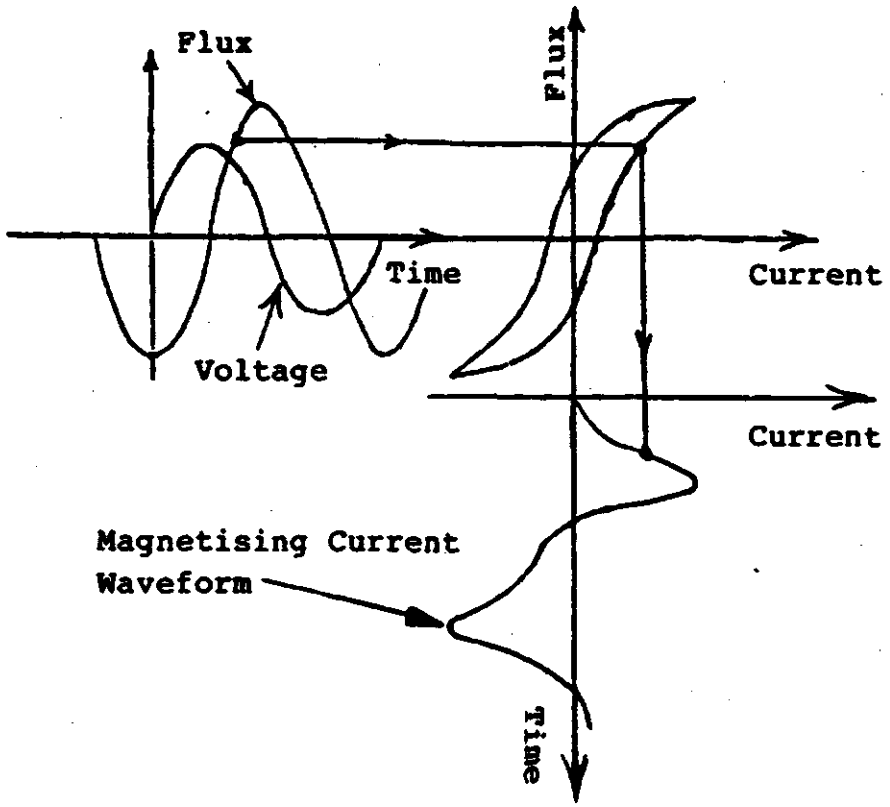

Figure 2.11: Magnetising current waveform.

Transformers are usually designed to operate near the knee of the magnetising curve. If such transformers are subjected to a 30% rise in voltage, the excitation current distortion increases substantially. The problem of harmonic generation from over-voltage is particularly aggravated in the case of transformers connected to large converter loads. As shown by Bowles[46], voltage at the converter terminal can reach as

high as 143 percent following a load rejection, thus driving the transformer deep into saturation. Figure 2.12 shows the relative magnitudes of harmonics of the magnetising current with respect to the percentage of the nominal voltage. The magnetising current of the fundamental frequency is plotted as a percentage of the nominal current of the transformer, whereas all harmonic components of the magnetising current are plotted as percentage of the magnetising current of the fundamental frequency.

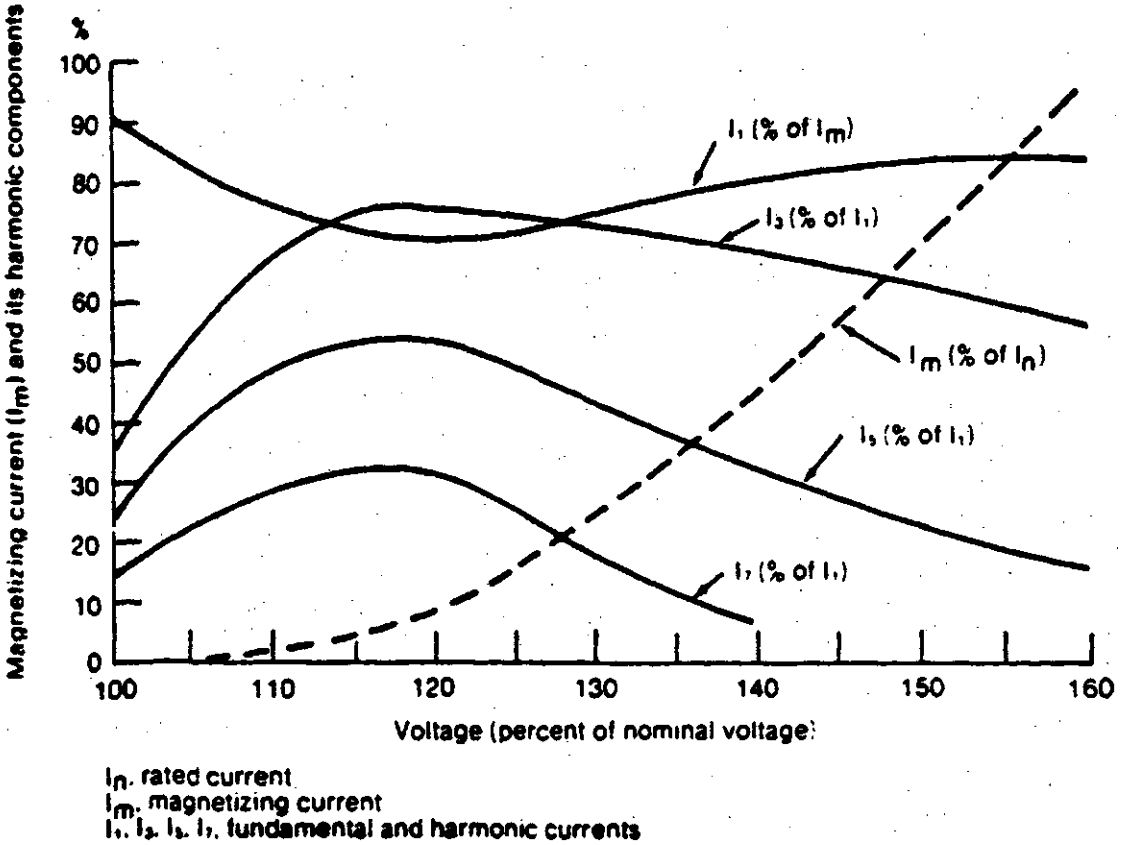

Figure 2.12: Harmonic components of magnetising current[27].

2.3.3. Arc furnaces

Arc furnaces generate harmonics due to the non-linear arc voltage-current characteristics. The harmonic voltages produced are highly variable during various phases of the arc. During the meltdown, the arc is unstable and any change in the arc length is followed by a sudden change in the current magnitude. The sudden change in current causes a voltage flicker. During the period of refining, the arc is more stable and the current is basically a triangular waveform due to the non-linear resistance of the arc.

Figure 2.13 shows the frequency spectrum[47] of the current during melting and refining periods. Such variations in harmonic current with respect to time can best be displayed by a probabilistic plots as shown in Figure 2.14. In Figure 2.14 the fundamental and harmonic components of the current are plotted on two different current scales.

2.3.4. Rotating machines

If the magnetic flux in the air gap of an ac generator is distributed sinusoidally around the air gap, then the e.m.f. induced in the stator winding is also sinusoidal. However, the flux is never exactly distributed in this way and hence the voltage induced contains harmonic voltages. Magnitudes of the harmonic voltages induced depend upon the magnitudes of the harmonic fluxes, the effective electrical phase spread of the windings, the coil spans, and the method of inter-phase connections. The harmonic magnitudes can be minimised by suitably choosing the winding distribution factors and the coil span factors.

The variation in the air gap permeance due to slots also causes harmonic flux components in the air gap. This phenomenon, however, can be minimised by (i) skewing the slots; (ii) offsetting the pole shoes in successive pairs of poles, displacing the centre line of the damper bars in successive pole faces. By using various correcting factors[48], the generation of the harmonic voltages is minimised greatly. The magnitudes of harmonic voltages produced by a typical utility type synchronous generator are between 1% - 3% of the fundamental.

Harmonic components of current are produced by induction motors as a result of the non-sinusoidal m.m.f. distribution. These harmonics are dependent on the speed of the motor; for example if f_1 is the fundamental frequency, λ_1 is the wavelength, and s is the slip in per unit, then a harmonic component of order n in the rotor m.m.f. induces an e.m.f. in the stator at a frequency of $f_1[n\text{-}s(n - 1)]$.

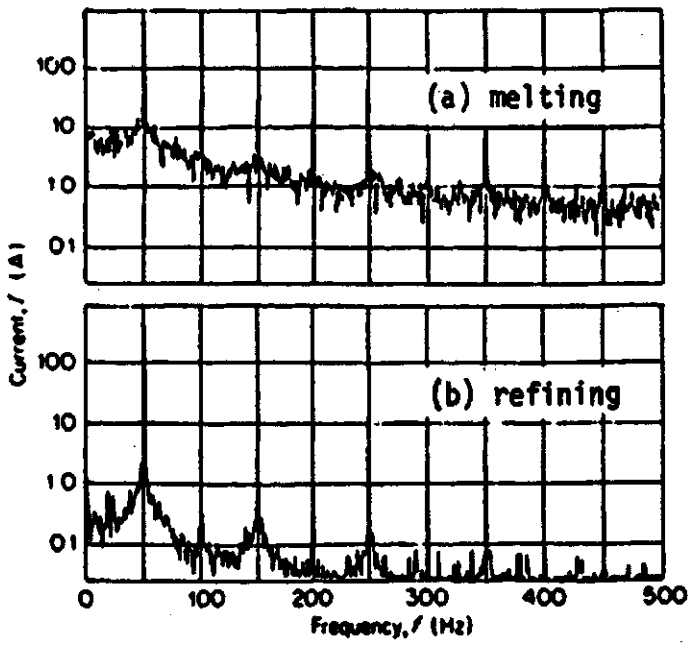

Figure 2.13: Current harmonics spectrum of an arc furnace.

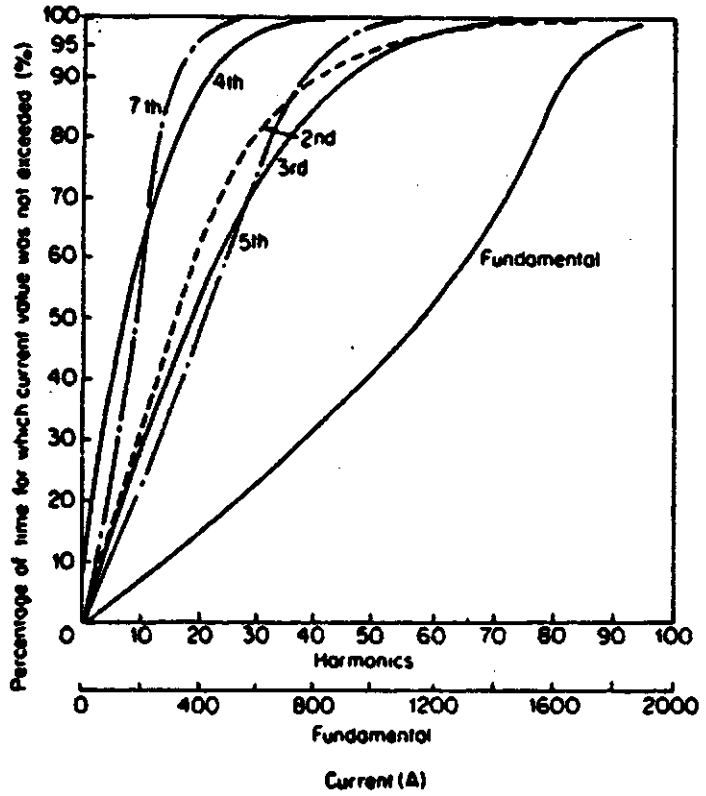

Figure 2.14: Probabilistic harmonic magnitude plots.

Harmonic currents can be produced also by an electrical asymmetry such as an unbalanced rotor winding, pole unbalance. Such an unbalance can produce the uncharacteristic harmonics as well. As shown by Wallace[49] et.al., harmonic current magnitudes produced by induction motors are typically less than 3.0% of the fundamental. The relative magnitudes of harmonics produced by a six pole machine running at a speed of 0.9 per unit are reproduced from reference[49] in Table 2-1.

There are several other non-linear loads such as fluorescent lighting, static uninterruptible power supplies, static frequency converters, and single phase non-linear loads. These sources are not considered in this thesis, because their major impact is on the distribution network and not on the transmission network[6].

Table 2-1: Typical harmonic current produced by the slip-ring induction motor.

Frequency (Hz)	Current (Percent of I_1)
20	3.0
40	2.4
50	100.0
80	2.3
220	2.9
320	3.0
490	0.3
590	0.4

2.4. Discussion on Harmonic Sources

In the foregoing section, various harmonic sources are described briefly. The relative magnitudes of harmonics of voltages and currents produced by these sources are also presented. The ac/dc converter stands out as the strongest harmonic source of all. This fact is also supported by field experience reported by Pillegi[50] et al. The magnitude of the fifth harmonic current from a six-pulse ac/dc converter is about 20% of the fundamental and in comparison, the maximum harmonic voltage produced by the

synchronous machine and the induction machine is about 3% of the fundamental. Another strong source of current harmonics is the transformer, particularly when saturated. Nevertheless the percentage of harmonic current produced by the transformer, under normal operation, is quite small compared to the load current, particularly so in the case of a power transformer used in the transmission network. There are harmonics in the transformer current during the initial excitation of the transformer due to inrush of the current. Such harmonics, however, are not the subject of this thesis due to their non-stationary nature. Arc furnaces are also major sources of harmonics, but the harmonics produced are quite variant during the melting process.

In the present application, the ac/dc converter is taken as the main source of harmonics. The methodologies are developed to calculate numerically the harmonic currents of ac/dc converters. Harmonic current and voltages from ac machines are ignored due to their relatively smaller magnitudes. The harmonic currents of transformers are included, however, their magnitudes are mostly obtained from experimental results.

Models of other miscellaneous elements, such as arc furnaces, static VAR compensators, and filters are not presented in detail. As shown earlier, estimation of harmonics of arc furnaces is quite difficult due to the time variation in the harmonic contents. The specific topic of arc furnaces is not treated in this report. Although no model of other equipment generating harmonics is discussed, the algorithm developed has the provisions for the inclusion of the harmonic currents injected by miscellaneous equipment as described in subsequent sections of this thesis.

The converter/inverter systems for integrating the alternate energy sources into a fixed frequency grid are also not included in this thesis, since these devices are not yet used extensively.

2.5. Conventional Load Flow Studies

In carrying out the fundamental frequency load flow studies, an iterative process of computation is used to determine the load bus voltages from the prior knowledge of the generator bus voltages and of the value of loads on the power system. There are three basic sets of equations required to solve for the load flow calculations at the fundamental frequency. These are as given below.

1. Network performance equations such as $V_{bus} = Z_{bus} I_{bus}$ or $I_{bus} = Y_{bus} V_{bus}$, where V_{bus}, I_{bus}, Z_{bus}, and Y_{bus} are bus voltage, current, impedance matrix and admittance matrix respectively.

2. Bus loading equations i.e. $P_i - jQ_i = V_i^* I_i$, where i is a bus node, P_i, Q_i, V_i^*, and I_i are active power, reactive power, conjugate of bus voltage and bus current respectively.

3. Line flow equations i.e. $I_{ij} = (V_i - V_j)Y_{ij} + V_i Yc_{ij}/2$, where i and j are bus nodes, Yc_{ij} is the total line charging admittance, Y_{ij} is the admittance between two nodes, and V_i is the ith node voltage and I_{ij} is the line current between nodes i and j.

Solutions of such a set of equations is obtained iteratively using the Gauss method, the Gauss-Seidel method, or the Newton-Raphson method. The formulation of these equations assumes that all quantities are referred to the fundamental frequency with prior knowledge of source bus voltage and power at a PV bus. Also the criterion of mismatch of power or voltages for the convergence of the solution of the load flow equations is valid only at the fundamental frequency. The admittance and the impedance matrices are also calculated for the fundamental frequency.

The power flow at harmonic frequencies is very much different from that at the fundamental frequency. One of the primary differences is that there is no initial knowledge of generation of harmonic voltages or harmonic currents and also there is no known value of harmonic load on the system. The harmonic signal (voltage or current)

generation can only be estimated from the dynamic interaction of the power system network and the harmonic generating equipment. The models used by Tschappu[51] and by Emanuel[22] demonstrate the difference between the power flows at the fundamental and the harmonic frequencies. With reference to the single machine system shown in Figure 2.15(a), the sinusoidal voltage generator supplies power P_1 to the load point. The major portion of this power flows into the load, P_L, a portion of it is consumed as loss in the system resistance (P_S) and a small portion of flows into the converter (P_C). A major part of the converter power (P_C) is transformed into the harmonic power P_H. In Figure 2.15(b), the flow of harmonic power is shown where the power P_{SH} is fed back to the power system supply components and part of the harmonic power P_{LH} is fed into the load.

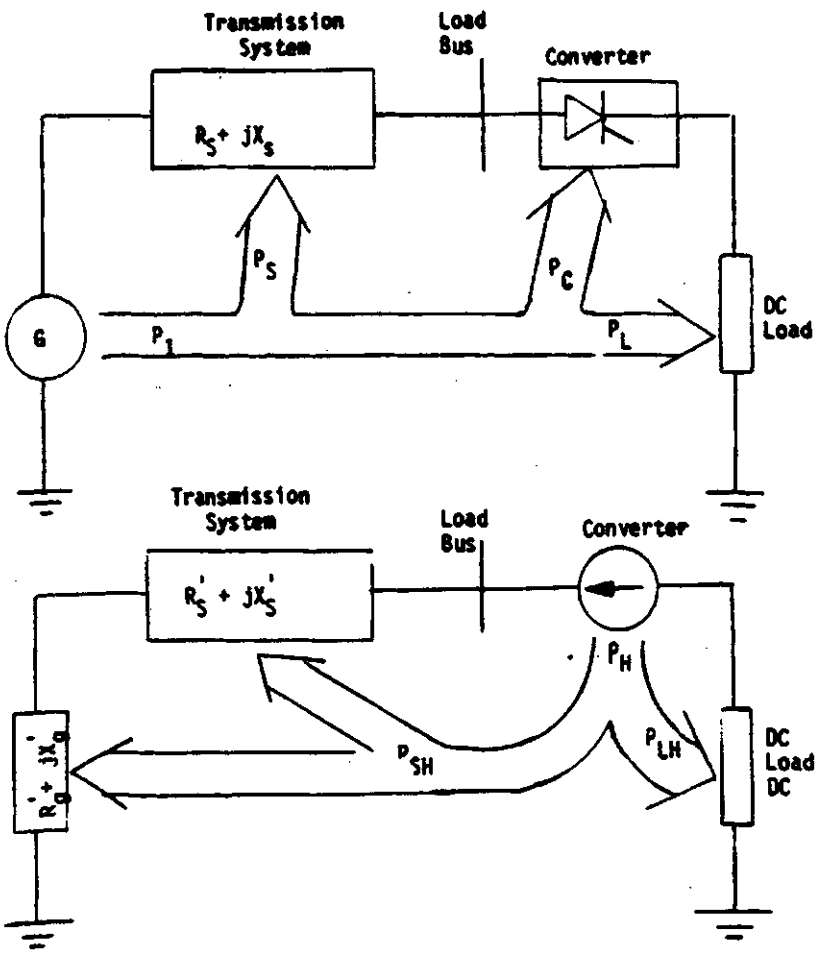

Figure 2.15: (a) Fundamental power flow;
(b) Harmonic power flow.

The formulation of equations for the load flow studies takes care of the conditions shown in Figure 2.15(a). The methodology is not suitable for the study of the case shown in Figure 2.15(b) due to the fact that harmonic power, also called distortion power, is not accounted for. Moreover, the harmonic power converted by the converter can not be explicitly represented by the power equations used in the conventional load flow studies. Thus it becomes imperative either to extend the load flow models by including the harmonic power equations or by employing a different set of equations to solve for the harmonic power flow. The simple strategy is to consider the power conditioning equipment as the sources of harmonic current injection into the power system network. The rest of the power system can be considered as a network of passive elements. These aspects are dealt with in Chapter 3.

2.6. Conclusion

In this chapter, the main sources of harmonics in the power system network have been briefly discussed. The static ac/dc converter system is shown to stand out as the main single source of frequency pollution due to the large stationary harmonic current injection into the power system at the present time. The concept of harmonic power flow is presented and it is shown that the converter can be visualised as a device to convert a portion of fundamental frequency power into harmonic power. The conventional load flow problem is discussed briefly and shown to be unsuitable for the analysis of the harmonic power flow. It is suggested that an iterative approach be used for the calculation of the harmonic interaction between the harmonic generating sources and the power system network.

3. POWER SYSTEM MODELLING FOR HARMONIC ANALYSIS

3.1. Introduction

The formulation of the harmonic frequency power flow problem is discussed and relevant assumptions are described in Chapter 3. Models of elements of the power system network for use in harmonic frequency power flow calculations are presented in this chapter. The analysis of the converter is carried out and the computation of the harmonic current injection from the converter is also presented. A phase shifting model of transformer is presented for the harmonic analysis. The transmission model to calculate the voltage profile on the transmission line is discussed. The justification for the independent treatment of each harmonic frequency is also included. A complete algorithm for the solution of the harmonic power flow is presented.

3.2. Formulation of Harmonic Power Flow Problem

As described in Chapter 2, the harmonic power flow problem can be visualised by considering the non-linear load as a source of current harmonics. The harmonic current demand of such a non-linear load arises due to its cyclical switching behaviour at the fundamental frequency. The power system can be either modelled as an admittance or an impedance network. In this manner, the system equations can be written to describe the harmonic current and voltage relation based upon the admittance or impedance matrix.

The set of equations so obtained for the harmonic power flow in a power system can be solved by employing several strategies. These are (i) linearized current injection technique; (ii) non-linear time domain simulation of the system; and (iii) non-linear frequency domain analysis.

The first technique is based on the assumption that the current supplied to the converter has a square waveform. Therefore the current harmonics are primarily functions of the fundamental current magnitude and are independent of the voltage waveform. With this linearization, the steady state response of the power system can be found by solving the admittance or impedance matrix equations for each harmonic frequency. The advantage of this method is higher computation efficiency while giving up some accuracy due to the square wave estimation of the line current of a converter. This method gives an approximate solution and ignores both the commutation of the converter devices and changes in the bus harmonic voltages with each iteration. This method is prone to error when there is interaction between the harmonic sources and the network voltages, such as, in the case of a converter load.

In the second method a set of differential equations are used to define the conduction state of the converter. The solution is obtained from integrating the differential equations using a small step size. The converter is modelled as a set of ideal switches with a linear load. The accuracy of this method depends upon the model of the load, source and the transmission network. The frequency domain models that treat the fundamental and harmonic frequencies separately are not appropriate for this method. Also the load and source modelling is somewhat difficult with this method. The finite commutation delay in converter devices is also ignored in order to simplify the complexities of equations.

The third alternative, chosen for implementation in this thesis, is based on the non-linear frequency domain analysis. Given an initial estimate of the current waveform of the converter, the harmonic voltages at system buses are determined from the system admittance matrix equation, i.e. $[I] = [Y][V]$. A new estimate of the current waveform of the converter is obtained from the new bus voltages including the harmonic voltages. This cycle is repeated until convergence in the magnitude of the harmonic

voltages on all nodes in the power system is obtained. The convergence criterion is the change in harmonic voltages at the system buses. This method is chosen for the implementation. The non-linear model of the converter is coupled with the admittance matrix of the system to find an iterative solution. This technique can be considered as an extension of the current injection technique. In this method the system parameters have to be formulated for each frequency. Figure 3.1 gives a flow chart of the algorithm for the frequency domain analysis.

The success of the method depends largely upon accurate modelling of the power system equipment and the harmonic current injecting load. There are several types of equipment used in the power system, and modelling of some of these is described in the following section. In addition, there are different types of electrical loads on the power system. Models for some of these loads for the harmonic analysis are also included in the following subsections.

3.3. Modelling of Power System Equipment

The thrust of the modelling is to find the most appropriate circuit model of each element of the power transmission network for the harmonic analysis. In such models, the main emphasis is attributed to the impedance and phase shift due to the device at the harmonic frequency of interest. Other factors such as the skin effect, balance, and unbalance condition also play significant roles. In the case of a transmission line, the skin effect influences both inductance and resistance appreciably at higher frequencies. All these factors are taken into account while modelling the power system equipment.

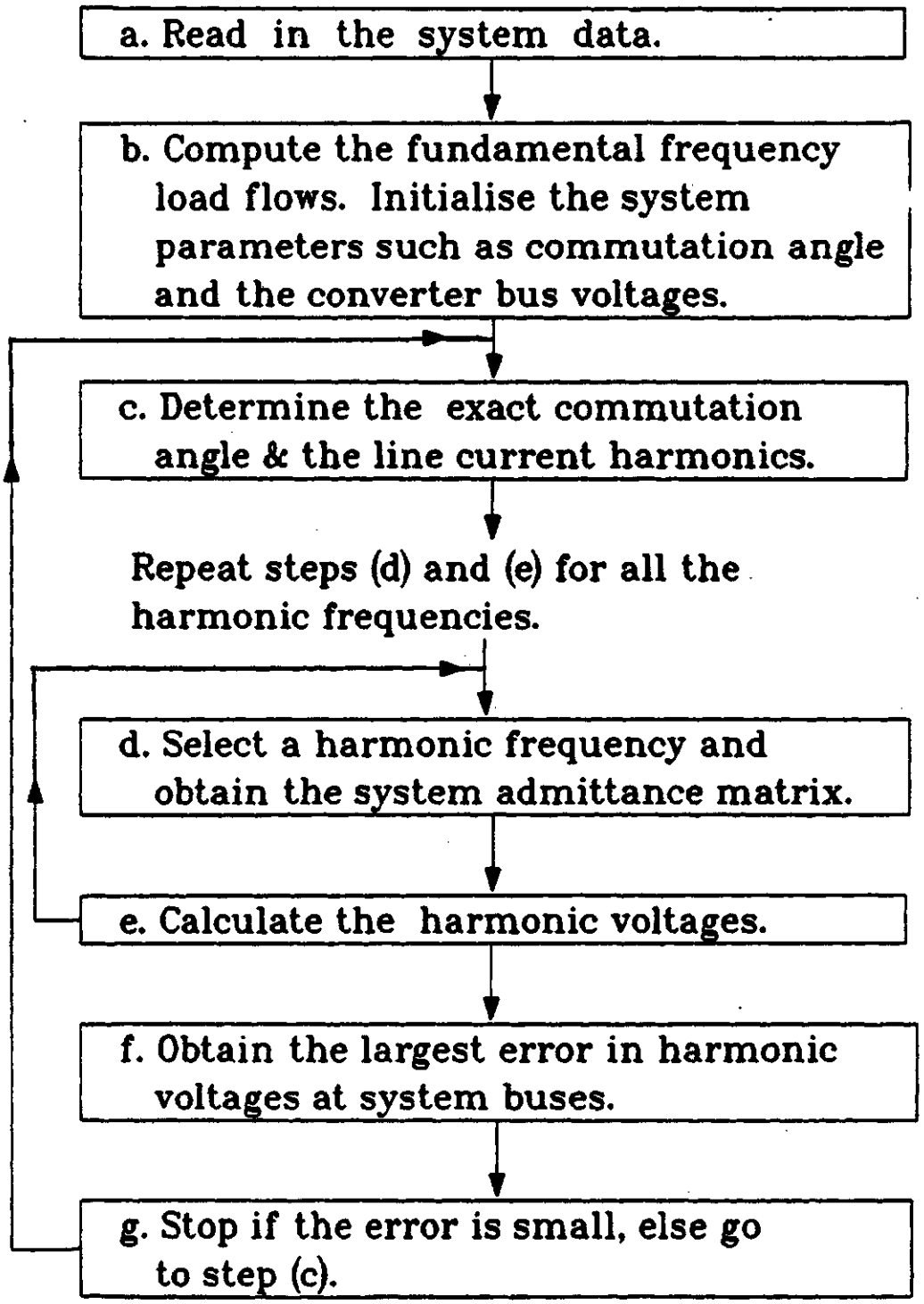

Figure 3.1: Flow chart for non-linear frequency domain analysis.

3.3.1. Static power converter

Static power converters have found extensive application in industry; unfortunately they produce large harmonic current injection into the power system. The amount of harmonic current injection depends on the type of load, finite commutation delay, and the pollution of the power system. In this section, the analysis is presented to illustrate the computation of the commutation delay of the converter excited by the polluted power system. The computation of the ac line current harmonics of the converter is also given.

Assume that the bus supplying the converter has the ac voltages given by equation (3.1), where the line A to neutral voltage is taken as the reference. Symbol δ_k is the sequence indicator, e.g. δ_k is 1 for positive sequence harmonics, -1 for negative sequence harmonics, and zero for zero sequence harmonics. Also assume that the firing angle of the converter is α. Let R_n, L_n and R_d, L_d be resistances and inductances of the converter transformer and the dc load, respectively, as shown in Figure 3.2. The conduction pattern of the converter for this condition is shown in Figure 3.3. Since there is a finite commutation delay, the current in each ac line is somewhat trapezoidal rather than being a square waveform and can be divided in several conduction zones.

$$
\begin{aligned}
v_{ab} &= \sum_{k=1,3,5,..} V_{Lk}\ cos(k\omega t + \frac{\pi\delta_k}{6}) \\
v_{bc} &= \sum_{k=1,3,5,...} V_{Lk}\ cos(k\omega t \pm \frac{\pi\delta_k}{2}) \\
v_{ca} &= \sum_{k=1,3,5,...} V_{Lk}\ cos(k\omega t + \frac{5\pi\delta_k}{6}).
\end{aligned}
\tag{3.1}
$$

During the commutation of two SCR's, e.g. SCR1 and SCR3, the SCR with more forward positive voltage commutates the other SCR. If the SCR's are assumed to have no voltage drops across them, during the commutation time two ac lines see a short

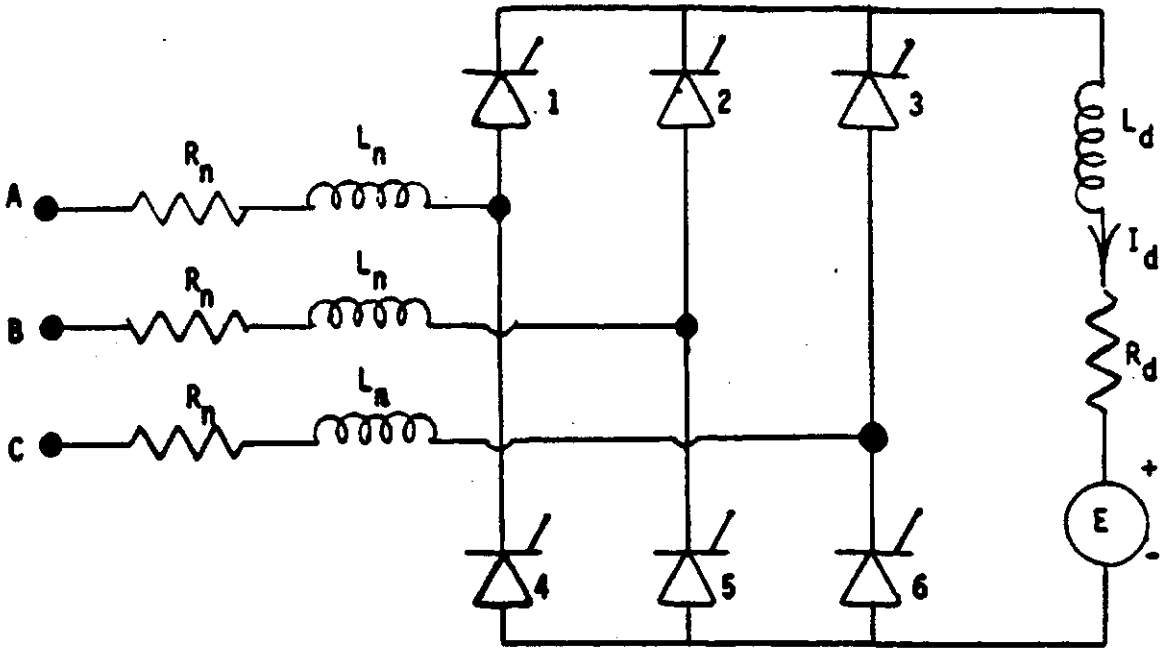

Figure 3.2: Bridge converter.

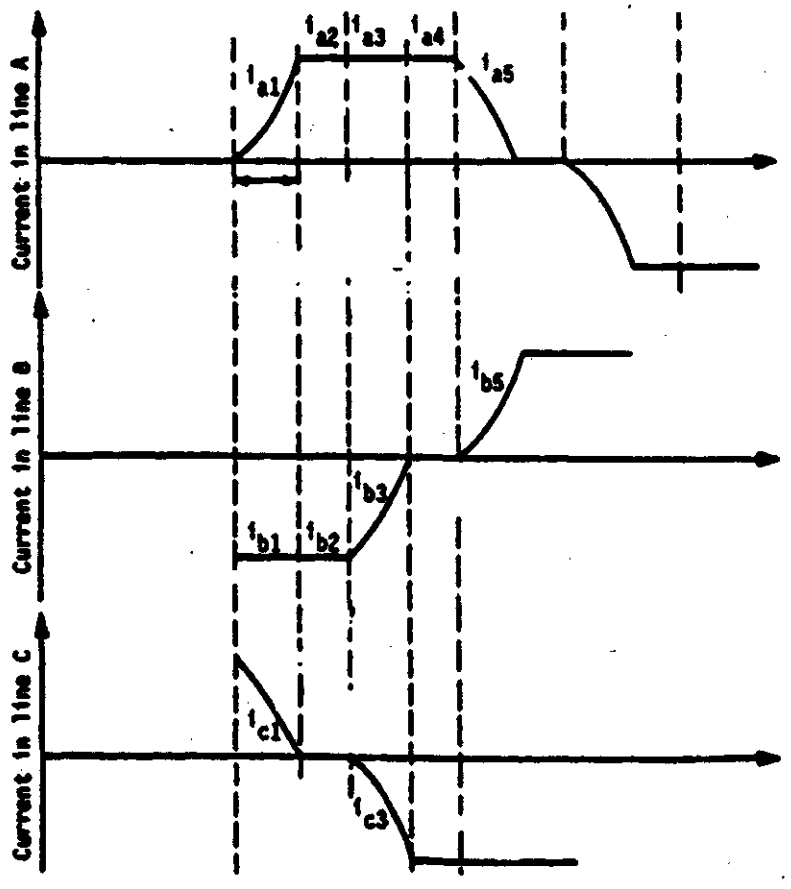

Figure 3.3: Conduction pattern of bridge converter.

circuit through the transformer and the series inductive snubber. Thus the commutation time is essentially determined by the character of the shorted circuitry. The harmonic spectrum of the converter bus voltage and the transformer impedance play significant role in determining the commutation delay. The objective here is to determine the harmonic content of the ac line current feeding the converter by taking into account the finite commutation delay and the harmonic voltages at the converter bus. In the following section, first a solution is obtained for the commutation delay followed by the computation of harmonics of the line current for the given harmonic voltages at the system bus.

The solution presented herein is valid under the following assumptions.

1. The firing sequence of the rectifier bridge is cyclic and balanced.

2. SCR's and diodes have negligible voltage drop across themselves when they are conducting current in the forward direction.

3. The commutation is natural and there is a finite commutation delay, i.e. self commutated bridges are not included in the analysis.

4. The power transformer feeding the converter has significant resistance. This gives rise to the exact solution at the cost of slight complexities.

5. The effect of harmonic bus voltages will be taken into account by the iterative nature of the harmonic power flow algorithm.

The current in line A, i_a, is symmetrical in both halves of the ac cycle. Therefore, the determination of i_a in one half is sufficient. There are five distinct time intervals in the positive half of the line current (line A), identified as i_{a1}, i_{a2}, i_{a3}, i_{a4}, and i_{a5} and shown in Figure 3.3. The computation of these currents is given as follows.

Consider the commutation period $[-\pi/3+\alpha,\ -\pi/3+\alpha+\mu]$, during which the line C (SCR3) is commutated by the on coming SCR1 in line A. Figure 3.4 represents the circuit configuration during the commutation interval. The governing current equations,

obtained by applying Kirchhoff's Current Law, are given by the set of equations (3.2), where operator D is d/dt. Similarly during the interval $[-\pi/3+\alpha+\mu, \alpha]$, lines A and B are conducting and the differential equations given by (3.3) govern the conduction.

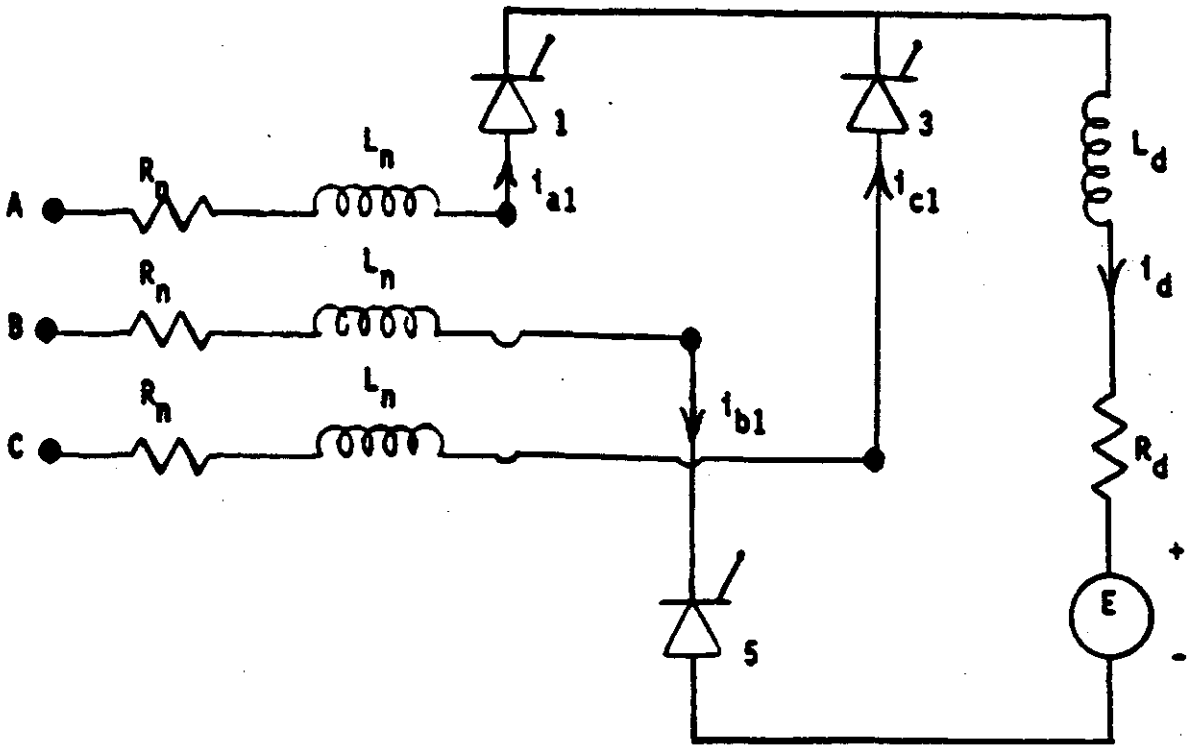

Figure 3.4: Bridge converter during commutation.

$$\begin{aligned} v_{ac} &= [R_n + L_nD][i_{a1} - i_{c1}] \\ v_{ab}-E &= (R_n+L_nD)i_{a1} + [R_n+R_d+(L_n+L_d)D]i_d \\ i_{a1} &+ i_{c1} = -i_{b1}. \end{aligned} \tag{3.2}$$

$$\begin{aligned} i_{a2} &= -i_{b2} = i_d \\ v_{ab}-E &= [R_n+ L_nD]i_{a2}+[R_n+R_d+(L_n+L_d)D]i_d \\ i_{c2} &= 0. \end{aligned} \tag{3.3}$$

Currents i_{a1}, i_{c1}, i_{b1}, i_{a2}, and i_{b2} can be obtained by the solution of equations (3.2) and (3.3). A complete step by step solution is given in Appendix A and the final results are as given below.

$$i_{a1} = A_{12}e^{-\theta/\omega\tau_{12}} + A_{11}e^{-\theta/\omega\tau_n} + f_{a1}(\omega t) - E/(3R_n+2R_d)$$

$$i_{c1} = A_{12}e^{-\theta/\omega\tau_{12}} - A_{11}e^{-\theta/\omega\tau_n} + f_{c1}(\omega t) - E/(3R_n+2R_d)$$

$$i_{b1} = 2A_{12}e^{-\theta/\omega\tau_{12}} + f_{a1}(\omega t) + f_{c1}(\omega t) - 2E/(3R_n+2R_d)$$

$i_{a2} = A_{22}e^{-\theta/\omega\tau_{22}} + f_{a2}(\omega t) - E/(2R_n+R_d)$

and

$i_{b2} = -A_{22}e^{-\theta/\omega\tau_{22}} - f_{a2}(\omega t) + E/(2R_n+R_d)$,

where,

$$f_{a1}(\omega t) = \sum_{k=1,3,5,\ldots} \frac{V_{Lk}}{Z_{12k}} cos(k\omega t + \delta_k \pi/6 - \phi_{12k}) - \sum_{k=1,3,5,\ldots} Z_{Tk} V_{Lk} cos(k\omega t + \delta_k \frac{5\pi}{6} + \phi_{Tk}),$$

$$f_{c1}(\omega t) = f_{a1}(\omega t) + \sum_{k=1,3,5,\ldots} \frac{V_{Lk}}{Z_{nk}} cos(k\omega t + \delta_k 5\pi/6 - \phi_{nk}),$$

$$f_{a2}(\omega t) = \sum_{k=1,3,5,\ldots} \frac{V_{Lk}}{Z_{22k}} cos(k\omega t + \delta_k \pi/6 - \phi_{22k}),$$

$|Z_{nk}|$ Angle $\phi_{nk} = R_n + jk\omega L_n$,

$|Z_{12k}|$ Angle $\phi_{12k} = 3R_n + 2R_d + jk\omega(3L_n + 2L_d)$,

$|Z_{22k}|$ Angle $\phi_{22k} = 2R_n + R_d + jk\omega(2L_n + L_d)$,

$|Z_{11k}|$ Angle $\phi_{11k} = R_n + R_d + jk\omega(L_n + L_d)$,

$$Z_{Tk} = \frac{Z_{11k}}{Z_{nk}Z_{12k}},$$

$$\tau_{12} = \frac{3L_n + 2L_d}{3R_n + 2R_d},$$

$$\tau_n = \frac{L_n}{R_n}, \quad and$$

$$\tau_{22} = \frac{2L_n + L_d}{2R_n + R_d}.$$

By virtue of there being a 3-phase balanced voltage supply, the solution for i_{a3}, i_{a4}, and i_{a5} can be obtained from shifting i_{b1} by $\pi/3$ radians , i_{a2} by $\pi/3$ radians, and i_{c1}

by $2\pi/3$ radians. In this manner the current for line A is defined completely by a set of five equations given in (3.4).

$$i_{a1} = A_{12}e^{-\theta/\omega\tau_{12}} + A_{11}e^{-\theta/\omega\tau_n} + f_{a1}(\omega t) - \frac{E}{3R_n+2R_d},$$

$$i_{a2} = A_{22}e^{-\theta/\omega\tau_{22}} + f_{a2}(\omega t) - \frac{E}{2R_n+R_d},$$

$$i_{a3} = 2A_{12}e^{-(\theta-\pi/3)/\omega\tau_{12}} + f_{a1}(\omega t-\pi/3) + f_{c1}(\omega t-\pi/3) - \frac{2E}{3R_n+2R_d}, \tag{3.4}$$

$$i_{a4} = A_{22}e^{-(\theta-\pi/3)/\omega\tau_{22}} + f_{a2}(\omega t-\pi/3) - \frac{E}{2R_n+R_d},$$

and

$$i_{a5} = A_{12}e^{-(\theta-2\pi/3)/\omega\tau_{12}} - A_{11}e^{-(\theta-2\pi/3)/\omega\tau_n} + f_{c1}(\omega t-2\pi/3) - \frac{E}{3R_n+2R_d}.$$

Equation (3.4) defines the current in line A in the positive half of the ac waveform and due to symmetry the current in the negative half is given by $i_a(\omega t-\pi) = -i_a(\omega t)$. Constants A_{11}, A_{12}, and A_{22} and commutation angle μ are determined from the continuity expressions for the current. The expressions obtained do not have any closed form of solution due to their transcendental nature and can only be solved by numerical methods. The detailed calculation of these equations is presented below.

3.3.1.1. Computation of the commutation interval

In the circuit of Figure 3.2, the current in line A at the instant of applying a trigger signal to SCR1 is 0 and starts building up. At the same instant the current in line C (SCR3) equals dc load current and starts reducing. During the commutation both SCR1 and SCR3 conduct, eventually SCR3 stops and SCR1 takes up the full load current. Therefore the following boundary conditions are valid during the interval $[-\pi/3+\alpha,\ -\pi/3+\alpha+\mu]$.

$$At\ \theta = \frac{-\pi}{3} + \alpha\ ;\ i_{a1} = 0. \tag{3.5}$$

$$At\ \theta = \frac{-\pi}{3} + \alpha + \mu\ ;\ i_{c1} = 0 \tag{3.6}$$

$$and\ i_{a1} = i_{a2}. \tag{3.7}$$

$$Also\ at\ \theta = \alpha\ ;\ i_{a2} = -i_{b3}$$

$$or\ i_{a2} = i_{c1}(\alpha-\pi/3). \tag{3.8}$$

The boundary condition given by (3.7) is because of the continuity of the current, since the current i_{a2} begins when i_{a1} ends. Applying the above mentioned boundary conditions, the following equations are obtained.

$$0 = A_{12}e^{-(\alpha-\pi/3)/\omega\tau_{12}} + A_{11}e^{-(\alpha-\pi/3)/\omega\tau_n} + f_{a1}(\alpha-\pi/3) - \frac{E}{3R_n+2R_d}. \tag{3.9}$$

$$0 = A_{12}e^{-(\alpha+\mu-\pi/3)/\omega\tau_{12}} - A_{11}e^{-(\alpha+\mu-\pi/3)/\omega\tau_n} + f_{c1}(\alpha+\mu-\pi/3) - \frac{E}{3R_n+2R_d}. \tag{3.10}$$

$$A_{12}e^{-(\alpha+\mu-\pi/3)/\omega\tau_{12}} + A_{11}e^{-(\alpha+\mu-\pi/3)/\omega\tau_n} + f_{a1}(\alpha+\mu-\pi/3) - \frac{E}{3R_n+2R_d} = A_{22}e^{-(\alpha+\mu-\pi/3)/\omega\tau_{22}} + f_{a2}(\alpha+\mu-\pi/3) - \frac{E}{2R_n+R_d}. \tag{3.11}$$

$$A_{12}e^{-(\alpha-\pi/3)/\omega\tau_{12}} - A_{11}e^{-(\alpha-\pi/3/\omega\tau_n} + f_{c1}(\alpha-\pi/3) - \frac{E}{3R_n+2R_d} = A_{22}e^{-\alpha/\omega\tau_{22}} + f_{a2}(\alpha) - \frac{E}{2R_n+R_d}. \tag{3.12}$$

The following variables are introduced in order to simplify the above equations.

$$\rho_1 = A_{11}e^{-(\alpha-\pi/3)/\omega\tau_n}, \tag{3.13}$$

$$\rho_2 = A_{12}e^{-(\alpha-\pi/3)/\omega\tau_{12}}, \tag{3.14}$$

$$\rho_3 = A_{22}e^{(-\alpha)/\omega\tau_{22}}, \tag{3.15}$$

$$\mu_1 = e^{-\mu/\omega\tau_{12}},$$

$$\mu_2 = e^{-\mu/\omega\tau_{22}},$$

$$\mu_3 = e^{-\mu/\omega\tau_n},$$

$$\delta = e^{\pi/3\omega\tau_{22}},$$

$$R_{21} = 2R_n + R_d,$$

and

$$R_{32} = 3R_n + 2R_d.$$

Using these constants, equations (3.9) through (3.12) can rewritten as below.

$$0 = \rho_2 + \rho_1 + f_{a1}(\alpha-\pi/3) - \frac{E}{R_{32}}. \tag{3.16}$$

$$0 = \rho_2\mu_1 - \rho_1\mu_3 + f_{c1}(\alpha+\mu-\pi/3) - \frac{E}{R_{32}}. \tag{3.17}$$

$$\rho_2\mu_1 + \rho_1\mu_3 + f_{a1}(\alpha+\mu-\pi/3) - \frac{E}{R_{32}}$$

$$= \rho_3\mu_2\delta + f_{a2}(\alpha+\mu-\pi/3) - \frac{E}{R_{21}}. \tag{3.18}$$

$$\rho_2 - \rho_1 + f_{c1}(\alpha-\pi/3) - \frac{E}{R_{32}}$$

$$= \rho_3 + f_{a2}(\alpha) - \frac{E}{R_{21}}. \tag{3.19}$$

Substituting the value of $\rho_2 - \frac{E}{R_{32}}$ from equation (3.16) into equation (3.19), equation (3.20) is obtained. Similarly substituting the value of $\rho_2\mu_1 - \frac{E}{R_{32}}$ from equation (3.17) into the equation (3.18), equation (3.21) is obtained. Finally equation (3.22) is obtained by multiplying equation (3.20) by μ_3 and adding the result to equation (3.21).

$$f_{c1}(\alpha-\pi/3) - f_{a1}(\alpha-\pi/3) - 2\rho_1 = \rho_3 + f_{a2}(\alpha) - \frac{E}{R_{21}}. \quad (3.20)$$

$$f_{a1}(\alpha+\mu-\pi/3) - f_{c1}(\alpha+\mu-\pi/3) + 2\rho_1\mu_3 = \rho_3\mu_2\delta + f_{a2}(\alpha+\mu-\pi/3) - \frac{E}{R_{21}}. \quad (3.21)$$

$$f_{a1}(\alpha+\mu-\pi/3) - f_{c1}(\alpha+\mu-\pi/3) - f_{a2}(\alpha+\mu-\pi/3) + \mu_3[f_{c1}(\alpha-\pi/3) - f_{a1}(\alpha-\pi/3) - f_{a2}(\alpha)] + (1+\mu_3)\frac{E}{R_{21}} - \rho_3(\mu_3+\delta\mu_2) = 0. \quad (3.22)$$

Equation (3.23) is obtained by multiplying equation (3.19) by μ_1 and subtracting equation (3.17) from the result. Similarly equation (3.24) is obtained by multiplying equation (3.16) by μ_1 and subtracting the result from equation (3.19). Finally equation (3.24) is subtracted from the equation (3.23) to obtain equation (3.25)

$$\mu_3\rho_3 + \mu_1 f_{a2}(\alpha) - E\mu_1/R_{21} = \rho_1(\mu_3-\mu_1) + \mu_1 f_{c1}(\alpha-\pi/3) - f_{c1}(\alpha+\mu-\pi/3) + E(1-\mu_1)/R_{32}. \quad (3.23)$$

$$\delta\mu_2\rho_3 + f_{a2}(\alpha+\mu-\pi/3) - E/R_{21} = \rho_1(\mu_3-\mu_1) + f_{a1}(\alpha+\mu-\pi/3) - \mu_1 f_{a1}(\alpha-\pi/3) - E(1-\mu_1)/R_{32}. \quad (3.24)$$

$$\rho_3[\mu_1-\delta\mu_2] + \mu_1[f_{a2}(\alpha) - f_{c1}(\alpha-\pi/3) - f_{a1}(\alpha-\pi/3)] - f_{a2}(\alpha+\mu-\pi/3) + f_{a1}(\alpha+\mu-\pi/3) + f_{c1}(\alpha+\mu-\pi/3) + E(1-\mu_1)/R_{21} - 2E(1-\mu_1)/R_{32} = 0. \quad (3.25)$$

Variables ρ_3 and μ are the only unknown variables in equations (3.22) and (3.25). Since these equations are transcendental in nature, therefore, no closed form of solution exists. The Newton-Raphson technique was used to solve for ρ_3 and μ numerically. To simplify the notation, equations (3.22) and (3.25) are rewritten as follows:

$$F_1(\rho_3,\mu) = \rho_3(\mu_3+\delta\mu_2) + f_1(\alpha+\mu-\pi/3) + \mu_3 A - E/R_{21} = 0, \tag{3.26}$$

$$F_2(\rho_3,\mu) = \rho_3(\mu_1-\delta\mu_2) + f_2(\alpha+\mu-\pi/3) + \mu_3 B - \frac{R_n E(1-\mu_1)}{R_{32}R_{21}} = 0. \tag{3.27}$$

Where

$$f_1(\alpha+\mu-\pi/3) = f_{a2}(\alpha+\mu-\pi/3) - f_{a1}(\alpha+\mu-\pi/3) + f_{c1}(\alpha+\mu-\pi/3),$$

$$A = f_{a2}(\alpha) + f_{a1}(\alpha-\pi/3) - f_{c1}(\alpha-\pi/3) - E/R_{21},$$

$$f_2(\alpha+\mu-\pi/3) = f_{a1}(\alpha+\mu-\pi/3) + f_{c1}(\alpha+\mu-\pi/3) - f_{a2}(\alpha+\mu-\pi/3),$$

and

$$B = f_{a2}(\alpha) - f_{a1}(\alpha-\pi/3) - f_{c1}(\alpha-\pi/3).$$

Simultaneous solution of equations (3.26) and (3.27) gives the solution of ρ_3 and μ. Other constants, namely, ρ_1 and ρ_2 are computed directly from equations (3.28) and (3.29), which are obtained by algebraic manipulation of equations (3.16) through (3.19).

$$\rho_1 + \rho_2 = \frac{E}{R_{32}} - f_{a1}(\alpha-\pi/3). \tag{3.28}$$

and

$$2\rho_2 - \rho_3 = f_{a2}(\alpha) - f_{a1}(\alpha-\pi/3) - f_{c1}(\alpha-\pi/3) + \frac{2E}{R_{32}} - \frac{E}{R_{21}}. \tag{3.29}$$

Once ρ_1, ρ_2, and ρ_3 are computed, other constants A_{11}, A_{12}, and A_{22} are obtained from equations (3.13), (3.14), and (3.15). From the knowledge of constants, the current equation for line current i_a given by (3.4) can be solved to determine the current waveform. In this manner, the current in the ac line A is completely calculated.

The harmonic content of the current in line A can be determined by calculating Fourier coefficients analytically from the current function defined by the set of equations (3.4). The analytical method would result in complex expressions due to the fact that there are five distinct conduction intervals in one ac cycle. Alternative to this is to compute the harmonic components using Fast Fourier Transform(FFT) method. Samples of the line current defined by the equation (3.4) are computed at regular time interval. The sample time interval is chosen such that the Nyquist criterion is satisfied. Moreover, the number of sample data in one cycle of the ac waveform equals 2^N, where N is an integer. The calculation of sampled data points in this manner minimises any error introduced by aliasing and windowing. The sampled data is calculated from the equation (3.4) for exactly one cycle. The Fast Fourier Transform mathod is used to compute the harmonic of the sample current waveform.

3.3.2. Transformer

H.S. Osborne[15] was the first to discuss the current harmonics due to the magnetising current of the transformer. Since then this has received little or no attention because of the fact that there has been substantial over-design built into transformers. For most applications, the transformer was operated in a near linear region. These days, due to the presence of non-sinusoidal waveforms in the power system, transformers are subjected to more non-linear operation.

Mahmoud et al.[26] described a lumped circuit equivalent model of a transformer which is reported to be valid up to 40th harmonic component. The model, as shown in Figure 3.5, includes leakage reactances, magnetising reactance, and core resistance of the transformer. In this investigation, the core resistance was assumed to be constant and the magnetising core reactance was assumed to vary linearly with frequency.

Although the aforementioned model has given satisfactory results, the

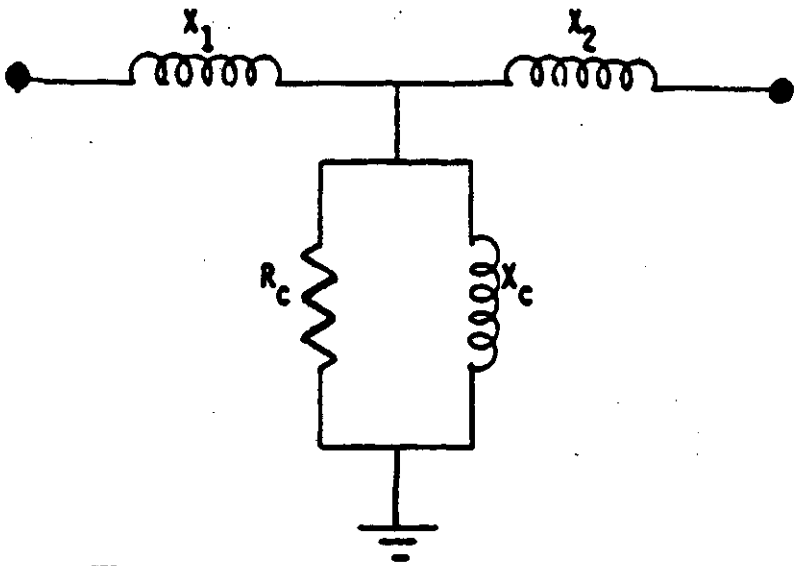

Figure 3.5: Simplified transformer model.

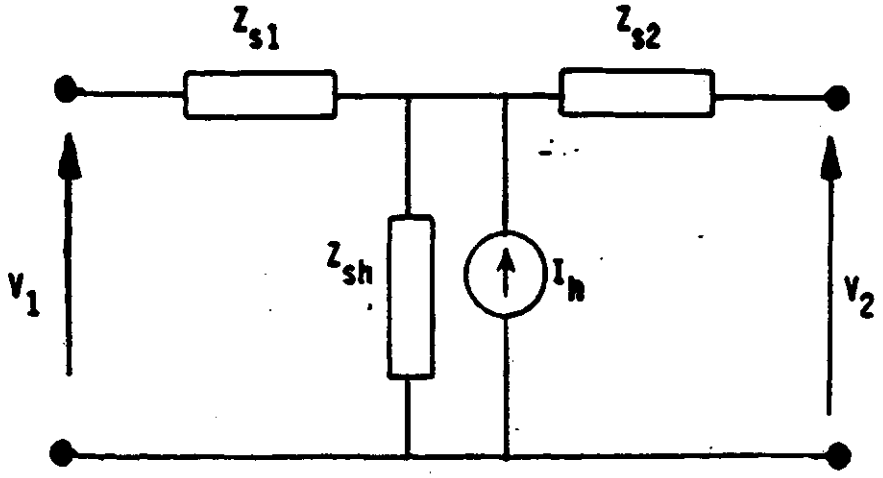

Figure 3.6: Szabados-Hill's transformer model.

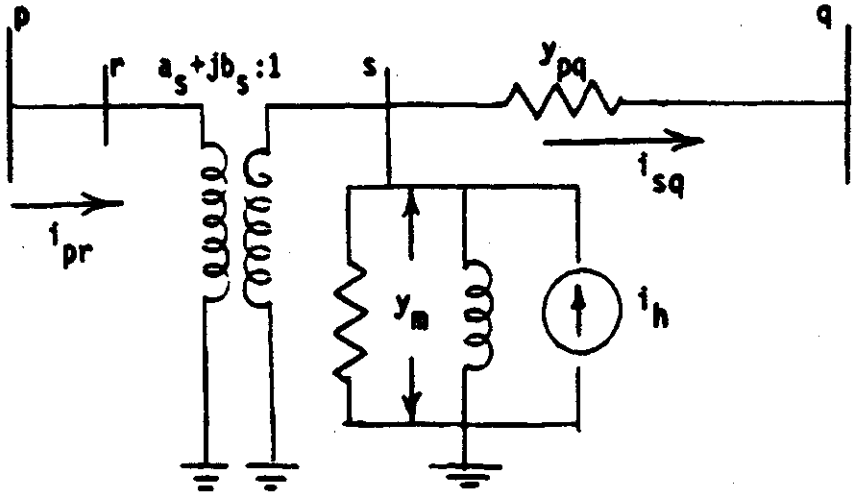

Figure 3.7: Transformer model at harmonic frequency.

model is erroneous as shown by Szabados[52] et al. Szabados experimentally showed that the core impedance does not vary linearly with the frequency. The impedance, in fact, is smaller for higher harmonic frequencies due to the saturation of the core. In the case of 3-phase transformers, the configuration also affects the saturation and as a result, it influences the harmonic impedance of the core. Nevertheless, it is shown that the linear monotonic relationship between harmonic order and the core impedance holds good up to the 9th harmonic order.

Due to the complex interactions caused by harmonic voltage excitation, there is no analytical expression to relate the core impedance and the higher harmonic order. It is best left to empirical or experimental computation of the transformer impedance. This effort is beyond the scope of this thesis but it needs further investigation.

In this study, Szabados-Hill's model[53], shown in Figure 3.6, was used for modelling of the transformer. The current source in shunt with the magnetising core represents the harmonic components of the magnetising current. Impedances are assumed to vary linearly with the frequency unless stated otherwise. With this assumption, models of Mahmoud and Szabados are similar.

The harmonic frequency currents flowing through a transformer are subjected to different phase shifts depending upon the sequence order of the frequency. Similarly the harmonic voltages suffer different phase shifts. An impedance or admittance model of a transformer should exhibit such a behaviour of the transformer at different frequencies. This is taken care of by applying the model of a phase shifting transformer[54]. The transformer model given in Figure 3.6 can be coupled with an ideal phase shifting transformer as shown in Figure 3.7. The admittance matrix Y_{bus} can be obtained in the following manner for each frequency of interest.

The ideal transformer is considered to have a complex ratio $[a_s+jb_s]:1$ (or $Ae^{j\delta_k\theta}:1$), where δ_k is 1 for positive sequence harmonic order such as 1st, 4th, 7th, 10th, -1 for the negative sequence harmonic order such as 2nd, 5th, 8th etc. and 0 for zero sequence harmonic order including all triplen harmonic components. The power is invariant through the ideal transformer and the current and the voltage experience a phase shift of $\delta_k\theta$ radians. Therefore the self admittances of nodes and mutual admittance of two nodes can be obtained from the application of Kirchhoff's Laws to the circuit shown in Figure 3.7.

$$Y_{pp} = \frac{i_{pr}}{E_p}, \quad when \quad E_p = 1 \ and \ E_q = 0$$

or

$$Y_{pp} = \frac{y_m + y_{pq}}{a_s^2 + b_s^2} \tag{3.30}$$

also,

$$Y_{qp} = \frac{-i_{sq}}{E_p}, \quad when \ E_p = 1 \ and \ E_q = 0$$

or

$$Y_{qp} = \frac{-y_{pq}}{a_s + jb_s}. \tag{3.31}$$

Similarly

$$Y_{qq} = \frac{i_{qs}}{E_q}, \quad when \ E_q = 1 \ and \ E_p = 0$$

or

$$Y_{qq} = y_{pq} \tag{3.32}$$

also

$$Y_{pq} = \frac{-i_{pr}}{E_q}, \quad when \ E_q = 1 \ and \ E_p = 0$$

or

$$Y_{pq} = \frac{-y_{pq}}{a_s - jb_s}. \tag{3.33}$$

The bus admittances of the transformer, given by equations (3.30), (3.31), (3.32), and (3.33) take care of the phase shift experienced by different frequencies. The admittances y_{pq} and y_m are updated for each frequency. The harmonics injected due to the magnetisation of the transformer are considered as current sources as shown in Figure 3.7. In order to incorporate this model of the transformer in the power system network, one virtual bus (either p or q) needs to be introduced, thus increasing the order of the system by 1 for each transformer.

3.3.3. Transmission line

The harmonic current and voltage distribution on a transmission line are dependent upon its capacitance, resistance, and inductance; the latter two are functions of frequency. The resistance of the transmission line is affected by higher frequency due to the skin effect. Direct current distributes uniformly throughout the conductor cross-section, whereas, at higher frequencies current tends to be distributed non-uniformly throughout the cross-section of the conductor. In a circular conductor the current density increases from the centre towards the surface. This gives rise to increased resistance due to the restricted area of the conduction. The increased resistance results in extra losses[55, 56].

Thus a correction needs to be applied to the resistance of the conductor at higher frequency. Stevenson[36] and Anderson[37] give a detailed analysis of the computation of the conductor resistance at higher frequency. Equation (3.34) is taken from reference 37, where ber and bei are real and imaginary Bessel functions; ber' and bei' are derivatives of real and imaginary Bessel functions, respectively. R_{dc} is dc resistance, k is the harmonic order, f is fundamental frequency, r is the radius of the conductor, and $mr = 0.0636\sqrt{\mu_r k f / R_{dc}}$, μ_r being the permeability of the media,

$$R_k = \frac{R_{dc} mr}{2} \quad \frac{ber(mr)\ bei'(mr) - bei(mr)\ ber'(mr)}{[ber'(mr)]^2 + [bei'(mr)]^2}. \tag{3.34}$$

For simplicity in computation, a look-up table approach is used to determine the resistance at a harmonic frequency. For a given mr, the value of the ratio R_k/R_{dc} is computed using Bessel function tables and then multiplied by the dc resistance to get the resistance at the frequency of interest. The change in resistance resulting from the computations is shown in Figure 3.8.

Also, it should be pointed out that in the case of stranded conductors, the skin effect is the same as in the case of solid conductors of the same cross-sectional area[57]. To keep the change of resistance due to skin effect in perspective, it should be noted that the combined effects of climate and the temperature rise due to loading of the line also alters the line resistance. In the development of the model, this has been left out, nevertheless, it is pertinent to incorporate effects of the environment.

The inductance of a transmission line is comprised of the partial self inductance of the conductor due to internal flux linkages, L_i, and the partial self inductance due to flux linkages outside the conductor, L_e. The transmission lines are composed of two or more strands electrically in parallel, called a composite conductor. The internal inductance, like resistance, is frequency dependent. Due to the skin effect the larger current density on the conductor surface reduces the internal flux linkages. This results in lower internal inductance as compared to the uniform current density case [see Figure 3.8]. Equation[36] (3.35) gives the formula for the calculation of the internal inductance of the conductor, where the variables are the same as defined in the equation (3.34).

$$L_k = \frac{4L_{dc}}{mr} \frac{ber(mr)\ ber'(mr) - bei(mr)\ bei'(mr)}{[ber'(mr)]^2 + [bei'(mr)]^2} \qquad (3.35)$$

The external inductance, L_e, is given by the equation (3.36), where s is the length of the conductor in meters, γ is the geometric mean radius, and μ_m is the permeability of the media surrounding the conductor. The total inductance, L ($=L_i + L_e$), is

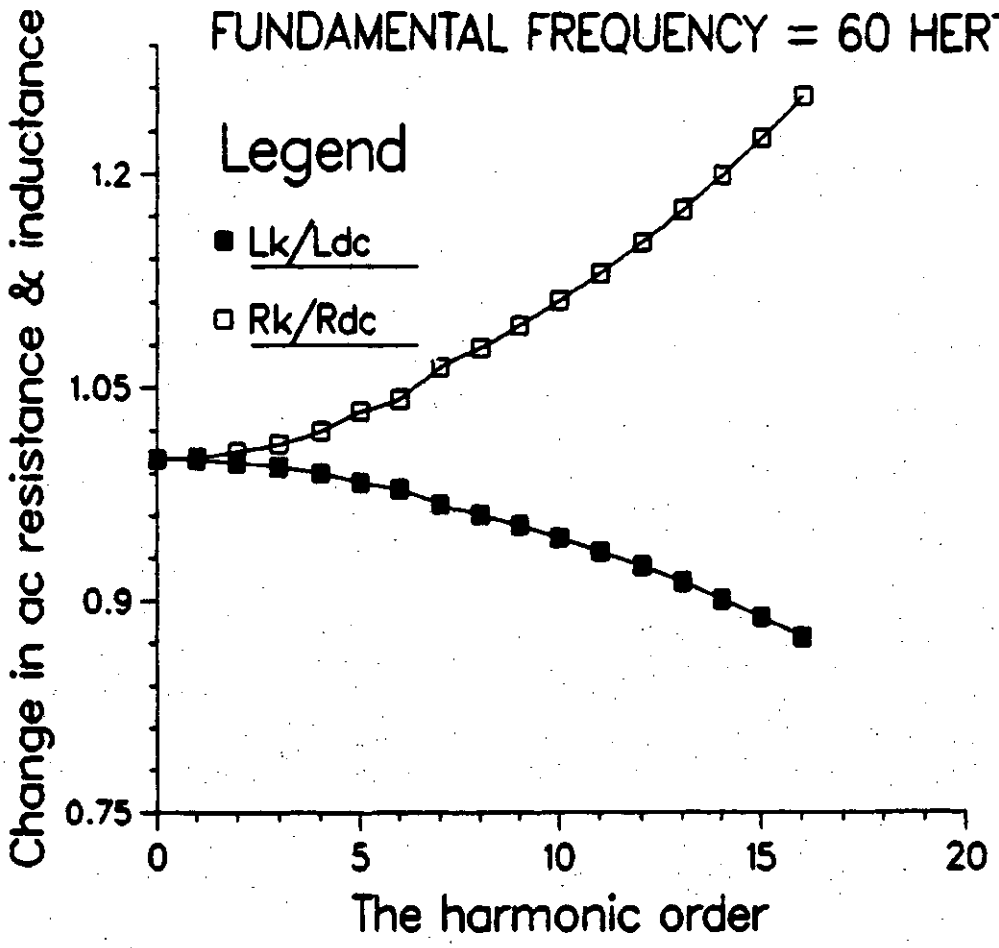

Figure 3.8: The ac resistance and inductance at harmonic frequency*.

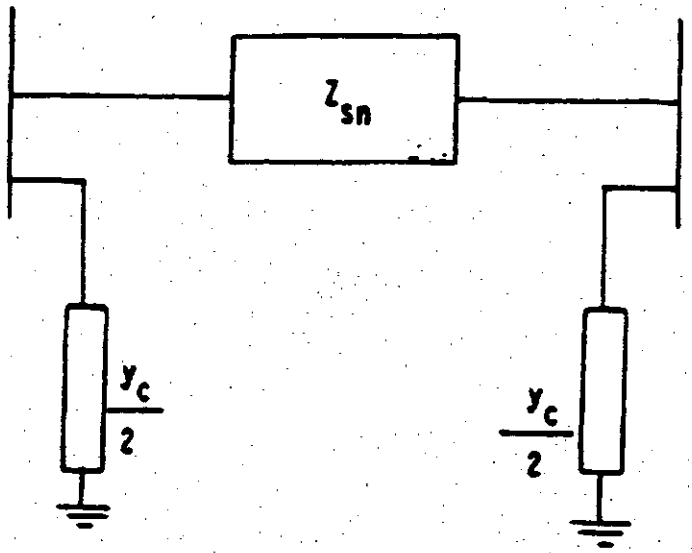

Figure 3.9: Nominal pi model.

*The relative change is shown for the conductor size whose dc resistance equals 0.47 ohms

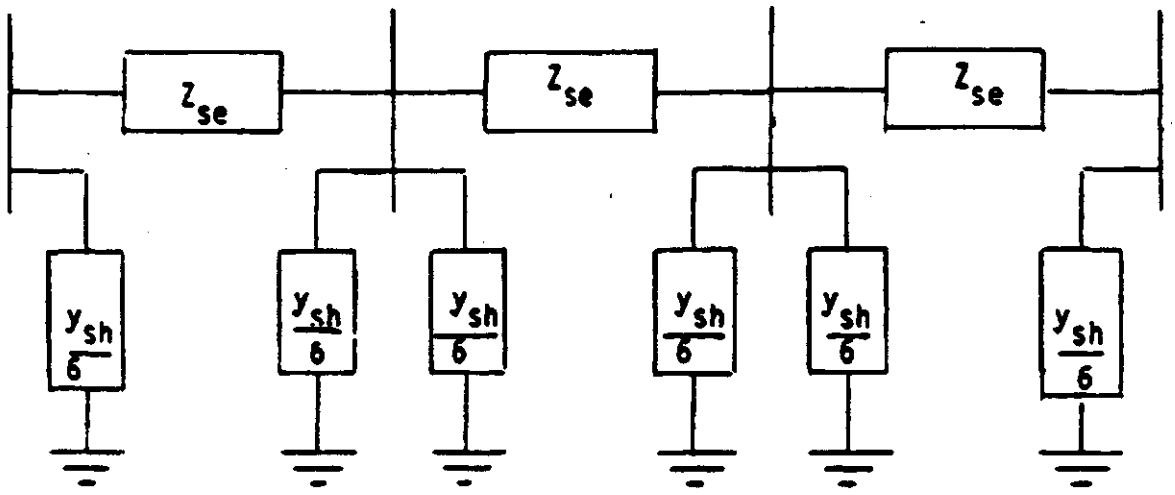

Figure 3.10: Transmission line model for 5th harmonic order.

then calculated for each phase with the assumption that either there is no neutral or it is a balanced three phase system. It is also assumed in the foregoing analysis that the lines are transposed at equidistant intervals, so that there is symmetry in the three phases.

$$L_e = \frac{\mu_m s}{2\pi}[Ln(\frac{2s}{\gamma}) - 1]. \qquad (3.36)$$

The shunt admittance of the overhead line is pure susceptance since there is negligible conduction between the wires or between wires and ground. The susceptance is purely capacitive and hence no correction need be applied to the value obtained from the table.

Once the parameters of the line are computed, the transmission line is modelled as a pi network. For harmonic analysis, the short line appears as an electrically long line at higher frequencies. The nominal pi model (Figure 3.9), commonly used to model a transmission line at power frequencies, gives reduced accuracy at harmonic frequencies. Arrillaga[47] et al. and Sharma[58] et al. proposed to use a number of nominal pi networks connected in series to model electrically long lines. However, it was shown in the references 25 and 54 that as the harmonic frequency increases, the accuracy reduces

drastically. For example by using 13 cascaded nominal pi sections for 13th harmonic calculation, there was 31% error[58] in the calculated results relative to the measured values.

The distributed nature of the transmission line, nevertheless, can be approximated by applying the correction to the nominal pi coefficients[25]. The model so obtained is called an equivalent pi model. The equivalent pi model is obtained by the solution of second order linear differential equations describing the wave propagation along the transmission lines[59]. If z is the series impedance per unit length of the line, y is the shunt admittance per unit length of the line, ρ is the propagation constant and s is the length of the line then the parameters for equivalent pi network are given by equations (3.37) and (3.38). The series impedance and shunt admittance are corrected by correction factors, which approach unity as a limit as ZY or ρs approaches zero.

$$Z_\pi = Z\frac{\sinh\sqrt{ZY}}{\sqrt{ZY}}, \tag{3.37}$$

and

$$\frac{Y_\pi}{2} = \frac{Y}{2}\,\frac{\tanh(\sqrt{ZY}/2)}{\sqrt{ZY}/2}. \tag{3.38}$$

$$\lim_{ZY\to 0} Z\,\frac{\sinh\sqrt{ZY}}{\sqrt{ZY}} = 1$$

also

$$\lim_{ZY\to 0} \frac{Y}{2}\,\frac{\tanh(\sqrt{ZY}/2)}{\sqrt{ZY}/2} = 1$$

or

$$\lim_{\rho s\to 0} Z_\pi = Z \text{ and } Y_\pi/2 = Y/2,$$

i.e.

$$\lim_{s/\lambda\to 0} Z_\pi = Z \text{ and } Y_\pi/2 = Y/2$$

or $\lambda >>> s,$

or the length of the line is much shorter than the wavelength of the signal.

The standing wave, which is characterised by fixed nodes and antinodes, can arise due to improper termination of the line at the frequency of interest. As a result, the maxima of currents and voltages are likely to occur at points other than at the receiving ends or sending ends. These local maxima could result in insulation damage, overheating or electromagnetic interference. It is thus important to calculate the maximum values of currents and voltages along the line.

One of the advantages of the cascaded nominal pi network model is that it gives an approximate profile of voltage along the line. In the case of an equivalent pi network, the information is obtained for sending and receiving ends only and one pi model is sufficient for the whole line. In order to obtain the voltage profile and still keep the accuracy of the model, it is decided to represent the transmission line by a number of cascaded equivalent pi networks. To keep the order of the system to a reasonable value, it was arbitrarily decided to create half as many cascaded equivalent pi models as the harmonic order. Therefore, there will be one equivalent pi model for 1st and 2nd harmonic order; two for 3rd and 4th harmonic order; three for 5th and 6th harmonic order and so on.

First the transmission line length is divided in the required number of the sections and then each section is represented by an equivalent pi network. For example, Figure 3.10 illustrates the representation of a 220.6 kilometre long line for analysis at the 5th harmonic order.

3.3.3.1. Discussion on transmission line model

The foregoing discussion on the model of the transmission line is valid only for the balanced condition. The balanced condition will exist particularly in the transmission system due to balanced loading and symmetrical transposition of the transmission line. However, at the high frequencies the assumption of the balanced

condition may not hold true if the length of one transposed cycle is shorter than the smallest wavelength[60] of interest. In cases where the wavelength exceeds the transposed cycle length, a more rigorous three phase model of the line based on the non-transposed line should be used. For example, if the speed of light is taken as a limiting velocity on the overhead transmission line, then frequencies up to 30 kHz can be studied if the transposed length is 10 kilometre or less. Similarly frequencies up to 15 kHz can be studied if the transposed length is 20 km or less and so on. In the event of an unbalanced condition, the three phase model of the transmission line should be used. Such a model is a coupled model. The complexity of a coupled model can be reduced by using modal analysis to decouple the set of equations. Such an investigation is left for the further research work to improve the accuracy of the transmission line model.

3.3.4. Synchronous machine

It is stated in Chapter 2 that the harmonic voltages produced by a synchronous generator are less than 3%. It can be assumed that synchronous generators do not introduce significant harmonic voltages into the power system network. Therefore, the generator can be represented passively by a shunt impedance at the generator terminal. Gardiner[61] suggested that if the resistance is neglected then the kth harmonic impedance of the machine is simply equal to k times its subtransient reactance value. This is due to the fact that when harmonic currents flow into the stator winding of the machines, they create a rotating flux at a speed greater than the synchronous speed (or speed of the rotor flux). This non-synchronous stator mmf produces rotor currents identical to those caused by the application of the negative sequence signals to the stator. Therefore, a synchronous generator can be represented by the negative sequence impedance for harmonic frequency analysis.

The negative sequence impedance[37] of a synchronous machine can be

easily obtained from equation (3.39), where L_d'' and L_q'' are subtransient inductances of direct and quadrature axes respectively. Arsneau and Szabados[62] showed through the measurement of parameters of a 3 kVA synchronous machine at harmonic frequencies that the results obtained from equation (3.39) agree closely with those of measured ones. An experimental test was also carried out on a 5 kVA synchronous machine by this author in the laboratory. The impedance of a 3-phase, 60 Hz. synchronous machine was measured by exciting it with a pure 3rd and 5th harmonic signals at one time. The resulting impedances were compared with those obtained through Gardiner's method. Table 3-1 gives the measured and calculated values. Clearly, the disagreement between two quantities is small. A maximum disagreement of 7.6% exists at the second harmonic frequency.

$$L_N = \frac{L_d'' + L_q''}{2} \tag{3.39}$$

Gardiner's model is used to represent the synchronous machine. The negative sequence inductance is multiplied by the harmonic frequency to obtain the equivalent reactive impedance. The calculation of the subtransient inductance is conveniently available and can be measured. The method of measuring subtransient inductance is given in the IEEE Standard Procedures[63], section 8.7.

Table 3-1: Harmonic impedances of a 5 kVA synchronous machine.

Negative Sequence Impedance = 1.51 Ohms			
Frequency Hertz	Applying a Pure Harmonic Frequency Signal X Ohms	Harmonic Multiple of Negative Sequence Impedance X Ohms	Percent Error
120	3.27	3.02	7.6
180	4.52	4.53	0.22
240	5.87	6.04	2.89
300	7.30	7.55	3.42

3.3.5. Load model

When carrying out harmonic penetration studies on a transmission system, it becomes very cumbersome to represent the system from generators right through to individual consumer loads. At some point down the network, the elements are aggregated into equivalent load centres. Utilities use equivalent load centres (or circuits) at the points of supply to represent the distributed load[35]. The distribution authorities then deliver power to individual consumers within a load centre.

These load centres are represented in terms of real power(P) and reactive power(Q) for load flow analysis at fundamental frequencies. However, an accurate model of the system load for harmonic analysis is difficult to determine, because the frequency-dependent characteristics are usually unknown and the load itself is changing continuously.

The most common load model used extensively is shown in Figure 3.11 where V is the nominal voltage, k is the harmonic order, and P_f, Q_f are real power and reactive power respectively at the fundamental frequency. This model was first suggested by Pesonen[64] et al. and has further been reported to give satisfactory results by Pillegi[35] et al. and McGranaghan[65] et al.

Industrial loads are comprised mainly of induction motors running in parallel. These motors can be bunched together into an equivalent single machine for fundamental frequencies[66]. Therefore, a single equivalent T-circuit can be used to represent the induction motor load at fundamental frequency as shown in Figure 3.12(a), where the windage, frictional and core losses are already subtracted from the fundamental real power. The following reasonable assumptions are made in order to simplify the calculations of the parameters of the induction motor for the harmonic analysis.

1. The reflected rotor resistance is small at harmonic frequencies, because the slip is large as given by the equation (3.40), where s is the slip at fundamental

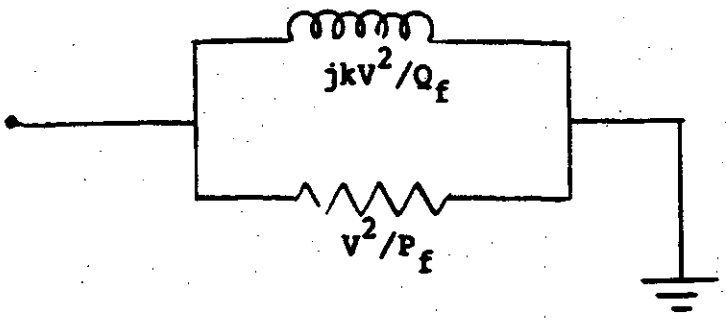

Figure 3.11: Load model for distributed load.

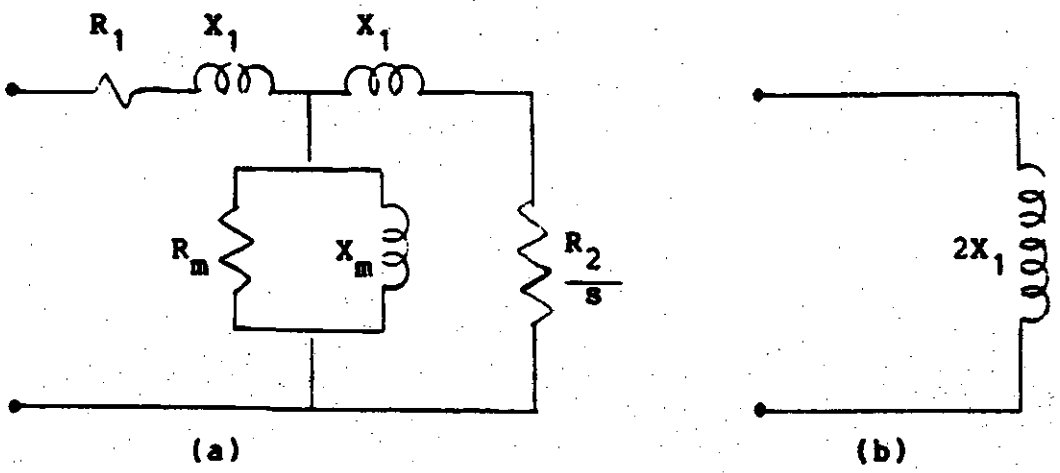

Figure 3.12: Equivalent circuit of the induction motor.

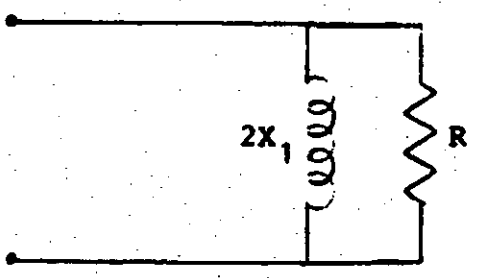

Figure 3.13: Final load model.

frequency, s_h is the slip at harmonic frequency, k is the harmonic order, n_s, and n_r are synchronous and rotor speeds respectively.

$$s_h = (kn_s - n_r)/n_s = k - 1 + s. \quad (3.40)$$

2. The magnetisation inductance can be neglected, since it is quite large compared to the rotor leakage inductance.

3. The rotor and stator leakage inductances are assumed to be equal as recommended by the IEEE Test Procedure[63].

4. The resistance of the stator windings is neglected for the analysis at higher frequency. Because the leakage reactive impedance at harmonic frequency is several times larger than the resistance.

5. The magnetising current is assumed to be 30% of the total input current. Usually the magnetising current is 30%-50% of the rated current because of the air gap. A lower limit is assumed.

For harmonic distribution studies, the representation of the induction motor can be reduced to the circuit shown in Figure 3.12(b), which is the leakage reactance of the stator and rotor windings. Murotani[67] has reported the use of a similar model where the leakage reactance was obtained empirically by taking 30% of the rating of the machine. More accurate calculation of the leakage reactance is obtained as follows.

If Q_l, P_l, V, and I are the reactive power, real power, terminal voltage and the total motor current respectively at fundamental frequency*, then from Figure 3.12(a) the following equation is obtained.

$$S_l = P_l^2 + Q_l^2 = 3V^2I^2,$$

Ignoring the current in the resistive branch of the core, the reactive power per phase of the motor is given by the equation (3.41).

*It is assumed that the constant core losses, friction and windage losses have been already subtracted.

$$\frac{Q_l}{3} = 1.49I^2X_1 + 0.09I^2X_m \tag{3.41}$$

The magnetising reactance is assumed to be approximately 35 times the leakage reactance, i.e. $X_m = 35X_1$. Substituting this in equation (3.41),

$$\frac{Q_l}{3} = 1.49I^2X_1 + 0.09I^2 35X_1$$

or

$$\frac{Q_l}{3} = 4.64I^2X_1$$

since

$$I^2 = \frac{P_l^2 + Q_l^2}{3V^2}$$

therefore,

$$\frac{Q_l}{3} = 4.64X_1\frac{P_l^2 + Q_l^2}{3V^2}$$

or

$$X_1 = \frac{Q_l V^2}{4.64(P_l^2 + Q_l^2)} \tag{3.42}$$

The fundamental frequency reactance can be easily calculated, since S_l, P_l, and Q_l are usually given. The leakage reactance given by equation (3.42) is for the fundamental frequency. The result of the above analysis is an approximate one, nevertheless, this model of the induction motor has proven to be quite satisfactory.

The consumer load is comprised mainly of induction motor type loads. An accurate consumer load model for harmonic analysis can be obtained by adding the resistive branch to the induction motor load model as shown in Figure 3.12(b). The resistance accounts for the real power which is assumed to be fixed. The final load model is shown in Figure 3.13 where X_1 is the 60 Hz reactance obtained from equation (3.42).

3.3.6. Other power system elements

Filters, capacitor banks, and inductors are assumed to be passive elements with constant values. The reactive impedance of such elements is linearly corrected for the frequency of interest. The static VAR compensator used for dynamic control of bus voltage and power factor is finding extensive application in the power system network. Although it can be treated as a filter, it produces appreciable current harmonics[68] in the system. In this study, the model of the static VAR compensator is assumed to be a filter with a shunt harmonic current source as shown in Figure 3.14. The harmonic generation, if given, can be included in the program. The proposed model necessitates the prior knowledge of harmonic current of the static compensator.

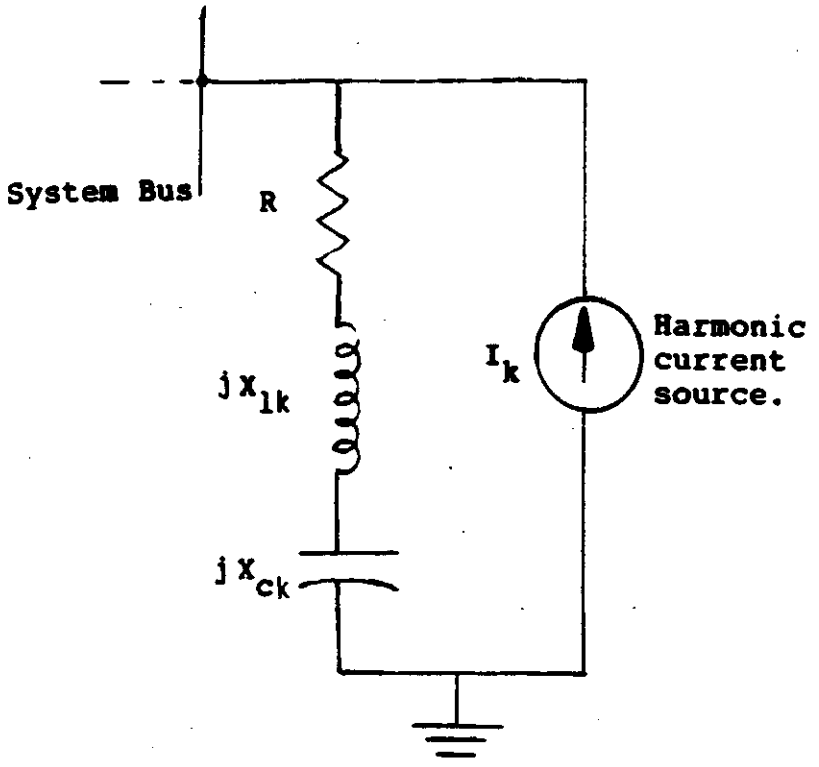

Figure 3.14: Static VAR compensator model.

3.3.7. Discussion

In the foregoing subsections, models of converter, transmission line, transformer, and load are described. The modelling of the converter is carried out by taking into account the dc current ripples and the characteristics of the dc load. The model also takes care of the interaction with the harmonic bus voltages in an iterative process. The computation of commutation angle is slightly complicated and has no closed form of solution due to the transcendental nature of equations. However, if the resistance of the transformer is ignored, some simplification of the results can be obtained. Simple analysis for the case when resistance of the converter transformer is ignored is discussed by Heydt[34] et al. Similar results can also be obtained from the aforementioned analysis presented herein by substituting zero for the resistance of the converter transformer.

The transmission line model is based on the equivalent pi representation. A cascaded number of equivalent pi networks are used to give the harmonic voltage profile on the transmission line. This helps in identifying the point of maximum stress in the transmission line. However, it must be emphasised that single line representation described in this report is valid only under the balanced condition.

Models for transformers and loads are valid only under the assumptions given in the respective subsections. The transformer model is based on the principle of the phase shifting transformer. This takes care of the different phase shifts experienced by different harmonic signals in case of three phase transformers. The load models are based on the aggregated power demands at a node in the transmission system. These models are approximate representations of loads, nevertheless, have been reported to give satisfactory results.

3.4. Algorithm

The methodology used in the harmonic flow algorithm is based upon the nodal equation formulation. The power system transmission network is considered as a network of admittances appropriate for the specific frequency of concern and harmonic current injections serve as sources of the excitation of the network. The system matrix equation describing this condition is given in the equation (3.43).

$$[V]\ [Y_{bus}] = [I], \tag{3.43}$$

where,

$$[V] = [V_1, V_2, V_3, \ldots V_n]^T,$$

$$[I] = [I_1, I_2, I_3, \ldots I_n]^T, \quad \textit{and}$$

$$[Y_{bus}] = \begin{vmatrix} y_{11} & y_{12} \ldots\ldots y_{1n} \\ y_{21} & y_{22} \ldots\ldots y_{2n} \\ y_{31} & y_{32} \ldots\ldots y_{3n} \\ \cdot\cdot & \ldots\ldots\ldots \\ \cdot & \ldots\ldots\ldots \\ \cdot & \ldots\ldots\ldots \\ y_{n1} & y_{n2} \ldots\ldots y_{nn} \end{vmatrix}.$$

The $[Y_{bus}]$ matrix is obtained directly by the given interconnection of the transmission network. Since the admittance of the power system network changes with the harmonic frequency, it is necessary to formulate the admittance matrix for each harmonic frequency. Vectors [V] and [I] are the harmonic voltage and current vectors respectively. The excitation current vector [I] is calculated for the line commutated converter system from the previous condition of the power system. The algorithm is designed for the line commutated converter. Other harmonic producing devices like transformers and static VAR compensators are not included. The harmonics injected from these devices are assumed to be known beforehand. It is assumed that the harmonic current values of these devices can be reasonably estimated and are not dependent on the voltage spectrum of the transmission system.

The equation (3.43) is then solved at each harmonic frequency to yield information about the harmonic voltages at the system buses. Initially the harmonic voltages at the converter bus are assumed to be small. The solution of the equation (3.43) gives new estimate of the harmonic voltages at all the system buses. The new estimate of the harmonic voltages is used to compute the new operating point of the converter. In this manner the calculation of the harmonic voltages at system buses is done iteratively until the mismatch in bus voltages of two consecutive steps is minimum. In each iteration of calculation, the converter equations are solved and the harmonic spectrum of the line current is computed. A complete structure of the algorithm is given in Figure 3.15. A computer program was written to execute the algorithm shown in Figure 3.15.

If N is the order of harmonics and M is the number of buses in the system, and N_v is the number of virtual buses included in the system, then the order of the equation (3.43) is $(M+N_v)x(M+N_v)$. Due to the symmetry and nature of interconnections of the power system, the system equations (3.43) are usually symmetric and sparse. The sparsity is further increased due to the addition of virtual buses. These properties, namely sparsity and symmetry, are exploited in the development of the computer program. The advantages of sparse methodologies are seen in the optimum use of memory allocation and the time of computation. The recent developments in heuristic algorithms pertaining to the sparse techniques have furthered the impact of such methods on the time of computation. This topic of sparse techniques and dynamic data structures is fully discussed in Chapter 4.

3.5. Single Frequency Behaviour

As mentioned in the last section, each harmonic frequency is dealt with independently. This is due to the fact that any cyclical repetitive waveform can be represented by a Fourier series comprised of the fundamental frequency plus integer

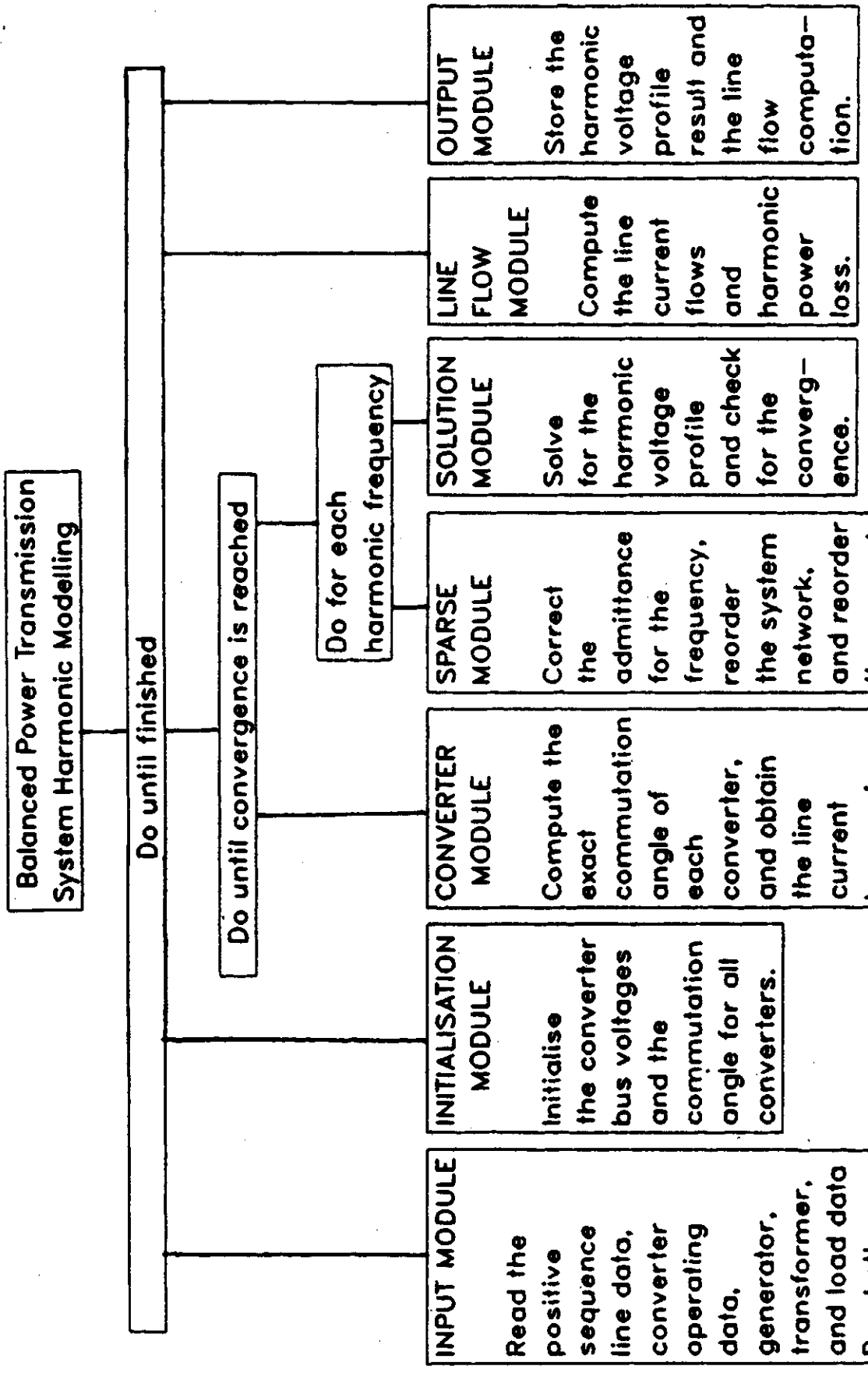

Figure 3.15: Algorithm structure for harmonic analysis of a balanced power transmission system.

multiples of the fundamental frequency**. If the system is a linear system such that the superposition theorem is applicable, each harmonic frequency can be considered separately. In the given problem, the converter load is a non-linear load. It is non-linear in the sense that it distorts the sinusoidal excitation.

Nevertheless, for a given value of firing angle α, the superposition theorem is equally applicable for the converter load. The converter with a fixed firing angle is like a device with fixed delay and as long as the delay is constant (time invariant), the superposition theorem is applicable. Therefore, with the assumption of constant firing angle of the converter, each frequency can be dealt with independently.

A transformer is also a non-linear device and the treatment of each frequency independently is not justifiable. But the emphasis of this thesis is more on lower order harmonics, and for that purpose the magnetising core of the transformer is considered constant and independent of the frequency. Under this assumption, the theorem of superposition is applicable.

The static VAR compensators can be considered similar to converters. They are dynamic in nature and the firing angles will be changing continuously. With the assumption of operation at a given firing angle (usually one at which the worst harmonic current will be required), the superposition theorem is applicable and the frequencies can be dealt with independently based upon Fourier transformation principles.

**The dc component is assumed to be zero because of the balanced and symmetric conditions of the power system.

3.6. Conclusion

In this chapter, the modelling of elements of power system network is carried out. The detailed analysis of the line commutated converter is presented and the exact computation of the finite commutation delay is obtained by taking into account the effect of harmonic voltage at the converter bus and the converter transformer paramters. The converter transformer is modelled exactly by including the leakage reactance and the winding resistance in the computation of the commutation overlap angle. Newton-Raphson method of numerical computation is employed for the solution of the transcendental equations of the converter. The transformer model presented in this chapter takes care of the phase shift experienced by different harmonic components. The voltage profile calculations on a transmission line are obtained by considering a cascaded network of equivalent pi's. Approximate models of the load and synchronous generators are also discussed.

A complete algorithm based upon the non-linear frequency domain analysis is discussed and justification of various assumptions made is included. The iterative approach is suggested to compute the harmonic voltages by employing the mismatch of harmonic voltages at all the buses of the power system.

4. IMPLEMENTATION OF THE HARMONIC POWER FLOW ALGORITHM

4.1. Introduction

In this chapter, the practical implementation of the harmonic power flow algorithm is given. Definitions of the power and the energy flow in a power system with a fundamental and harmonic frequencies are given. Modifications in the algorithm are presented to reflect the modified definition of the power and the energy in a non-linear system. A two bus example is used to illustrate the step by step calculation of the proposed algorithm. Also included in this chapter is a brief description of the sparse methods of representing network equations. The non-linear dynamic data structure is described for the implementation. This data structure is specially proposed here for harmonic analysis in power systems when the number of nodes may vary with the order of the harmonics. The use of a minimum degree algorithm in solving a set of simultaneous network equations and optimisation of the algorithm using elimination graph theory as proposed by George and Liu[7] are briefly discussed.

4.2. Definition of Energy in a Polluted Power System

In a single frequency electric power system, the apparent power S is given by $\sqrt{P^2+Q^2}$, where P is given by $EI\cos(\phi)$ and Q is given by $EI\sin(\phi)$. In a system where several frequency signals co-exist, the above definitions are not adequate as shown by Heydt[32] and Shepherd[38]. The new definitions of apparent and non-active power to handle power flow in systems where harmonic frequencies co-exist are given in this section.

Consider a power system where the voltage and the current in the system are given by equations (4.1) and (4.2). The average power P comprises the sum of powers due to all frequencies as given by the equation (4.3). The apparent power, S, defined as the

product of the total rms voltage and total rms current, is given by the equation (4.4)[69]. Equation (4.4) includes products of similar frequencies and cross products of unlike frequencies. The non-active power $\sqrt{S^2-P^2}$ includes two parts: the conventional reactive volt ampere, Q; and distortion volt amperes, D_r[70], which is also reactive in nature from the point of view of the fundamental frequency. Thus the apparent power can be broken into its parts as shown by equation (4.5).

$$e = \sqrt{2}\sum_{k=1}^{n} E_k sin(k\omega t+\alpha_k). \tag{4.1}$$

$$i = \sqrt{2}\sum_{k=1}^{n} I_k sin(k\omega t+\alpha_k-\phi_k). \tag{4.2}$$

$$P = \sum_{k=1}^{n} E_k I_k Cos(\phi_k). \tag{4.3}$$

$$S^2 = \sum_{k=1}^{n} E_k^2 \sum_{j=1}^{n} I_j^2. \tag{4.4}$$

$$S^2 = P^2 + Q^2 + D_r^2. \tag{4.5}$$

Heydt[32] suggests the use of the conventional reactive volt amperes definition given by $Q = \sum_{k=1}^{n} E_k I_k sin(\phi_k)$ in order to determine the distortion volt ampere by employing the formula $D_r^2 = S^2 - P^2 - Q^2$. As described earlier, at a non-linear node the reactive volt-amperes includes products of like frequencies and unlike frequencies. Although Heydt's definition can be used to arrive at a mathematical solution, such a definition of reactive volt-amperes can not be used to compute the value of the shunt connected compensating capacitance for the purpose of making unity power factor as shown by Shepherd[69] and others[69]. In essence it is difficult to separate the conventional reactive and distortion reactive power. In the analysis presented herein, the reactive and distortion volt-amperes are combined in one term referred to as non-active volt-amperes and denoted by QD. This is consistent with the argument, since the single frequency source must provide the net volt-amperes required by the nonlinear load. Also the separation of the reactive and distortion volt-amperes will not lead to any worthwhile results from the point of view of this thesis.

4.3. Modifications of the Algorithm

A source of single frequency can supply energy at the fundamental frequency only. As mentioned in Chapter 2, it is the harmonic generating load that converts some of the fundamental frequency power into harmonic frequency power. Figure 2.15 is re-drawn here in Figure 4.1 to illustrate the concept. The energy S_1 including P_1 and QD_1 is supplied to the converter load, the converter converts a part of that energy into the harmonic energy. The portion of the energy converted into harmonic power by the converter depends, among other factors, upon the ac terminal voltage. In other words, there is strong interaction between the power system and the converter operation[71].

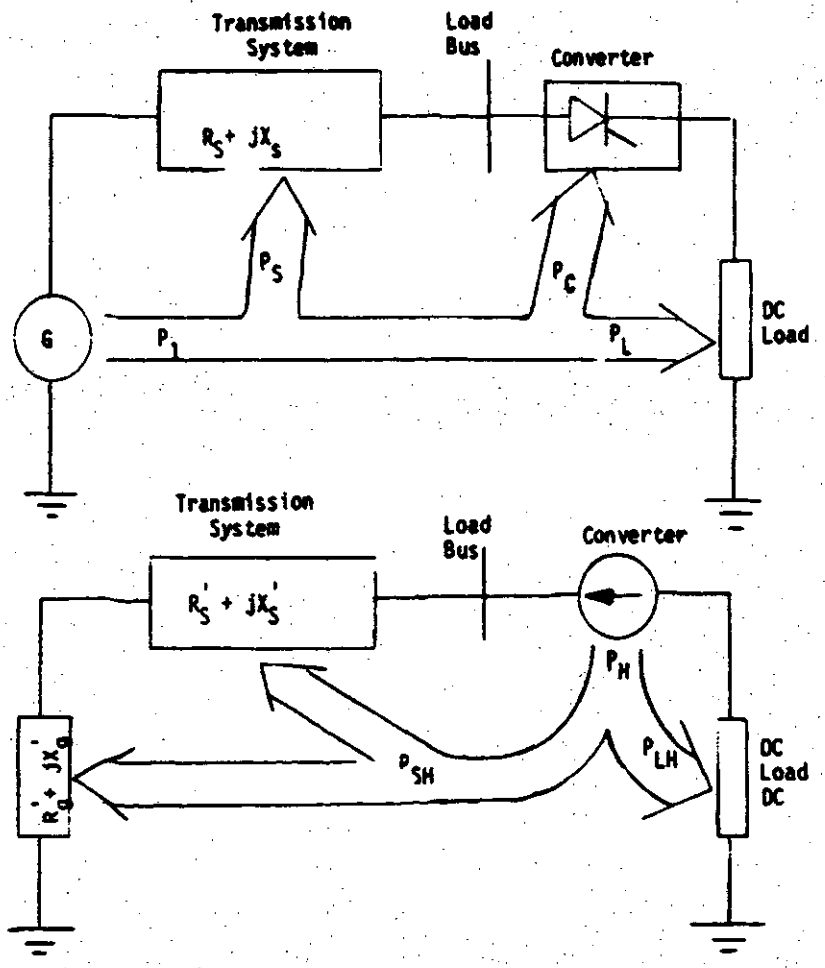

Figure 4.1: Harmonic energy flow.

Given a converter operating at a certain firing angle, power dissipated in the dc load may be known, but the apparent ac power supplied to the converter node by the electrical system can not be known until the harmonic power flow in the electrical system is determined; therefore, it is essential to carry out the fundamental frequency load flow calculations following the harmonic power flow computation each time. This process must be iterated to study the interaction of the converter and the power system. The iterations are stopped when the calculated power (both active and non-active) converges to a constant value.

Figure 4.2 gives an overall algorithm for the harmonic power flow calculation of an ac power system including the modification described above. Initially, the load flow studies are carried out at the fundamental frequency using the Newton Raphson method. Following this, the harmonic network solution is achieved in an iterative manner to determine the harmonic voltage profile of the power system. The net power at the converter node, given by the equations (4.3) and (4.4), is computed. The whole process is reiterated again as shown by the outer loop in Figure 4.2. Exit from the outer loop in the algorithm occurs when the steady state value of the net volt-ampere at the converter node is obtained.

In this manner, an interaction of the performance of the converter and the power system is obtained. The value of the commutation angle and the harmonic spectrum of the line current of the converter are exact values without any ideal assumptions regarding the converter or the power system.

4.4. Two Bus Example

A two bus example is considered to illustrate the steps of execution of the algorithm. This example is taken from the literature[32, 34].

Consider the two bus system shown in the Figure 4.3, where a single

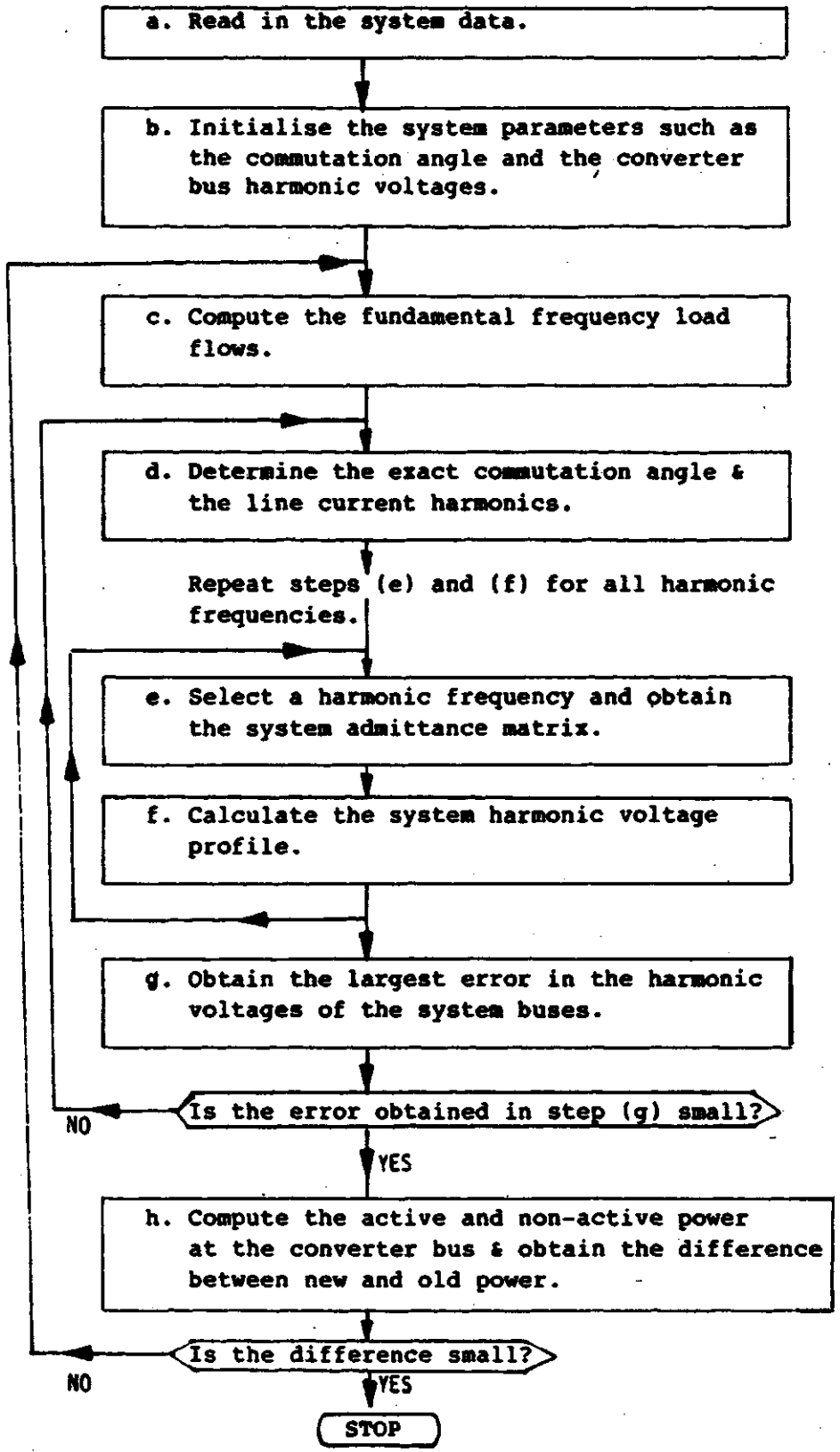

Figure 4.2: Modified algorithm for harmonic power flow.

frequency generator is supplying energy to a converter node through a transmission line. The transmission line is 20 miles long and the relevant data for the system is given in the Table 4-1. The objective is to determine the harmonic voltage profile on the transmission line and the net power delivered to the converter load at the fundamental frequency.

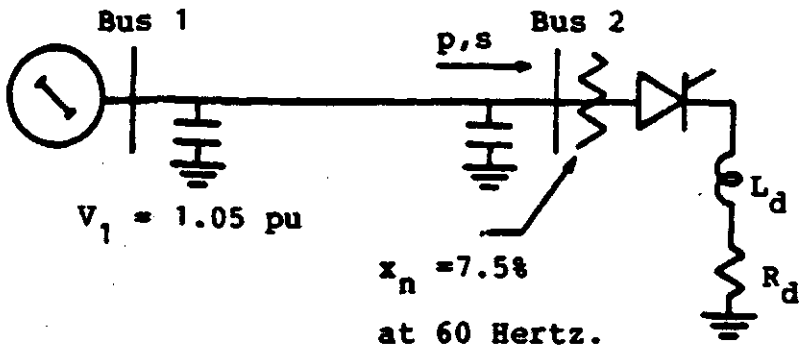

Figure 4.3: Two bus system.

1. Step 1: The load flow study is first performed to determine the fundamental voltage at the converter bus(es). For the first iteration, the real power at the converter node is initialised to the specified power of the dc load. The non-active (reactive) power is initialised by assuming that the converter is an ideal one, i.e. QD = P*tan(α). Using these values of P and QD at the converter node, the fundamental frequency load flow is computed.

2. Step 2: The fundamental frequency voltage at the converter node is obtained from step 1. The next step is to compute the commutation angle and the harmonic spectrum of the line current of the converter. During the first time execution of the Step 2 the harmonic voltages at the converter node are initialised to small values of 0.01 per unit with zero phase[34, 58]. In the subsequent iteration, the actual harmonic voltages at the converter node are used. Also, the commutation angle is initially assumed to be zero. The converter algorithm is based on the mathematical analysis presented in Chapter 3.

3. Step 3: After a steady state solution of the commutation angle is obtained in Step 2, the line current waveform of the converter is computed using equations

Table 4-1: Parameters of two bus example.

Base Values
S_base = 6.25 MVA, V_base = 25 kV,
I_base = 144.34 Amperes, and Z_base = 100 Ω.
Transmission Line Data
r = 0.385 Ω/mile, x_l = 0.55 Ω/mile,
$x_c = 0.1281*10^6$ Ω-mile, and length = 20 miles.
Generator Data
Terminal Voltage = 1.05+j0 per unit,
Z_n = negative sequence impedance at 60 Hz. = 0.0 + j0.0001 per unit.
Transformer Data
Leakage reactance = 0.075 per unit, Ratio = $1:1e^{-j\delta_k 30°}$.
The mutual reactance is neglected since it is a power transformer.
Converter Data
Six-pulse fully controlled rectifier,
delay angle α = 21.0°, R_{DC} = 300 Ω, and
L_{DC} = 1.202 Henries.

given in Chapter 3. From the digitised line current, an FFT software package is used to compute the harmonic spectrum of the line current.

4. Step 4: Choosing one harmonic frequency at a time, the transmission network is modelled as an admittance network and the voltage profile on the transmission line is computed. This is repeated for all harmonic frequencies whose current injection is larger than 1% of the fundamental frequency current.

5. Step 5: Using the new harmonic voltages at the converter node, steps 2, 3, and 4 are repeated until the maximum change in the harmonic voltage at any bus (node) in the power system between successive iterations is very small(10^{-5}).

6. Step 6: The power demand at the converter node, including the harmonic power, is computed using equations (4.3), (4.4), and (4.5). The total real power P and total non-active power QD (both reactive and distortion) is used as the net new power demand at the converter node for the purpose of the load flow studies at the fundamental frequency.

7. Step 7: Steps 1 through 6 are repeated with the new operating point until the computed changes in power demand at the converter node between successive iterations is very small(10^{-4}).

Table 4-2: Simulated test results for two bus example.

Trial No	Fundamental* Load Flow	Converter Computation	Harmonic Power Computation at the Converter Node
1	P = 0.40 Q = 0.20 V_2 = 0.9827 θ_2 = -1.85	Harmonic Current Vector computed	P = 0.4859 QD = 0.26650
2	P = 0.4859 Q = 0.2665 V_2 = 0.9823 θ_2 = -1.86	Harmonic Current Vector computed	P = 0.4855 QD = 0.26633
3	P = 0.4855 Q = 0.2633 V_2 = 0.9824 θ = -1.859	Harmonic Current Vector computed	P = 0.4856 QD = 0.26635
4	P = 0.4856 Q = 0.26635 V_2 = 0.9824 θ_2 = -1.86	Harmonic Current Vector computed	P = 0.4856 QD = 0.26635
5	P = 0.4856 Q = 0.27735 V_2 = 0.9824 θ_2 = -1.86	Harmonic Current Vector computed	P = 0.4856 QD = 0.26635

* Fundamental frequency voltage at bus 2

For the two bus example, Table 4-2 gives the results of iterations. Input and output information of each iteration (trial) is shown in Table 4-2. For simplicity, results of steps 2, 3, 4, 5, and 6 are grouped together, since the final objective is to obtain the voltage profile and the power deamand at the converter node.

Figure 4.4 illustrates the change in active and non-active power (the

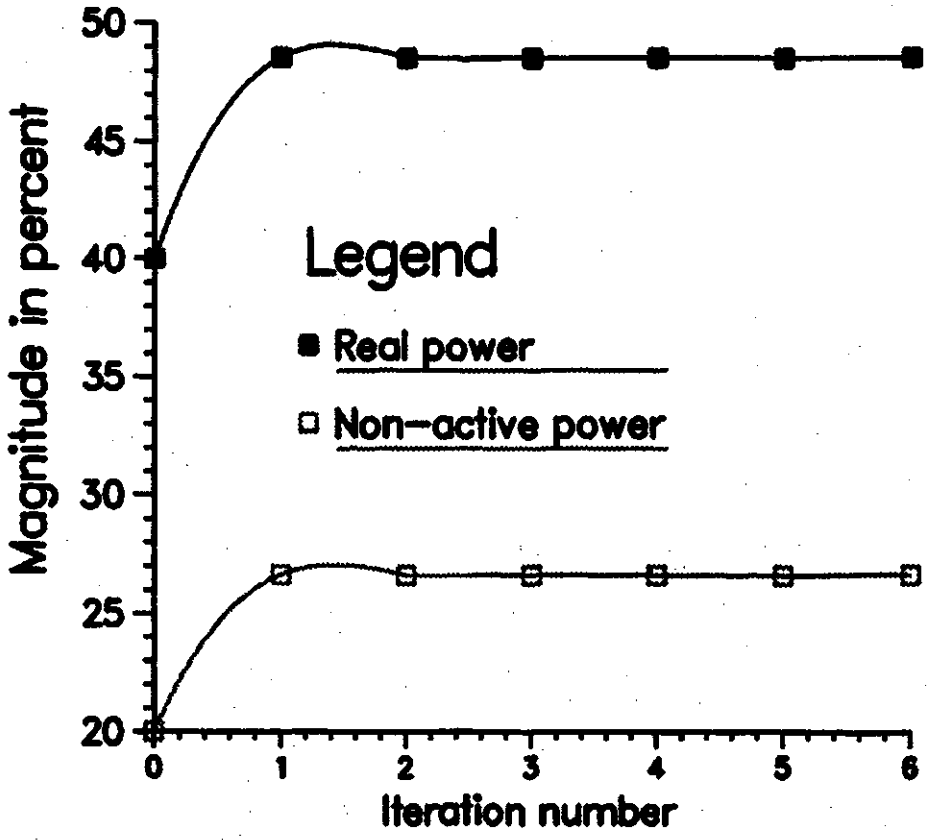

Figure 4.4: Change in power demand at the converter node versus iteration number.

reactive and the distortion power) versus the iteration number. The convergence of the program is achieved when the change in power demand at the converter node reaches its steady state value as shown in Figure 4.4.

4.5. Sparse Matrix Application

The methodology used in the harmonic flow algorithm is based upon the nodal equation formulation as given by equation (4.6). The power system transmission network is considered as a balanced network of admittances, appropriate for a specific frequency of concern. The harmonic current injection serves as the excitation source of the network(Step 4). In equation (4.6), [Y] represent the system admittance matrix, [I] represent the current injection vector, and [V] represent the bus voltage vector. For a balanced power system, the admittance matrix is symmetric and quite sparse. The sparsity is further increased due to the introduction of the virtual nodes in the power system for purpose of harmonic analysis.

$$[I] = [Y][V]. \tag{4.6}$$

In order to optimise the storage and number of operations in solving such a sparse system of equations, it is important to exploit the sparsity of the system[72]. Further optimisation can be achieved by using Cholesky's method of solution of system equations given by (4.6). Cholesky's algorithm employs lower triangular and upper triangular factorisation of the matrix [Y]. Such a factorisation results in two sets of equations given by (4.7) and (4.8).

$[Y][V] = [I]$, *factoring* $[Y]$,

$[Y] = [L][U]$,

therefore the system equations are

$[L][U][V] = [I]$ *or*

$$[L][x] = [I], \tag{4.7}$$

and

$$[U][V] = [x]. \tag{4.8}$$

Since the power system admittance matrix is a symmetric matrix, therefore $[L] = [U]^T[D]$, where [D] is a diagonal matrix. Thus the system equation [Y][V] = [I] can be written as $[U]^T[D][U][V] = [I]$. Then [V] is obtained by solving two sets of equations $[U]^T[D][x] = [I]$ and $[U][V] = [x]$.

Sato and Tinney[8] presented an algorithm which is based upon the above method. The algorithm is as given by the equation (4.9), where [U] is the factored upper triangular matrix of a square and symmetric matrix [A], U_{ij} is the negative of the element in i^{th} row and j^{th} column of [U] and D_{ii} is the reciprocal of the i^{th} pivot element in the factoring process. If [b] is the excitation vector, then the algebraic operation $U_{ij}([b])$ is defined as below.

Theorem 1: $U_{ij}([b])$ is an operation whereby one multiplies the j^{th} element of the vector [b] by U_{ij} and adds the product to the i^{th} element of the vector [b] to obtain the new i^{th} element of the solution vector [x]

$$[x] = (U_{12}(U_{13}(\ldots(U_{n-1,n}(D_{nn}(\ldots(D_{11} (U_{n,n-1}(\ldots(U_{31}(U_{21}([b])))\ldots)))\ldots)))\ldots))). \quad (4.9)$$

Tinney's algorithm is same as the Cholesky's method and both these methods require that the system admittance matrix be factored. If a sparse matrix is factored it suffers fill[7], i.e. the factored matrices may have more nonzero elements than the original matrix. This will result in an increased memory storage requirement and more number of steps of computations. This situation can be avoided if the system is carefully reordered. Much of the effort of exploiting the sparsity of the system is spent in finding the optimum order***.

The most commonly used algorithm for finding low-fill ordering is the so called minimum degree algorithm. This is a symmetric variant of the strategy proposed by Markowitz[74]. During the Gaussian elimination process in factoring of [Y], the rows and columns are interchanged at the beginning of each elimination step so that the pivot row and column have a minimum number of nonzero elements. In this manner the rows with minimum degree (minimum number of nonzero elements) are first used as the pivot rows. This algorithm has been reported to have given the best possible results[7, 73, 75, 76].

4.5.1. Limitations of minimum degree algorithm

There are two main disadvantages of the minimum degree algorithm. Firstly there is a likelihood of ties between two or more rows with the same degree. Secondly, the number of new fills created are not predictable beforehand; the partial elimination is required before determining new pivot row and column. Therefore the storage requirements of the algorithm cannot be predicted explicitly.

***Note that ordering and storage allocation problems for sparse positive definite systems, such as a balanced power system nodal equations, are both different and easier than those for the general sparse matrix. For a general sparse matrix, some form of pivoting is necessary to ensure numerical stability[73].

In general the following points are to be noted with respect to the minimum degree algorithm.

1. There is a likelihood of ties between rows and columns of the partially factored matrix, i.e. there could be more than two row-column pairs that have the same degree. Therefore, there has to be some arbitrary tie breaking strategy. In the present application, the ties are broken by selecting the occurrence of the minimum degree of the first row inspected. The different strategies of breaking ties has not been proven to show any critical effect on the algorithm. These strategies are arbitrary ones without any theoretical proof of being good, bad, or otherwise[72, 73].

2. The ordering selection depends upon the partially factored matrix, which requires that the partially factored matrix be known prior to execution. This obstacle is circumvented by using the graph theory as given in the subsequent sections. The use of elimination graph theory mitigates the unpredictability of the storage requirements. Moreover by employing dynamic memory structures, the problem of explicit declaration of static storage space is avoided.

3. The constant vector [I] should be reordered and the final results should also be reordered back to the original order.

4. The elements in the factored matrix may be quite spread.

4.5.2. Application of graph theory

The minimum degree algorithm requires the prior knowledge of the partially factored matrix. This can be if the graphical analogy is used to represent a interconnected system such as the power transmission network. In this subsection, the application of the graph theory is briefly discussed. A complete set of definitions pertaining to graph theory is given in the appendix B. Definitions of terminology used in the proposed algorithm are given here briefly[7].

Graph G = (X,E) is comprised of a finite set X of nodes and a finite set E of edges that connect the nodes. A graph $G' = (X',E')$ is a subgraph of $G = (X,E)$ if X' #⊂# X and E' #⊂# {E plus the new edges in X'}.

Nodes x and y are said to be **adjacent** if {x,y} is an edge in E.

Degree of a node x in a graph is the number of nodes adjacent to x and is denoted by |Adj(x)|. Figure 4.5 illustrate a graph representation of a 9 bus power system, then,

Adj(a) = {s4} and Adj(c) = {b,d,s1,s3},

also, degrees are

|Adj(a)| = 1 and |Adj(c)| = 4.

Let S be a subset of X and y be a node in X but not in S, i.e. $y \in (X-S)$. Then the node y is said to be **reachable** from a node x in the set X through the set S if there exists a path $(y,v_1, \ldots,v_k,x)$ such that node $v_i \in S$, for $0 \le i \le k$. Here k can take the value of 0 as well, i.e. a node x adjacent to y, but not in S, is defined as reachable from y through S. If S comprises s1, s2, s3, and s4 in Figure 4.5, then

$$Reach(y,S)=\{x \in X-S | x \text{ is reachable from } y \text{ through } S\} \quad (4.10)$$

or applying to the graph shown in Figure 4.5,

Reach(y,S) = {a,b,c}, similarly

Reach(b,S) = {d,y},

Reach(a,S) = {y}, and Reach(c,S) = {b,d,y},

so on and so forth.

In the graph representation of the power system network, the definition of reachability of node can be employed to determine the new order of the graph without actual elimination. This will avoid the need of prior knowledge of the partially factored matrix. Consider the graph shown in Figure 4.6 where double circled nodes have been eliminated and are, therefore, members of subgraph S. Rest of the nodes remains to be eliminated. The next node to be eliminated is the one whose reachability through S is minimum. As shown in Figure 4.6, node d has a minimum degree based upon the

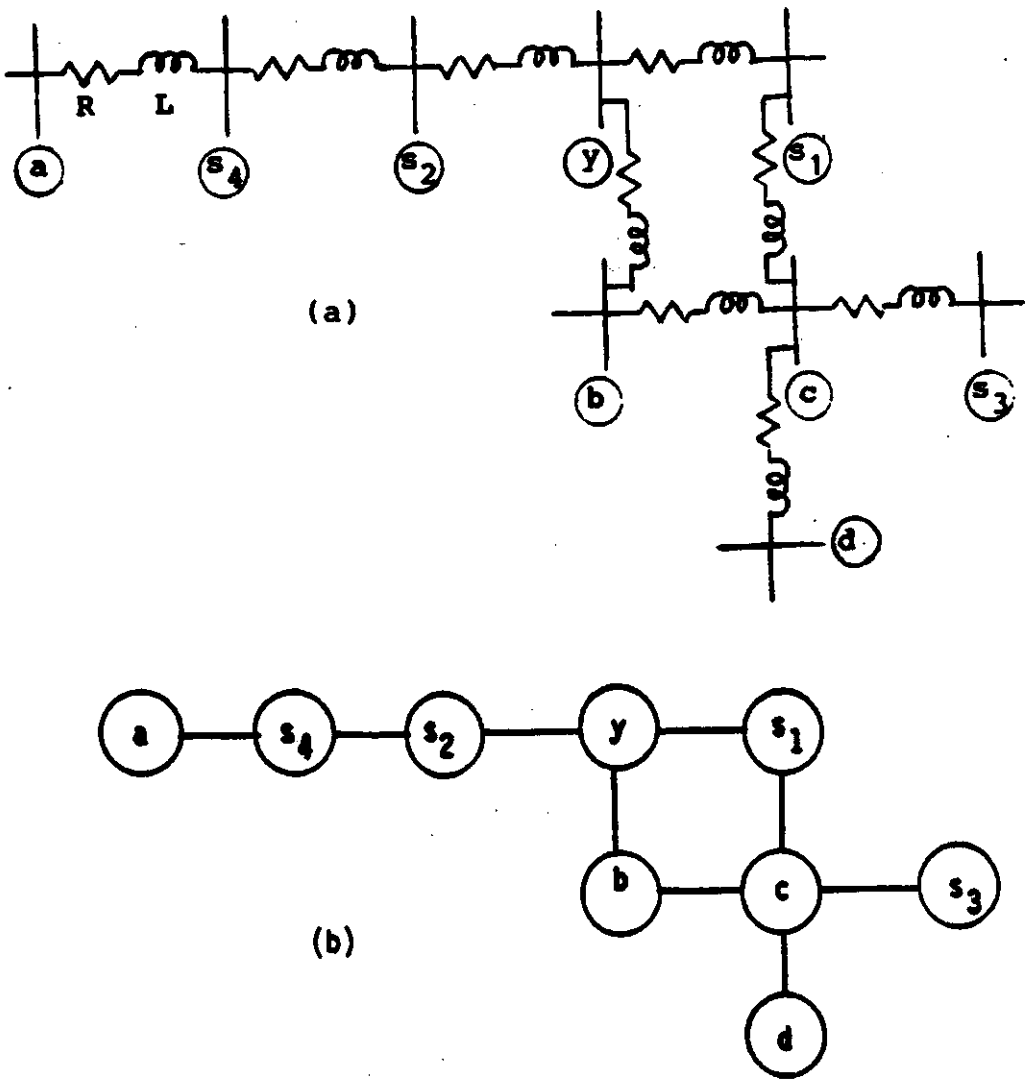

Figure 4.5: A graph representation of a power system; (a) Power system network; (b) Graph representation.

definition of Reach(d), therefore node d is the next node to be eliminated. In this manner same graph storage can be used for the whole process and the storage requirement can be predicted. Double circled node in Figure 4.6 identifies an eliminated node (row) of the matrix. The algorithm for reordering in terms of reach set is given as below, where ϕ indicates an empty graph.

1. Step 1: Initialisation. $S \leftarrow \phi$.

   $Deg(x) \leftarrow |Adj(x)|$ *for all* $x \in X$

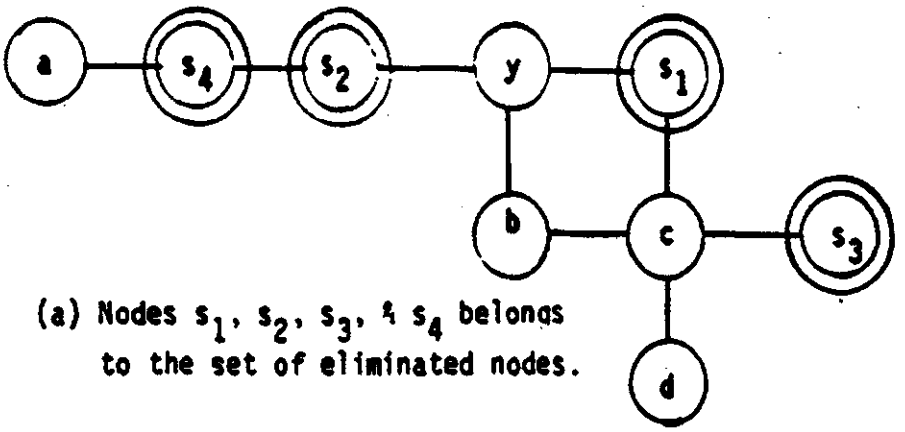

(a) Nodes s_1, s_2, s_3, & s_4 belongs to the set of eliminated nodes.

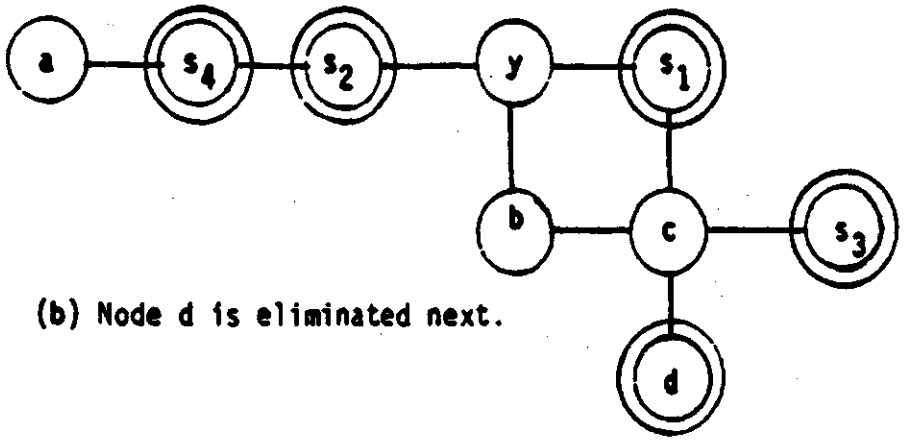

(b) Node d is eliminated next.

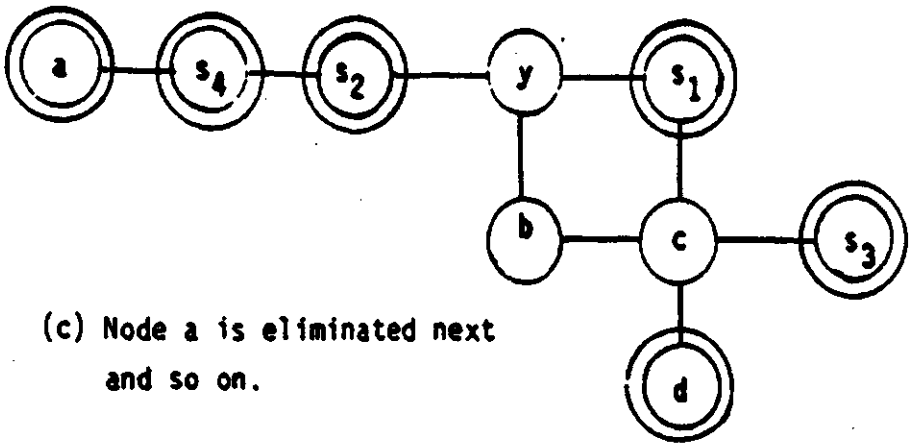

(c) Node a is eliminated next and so on.

Figure 4.6: Example of an elimination graph.

2. Step 2: Minimum degree selection. Pick a node $y \in X-S$ where $Deg(y) = min_{x \in X-S} DEG(x)$.
   Number the node y next and set $S' = S \cup \{y\}$.

3. Step 3: Update the degree for rest of the graph.
   $Deg(u) = |Reach(u,S')| \text{ for } u \in X-S'$.

4. Step 4: If $S' = X$ then stop. Otherwise, set $S \leftarrow S'$ and go to Step 2.

The above algorithm gives a new order of the system matrix based upon the minimum degree. There is no or very little improvement in the time of computation of this algorithm. However, the storage requirement is predictable. Further reduction in time of computation can be achieved through the mass node elimination and mass degree update as suggested by George and Liu[7, 77]. These methodologies are not pursued further in this thesis.

4.6. Data Structure

As described in the last section, the storage requirement was made more predictable by the use of minimum degree algorithm based upon the graphical elimination process in solving the set of simultaneous equations. But in the case of harmonic analysis such as the one proposed in Chapter 3, the order of equations will vary with the harmonic order, i.e. the order of system equations increases with higher harmonic order. This is due to the fact that virtual nodes are introduced in the transmission network in order to determine the harmonic voltage profile. In case of static data declaration, vectors and arrays should be properly dimensioned, otherwise the program will crash exit. Such a static data structure (e.g. dimensioned vector and arrays) may render itself inadequate in cases where the order of system equation is variable. One obvious solution is to declare the largest dimensions of all static arrays and vectors.

Furthermore, during reordering and factorisation of the system bus matrix, much updating and traversing of data is required. This leads to a search for data structure that will take more account of the data organisation.

The dynamic data structure is suitable for both preventing the crash exit of the program due to improper dimensioning of arrays and for efficient data traversal. Such a data structure is linked through pointers. The storage is allocated or deallocated as per the requirement of the program during its execution. The traversal and updating of data can be made efficient through the use of more elaborate recursive data traversal algorithm[78, 79].

In the case of the transmission network, the structure of the [Y] matrix is obvious from the structure of interconnections of the power system. For example, in case of the transmission network shown in Figure 4.7(a) there are three buses. For harmonic analysis, there will be some virtual nodes included as described in Chapter 3. Assuming one virtual bus (or node) is introduced in each transmission line and one virtual bus is needed for each transformer, then Figure 4.7(b) illustrates the system for harmonic analysis. This network is then converted to the graph of nodes as shown in Figure 4.7(c).

The minimum degree algorithm as described earlier can be implemented on this graph and a case of minimum fill will occur if the nodes(or buses) are numbered in the order of increasing interconnections. A data structure to store such a network is shown in Figure 4.8, where NBN, and OBN are new bus number and old bus number respectively. Initially NBN is given the value 0 and OBN is the original number of the bus given by the user. DEG denotes the degree of the node, or the number of nodes linked to the right of a head node. RPTR and DPTR are right and down pointers respectively. Such a data structure is called a linked data structure and is dynamic in nature. This type of data structure lends itself for recursive algorithms. Some refinements are carried out in the

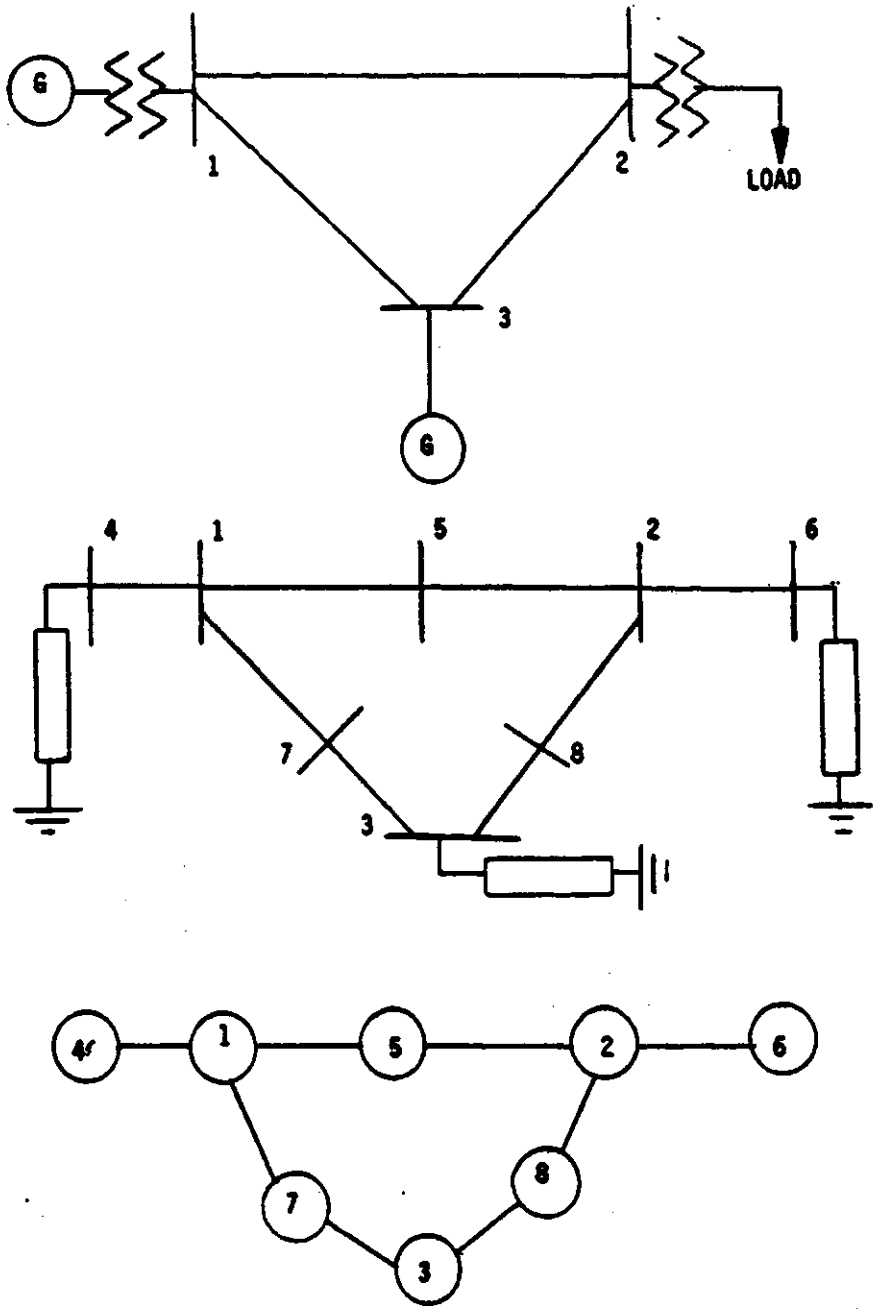

Figure 4.7: Example of a transmission network.

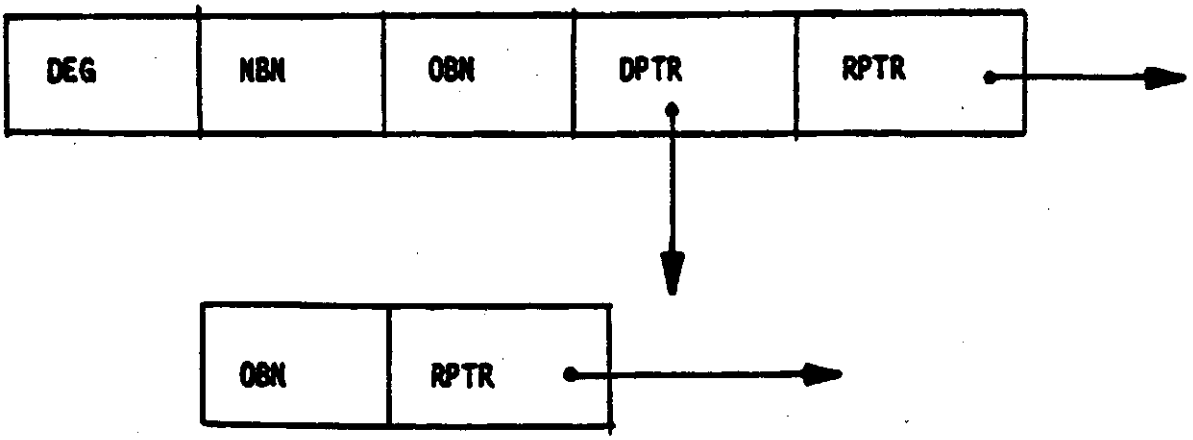

Figure 4.8: Storage of nodes.

algorithm given in the section (4.19) in order to implement the algorithm using a dynamic data structure. The new algorithm is given in the next section.

For the purpose of clarity, the following terms are defined. **Head node** refers to the node containing two pointers RPTR and DPTR. **Data list** refers to the list of nodes containing only one pointer RPTR and is linked to a head node.

4.7. Final Algorithm for Minimum Degree Selection

The final algorithm uses the dynamic data structure as described in aforementioned subsection. The reachable set concept is used in a recursive manner to determine the new order of nodes. Each step of the algorithm is briefly described in the following section. At the end of the algorithm the linked list structure contains the new order of the system equations.

1. Step 1: Initialisation. The original network is stored in the data structure as shown in Figure 4.8 and degree of each node, given by the number of nodes to its right, is computed.

2. Step 2: Minimum Degree Selection. Pick a node of minimum degree and number it next. For example, in Figure 4.9, node 4 is first minimum degree node and is numbered as 1 in the new ordering scheme. Repeat the following steps for each of its reach nodes linked through its pointer;

   a. delete the node;
   b. pick the same node in the head node list;
   c. if a NBN is 0 then do the following else return;
   d. decrease its degree by one;
   e. check if the new degree is same or less than the previously selected minimum degree;
   f. if yes then renumber it as the next node and return to Step 2.

3. Step 3: If all the nodes have been renumbered then stop else go to Step 2.

In this manner, node 6 in Figure 4.9 is chosen next and numbered 2 in the

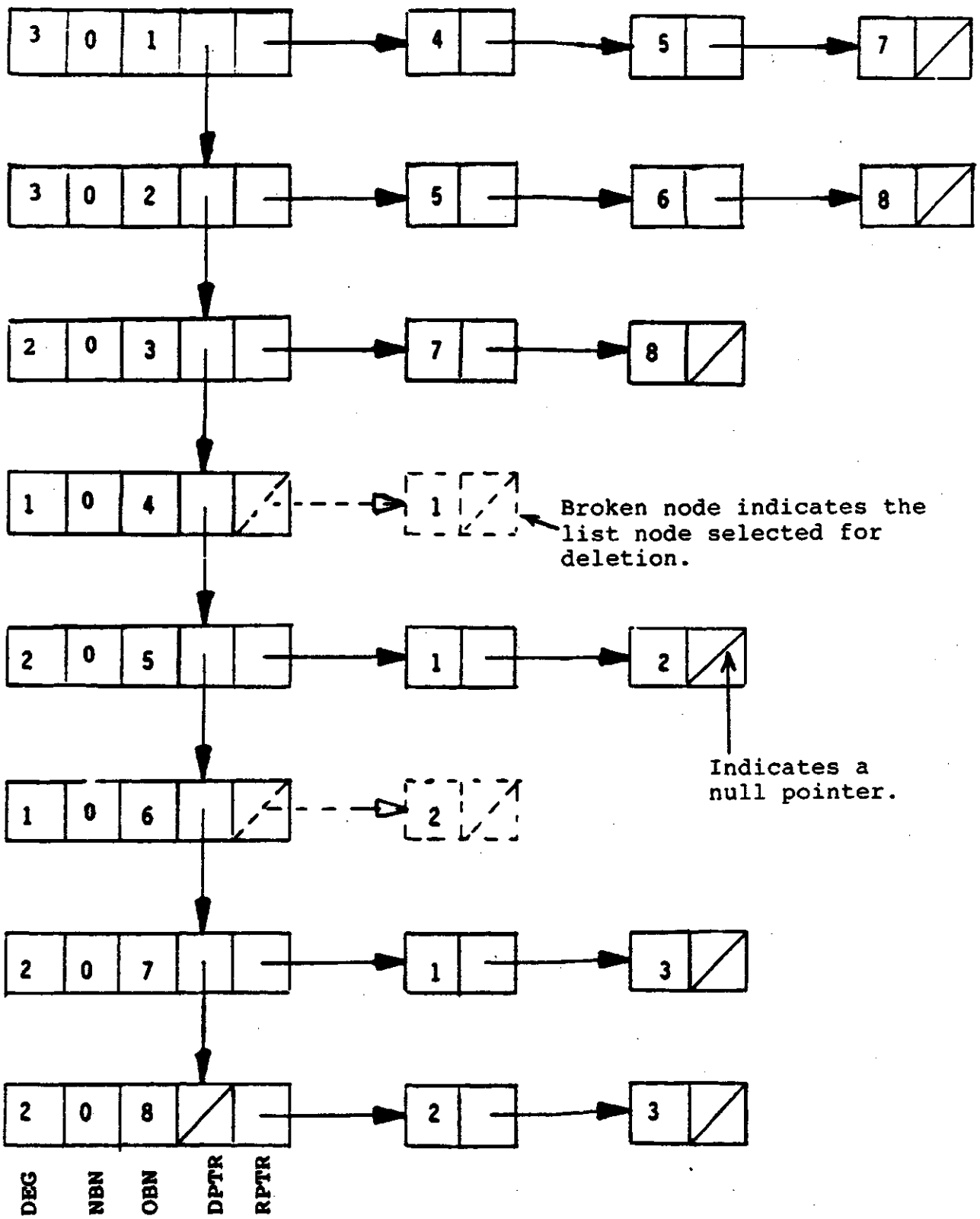

Figure 4.9: Example of reodering.

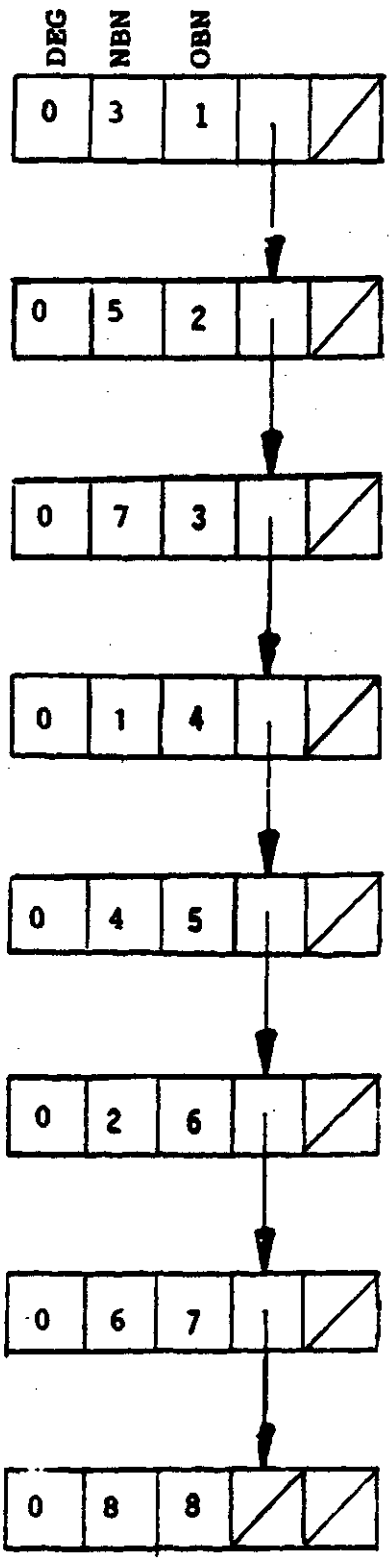

Figure 4.10: New order of the system matrix.

new order. All the rest of nodes have the same degree and are numbered consecutively. The new order is identified by the NBN column in Figure 4.10. The final data list contains the old and the new node numbers. This information is later retrieved to renumber the result back to the original order. The storage requirement is predictable, since the maximum storage is the one required for the original network. Also the ordering algorithm is such that it does not require prior information of the partially factored matrix. The information of the new order is used to reorder the system buses.

4.8. Elimination Process

The reordered system is now ready for the process of elimination. The elimination process based on the Gaussian method is performed on the [Y] matrix. Therefore, first the admittance matrix is formed from the given data and the new order of nodes. The direct method is used to obtain [Y] from the line parameters. The constant vector [I] is reordered in accordance with the new order.

Due to symmetry of the system, only the upper half of the matrix is stored. The storage of the upper half of the matrix is done in a similar manner as for the network. A head node contains the the diagonal element of the matrix. The right data list comprises of remaining nonzero elements in that row to the right of the diagonal. The head node is referred to as pivot node, denoted by P_{ii}. All other nodes connected to the right of a head node are called column nodes, denoted by C_{ij}. An example is shown in Figure 4.11. In order to use the minimum storage, the head node contains the row number and the pivot value, whereas the right list node contains only the column number and the column node value[****]. Such a data structure is dynamic in nature and also, the recursive algorithm is quite easy to implement. The Gaussian elimination algorithm is then implemented in the following recursive manner.

[****]In case of real number, only one value is stored whereas in case of complex number, two numbers are stored separately

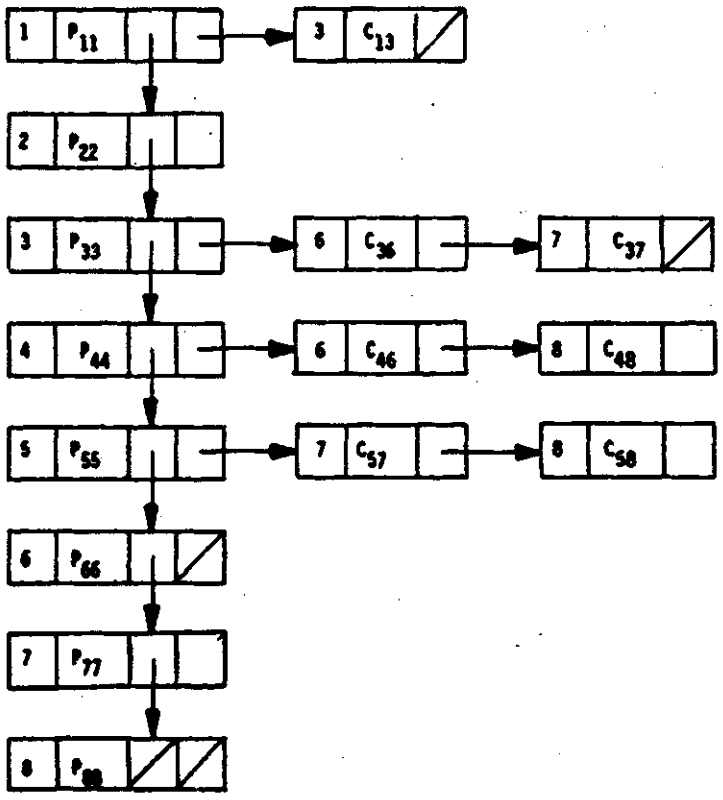

Figure 4.11: Storage for the admittance matrix.

1. Step 1: Pick a pivot node and for each of its column node in the data list perform Steps 2 and 3.

2. Step 2: Chose the head node whose row is same as the column number of the selected column node. Obtain the new value of each node in the currently selected data list, i.e. if n is the pivot node and j is the column number of the column node selected in Step 1 then

$$P_{jj} = P_{jj} - \frac{C_{nj}C_{nj}}{P_{nn}}$$

$$for\ k > j$$

$$C_{jk} = \begin{cases} C_{jk} - C_{nk}C_{nj}/P_{nn}, & C_{jk} \neq 0 \\ -C_{nk}C_{nj}/P_{nn}, & C_{jk} = 0 \end{cases}$$

3. Step 3: Stop if all the pivots are exhausted else go to Step 1.

Although the reordering algorithm guarantees a minimum number of fills, nevertheless there are going to be some newly created column nodes in Step 2. The dynamic nature of the data will provide the flexibility of creating more nodes if needed.

This is the main reason why the dynamic data structure is chosen. Except for the creation of new nodes, the factored upper triangular matrix is stored in the same data structure. Finally, the solution of the system equation is obtained using Sato and Tinney's algorithm given by the equation (4.9). This algorithm is easily implemented due to its recursive nature. Also there is no need to transpose the U matrix. After the final solution is obtained, the result is transformed back to the old order of the nodes (buses).

4.9. Discussion

The computer module for the sparse implementation was divided into four main subroutines; Reodering program; Elimination program; Solution program; and Orderback program. As an example, the sparse module was executed for a small system of the order of N. Table 4-3 gives the statistics of the results of the program pertaining to the computation and memory requirements*****. The system considered for the example was a real number system. In case of complex numbers, the storage will be larger since each value node will contain two numbers (i) real and (ii) imaginary. The comparison is carried out with the IMSL example subroutines which do not use any sparse methodologies. It is obvious that the total time of computation is quite large for sparse systems. It becomes comparable only for highly sparse systems.

With the very fast change of technology, memory allocation is becoming less of a problem. In the face of this argument, it may look foolish to optimise the storage requirement. However, the objective of the algorithm is to optimise and provide means for a predictable memory. The minimum degree algorithm presented here certainly uses predictable memory. However the elimination program has some uncertainty of the memory allocation. Nevertheless that uncertainty is minimised by the minimum degree algorithm. Also with the dynamic data structure the uncertainty, however large, is of no

*****Each pointer uses up two word of memory on VAX/VMS computer system

Table 4-3: Statistics of the algorithm.

Order of the system	Number of Nonzero Elements	Sparsity (Percent)	Estimate of Minimum Data Storage Required in Words		CPU Time	
			Sparse (Dynamic)	IMSL (Static)	Sparse Secs.	IMSL Secs.
25	259	58.5	693	700	0.11	0.04
50	550	78.0	1450	2650	0.60	0.11
50	346	86.2	1042	2650	0.40	0.08
65	513	87.8	1481	4420	0.70	0.18
50	178	92.8	706	2650	0.14	0.07

significance. With the minimum degree algorithm, the time of computation is certainly minimised for highly sparse systems.

The graph structure used for the minimum degree algorithm may seem similar to the quotient graph as suggested by George[77] et al. Nevertheless the algorithm used here is quite different. Since the concept of closure and neighbourhood are not used explicitly as suggested by George. It is highly recommended to use the mass degree and mass elimination process suggested by George to reduce the time of computation.

4.10. Conclusion

In this chapter definitions of power and energy at harmonic frequencies are given. The harmonic power algorithm is modified to accommodate the new concept regarding the distortion volt-amperes. Also included is a step by step illustration of the program as applied to a two bus power system example. A table of results is included for the example case. It is proven that given an appropriate first estimate of the power demand at the converter node, the convergence is successful. By the use of an iterative method of computation of harmonic power demand at the converter node, a true interaction of the power system and the converter is studied.

Also included is a review of the sparse matrix techniques. The graph theory implementation of the minimum degree algorithm is presented. The algorithm is adopted for the application to the power transmission network. An heuristic approach is used to minimise the number of fills in the Gaussian elimination process. The dynamic data structure used in the implementation lends itself for the recursive process and also optimises the storage allocation. A complete implementation of the algorithm is carried out in the VAX PASCAL Version V3.7 programming language.

5. APPLICATIONS OF THE HARMONIC POWER FLOW ALGORITHM

5.1. Introduction

In this chapter, the application of the harmonic flow program is illustrated. Four examples of power systems were taken for the study of the harmonic voltage profile computations. The first example, a five bus power system, is similar to the one given in the reference 34 and was used to show the accuracy of the program. There are three more example studies presented, namely the IEEE RBTS[80] five bus test system, SPC six bus system, and an industrial eleven bus test[34] system.

A series of simulated tests were carried out for the first example of five bus system. These tests were similar to those reported by Heydt et al. Tests were carried out for the purpose of comparison of the method used in this thesis and the one reported by Heydt[32, 33, 34]. A series of simulated tests were also carried out for each of the remaining three example systems to illustrate the effect of various parameters on the harmonic voltage profile. These Tests were carried out in order to highlight the use of the algorithm. The description of type of simulated tests performed is given in Table 5-1.

Table 5-1: Description of types of simulated tests.

Description of Test	IEEE RBTS System	SPC System	Industrial System
Variation of Rectifier Load	Test A1	Test B1	-
Variation of Delay Angle of the Converter	Test A2	-	-
Variation of VAR Compensation	Test A3	Test B2	Test C1

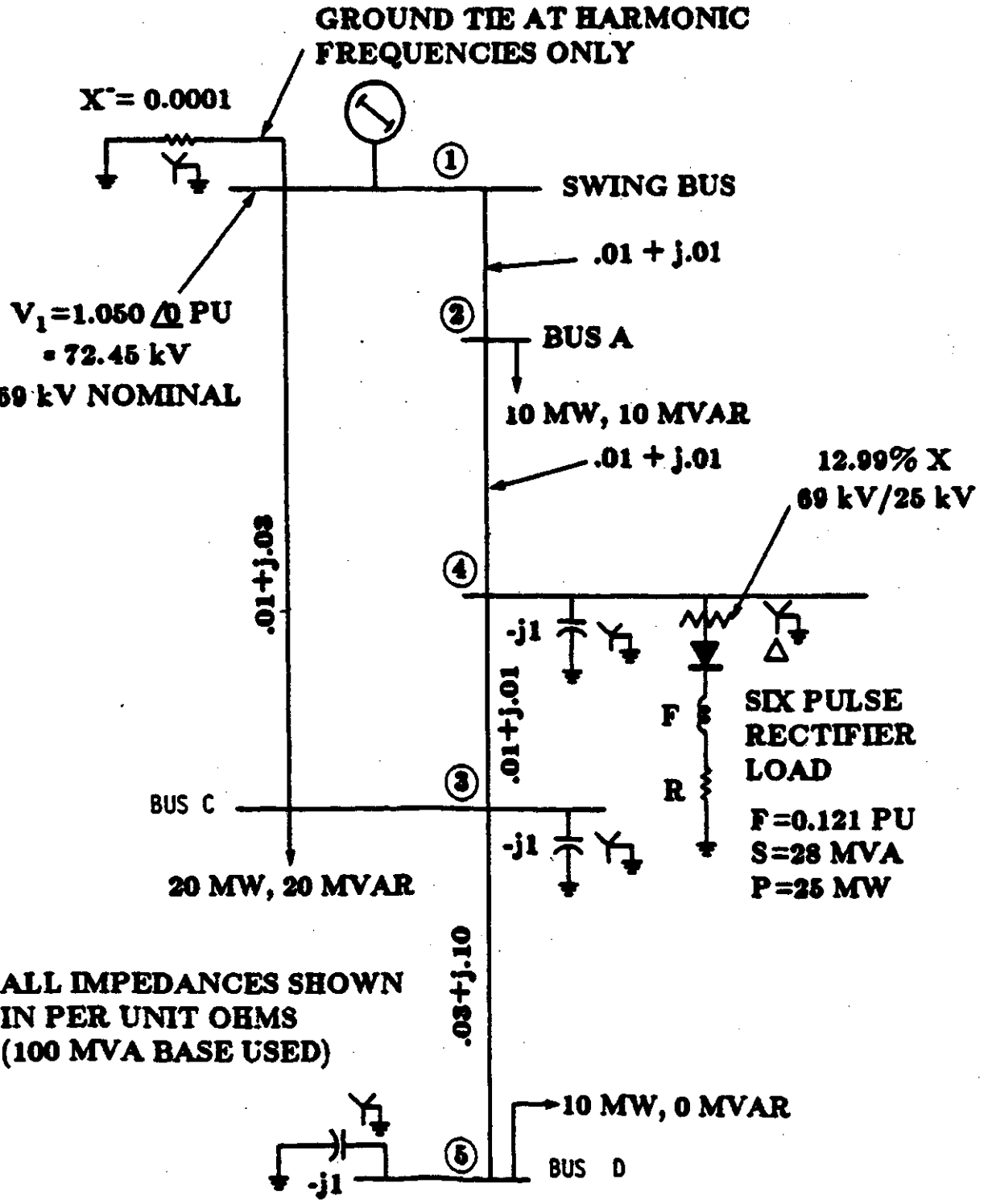

Figure 5.1: Five bus example.

5.2. Five Bus Example

A five bus example was taken from the work reported by Heydt, G.T.[34] et al. to show the accuracy of the methodology. The single line diagram of the system is shown in Figure 5.1. There are five buses in the system with the generator connected at bus 1. The system impedances in per unit and loads at several load buses are as shown in Figure 5.1. The ac/dc converter at bus 4 of the system is a line commutated converter operating at a delay angle of 22.5 degrees. The buses 3, 4, and 5 have capacitor compensation for power factor correction and are included to show the resonance condition.

In order to illustrate the accuracy of the program, the first test was similar to the one discussed by Heydt, G.T.[34] et al. The capacitive reactances at buses 3 and 4 were kept constant at -j1.0 per unit, while at bus 5, it was varied through -j0.2 p.u., -j0.3 p.u., -j0.4 p.u., -j0.5 p.u., -j0.6 p.u., -j0.8 p.u., and -j1.0 p.u. The results are shown in Figures 5.2 through 5.6. Figure 5.2 illustrates fifth harmonic voltage amplitudes at all buses as the capacitive reactance at bus 5 is varied. For low values of the shunt capacitive reactance, the voltage at the bus 5 collapses, whereas the voltages at the other buses rise. This is because the short circuit at the bus 5 due to small capacitive reactance causes more fifth harmonic current injection. This gives rise to the increase in the fifth harmonic voltage at the other nodes while the voltage at bus 5 collapses due to the short circuit. Figure 5.3 illustrates the fifth harmonic voltages for bus 3 and bus 5 taken from Heydt's work[34]. Clearly the results are very similar to the one obtained by the proposed methodology.

The slight difference seen at low values of capacitive reactance arises due to the difference in setting up the experiment. In the case of the experiment reported in this thesis, the power demand is allowed to change while keeping the delay angle of the converter constant; whereas the power demand, in case of Heydt's work, is kept constant

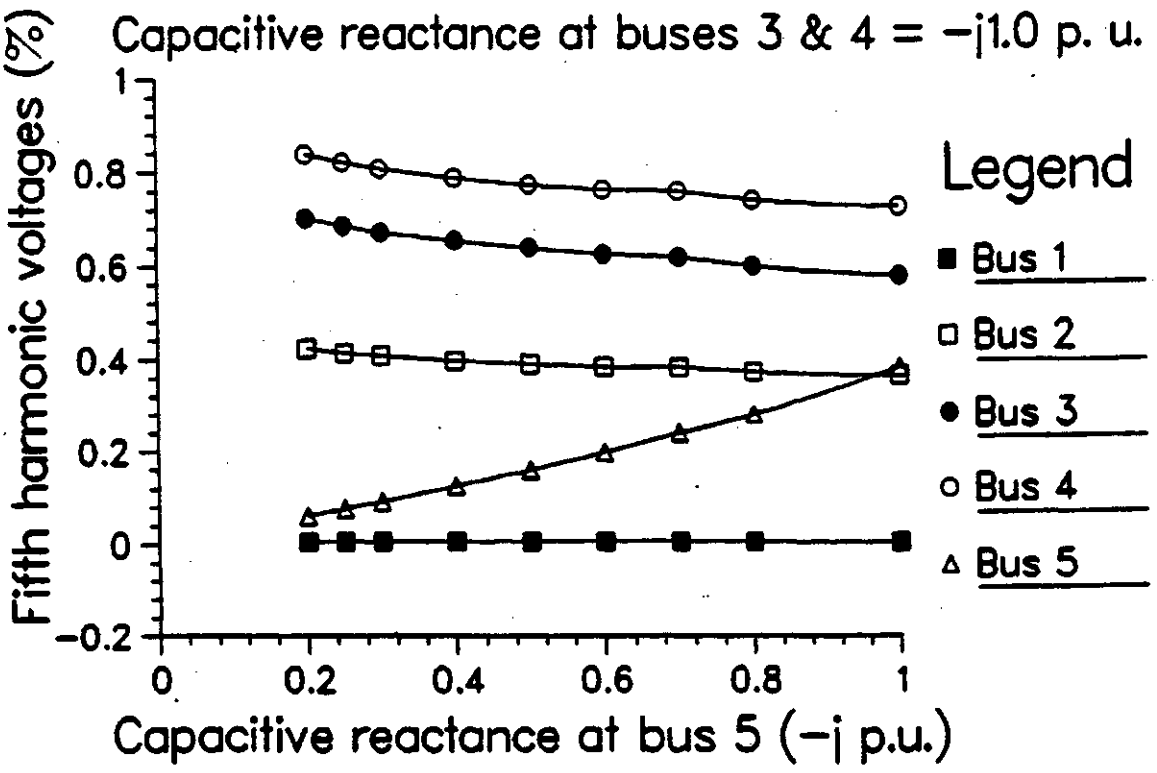

Figure 5.2: Fifth harmonic voltage magnitude(rms).

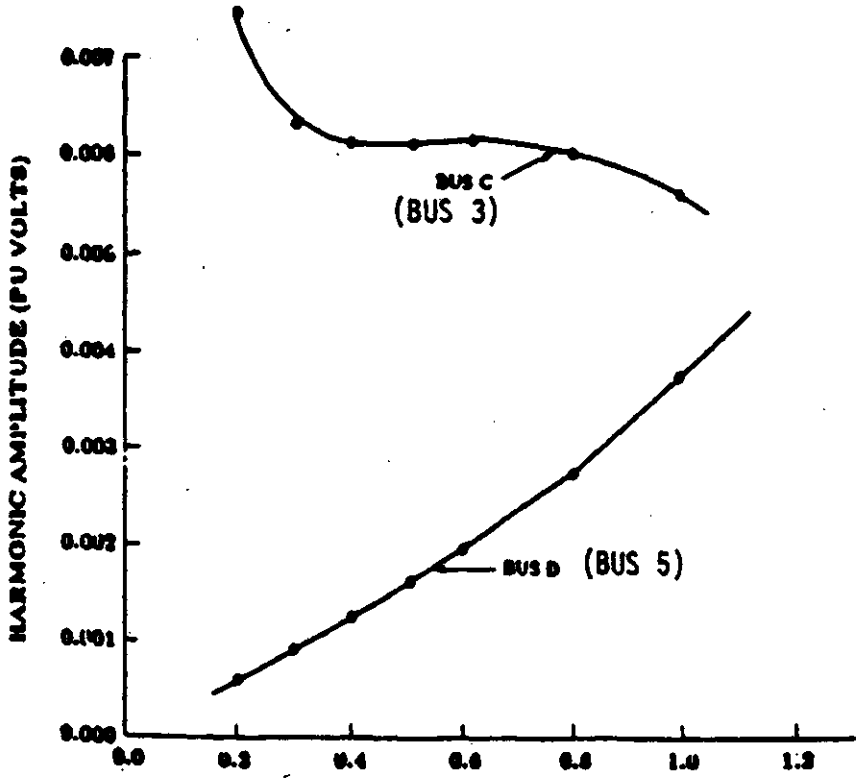

Figure 5.3: Fifth harmonic voltage magnitude(rms)[34].

while permitting the change in the operating point of the converter. Nevertheless, the pattern in change of the fifth harmonic voltage at bus 3 and 5 is similar in both cases.

The graphical representation of results may be misleading in the sense that the percentage of error between the two compared results is not perceptible. Table 5-2 presents the results computed by the author and the documented results presented in the reference 32, 33 and 34. The results are for the condition when the capacitive reactances at buses 3, 4, and 5 are -j1.0 per unit, -j1.0 per unit, and -j0.6 per unit respectively.

Table 5-2: Comparison of harmonic voltages for a five-bus example.

All values are given in percent.

	Computed Results		Heydt's Reported Results		Error(%)
Bus No.	Fundamental voltage.	Fifth harmonic voltage.	Fundamental voltage.	Fifth harmonic voltage.	In fifth harmonic voltage.
1	105.0	0.006	105.00	0.0057	5
2	106.88	0.383	106.91	0.3787	1
3	110.38	0.625	110.43	0.6182	1
4	108.99	0.762	109.05	0.7517	1
5	131.89	0.197	131.95	0.1946	1

Both fundamental and fifth harmonic voltages agree within 1% error. The magnitude of the fifth harmonic voltage at bus 1 is in disagreement by 5%, perhaps the error is larger due to small influence of the harmonic current at the generator bus. The condition of experiment in both cases is similar. It is encouraging to see that two methodologies, namely, the admittance method based upon the iterative Fourier principles used in this report and the Newton Raphson harmonic load flow studies agree closely.

Figure 5.4 illustrates the bus voltages for the 7th harmonic. The behaviour of seventh harmonic voltages is similar to that of the fifth harmonic voltage, except that there is a decrease in the magnitude when the capacitive reactance is between -j0.7 p.u. and -j0.8 p.u.

Figure 5.5 demonstrates the voltage profile on lines 1-3, 2-4 and 3-4. The line voltage profiles were made available due to the introduction of the virtual buses in the system. As expected, the harmonic voltage amplitude is largest at the converter node and reduces as one moves away from the converter node. There is no standing wave pattern on any line. The lines considered in the system are short lines.

Finally Figure 5.6 gives the change in the power demand at the converter bus while the compensation at bus 5 is varied. For the same passive load impedance on the dc side of the converter, the power demand increases. This is due to the fact that the compensation boosts the voltage at the converter node, as a result the power consumed increases. This further increases the harmonic current level and hence the harmonic voltage distrotion in the power system increases. In the series of these experimentations, the converter parameters such as dc load side impedance and the delay angle are kept unchanged. This is the reason why the power increases with the increase in bus voltage. Nevertheless the results obtained highlight the nature of the response of the system and the increase in power demand only increases the magnitude of the harmonic voltages.

The example of the five bus system was further studied by varying the capacitive reactance only at bus 3. The results are shown in Figures 5.7 through 5.10. The fifth harmonic voltages shown in Figure 5.7 go through a resonance when the capacitive reactance is about -j0.4 per unit. The magnitudes of the voltages are small owing to small harmonic current injection from the converter. Nevertheless it clearly exhibits a resonance condition which is potentially harmful in a real application and such a condition should be avoided.

The seventh harmonic component of the voltage exhibits a resonance condition as well, but at a value of capacitive reactance between -j0.7 per unit and -j0.8 per unit. As shown in Figure 5.8, other than the resonance condition, the seventh harmonic

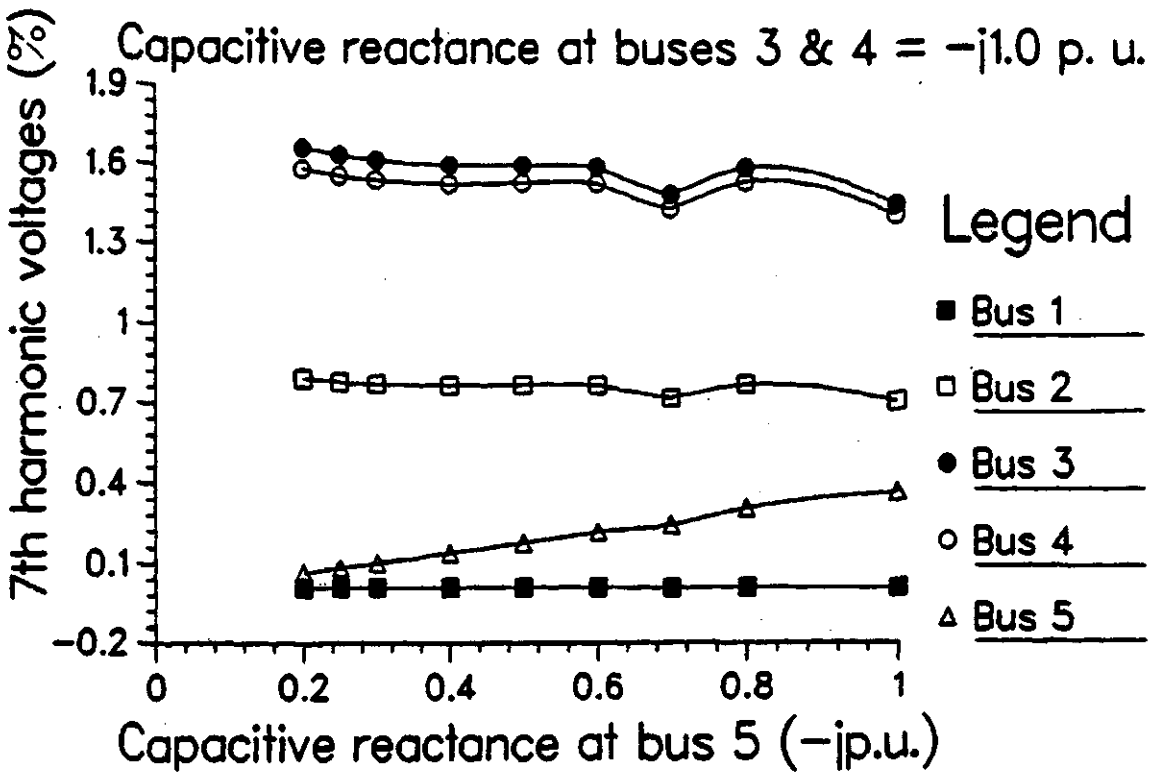

Figure 5.4: Seventh harmonic voltage magnitude(rms).

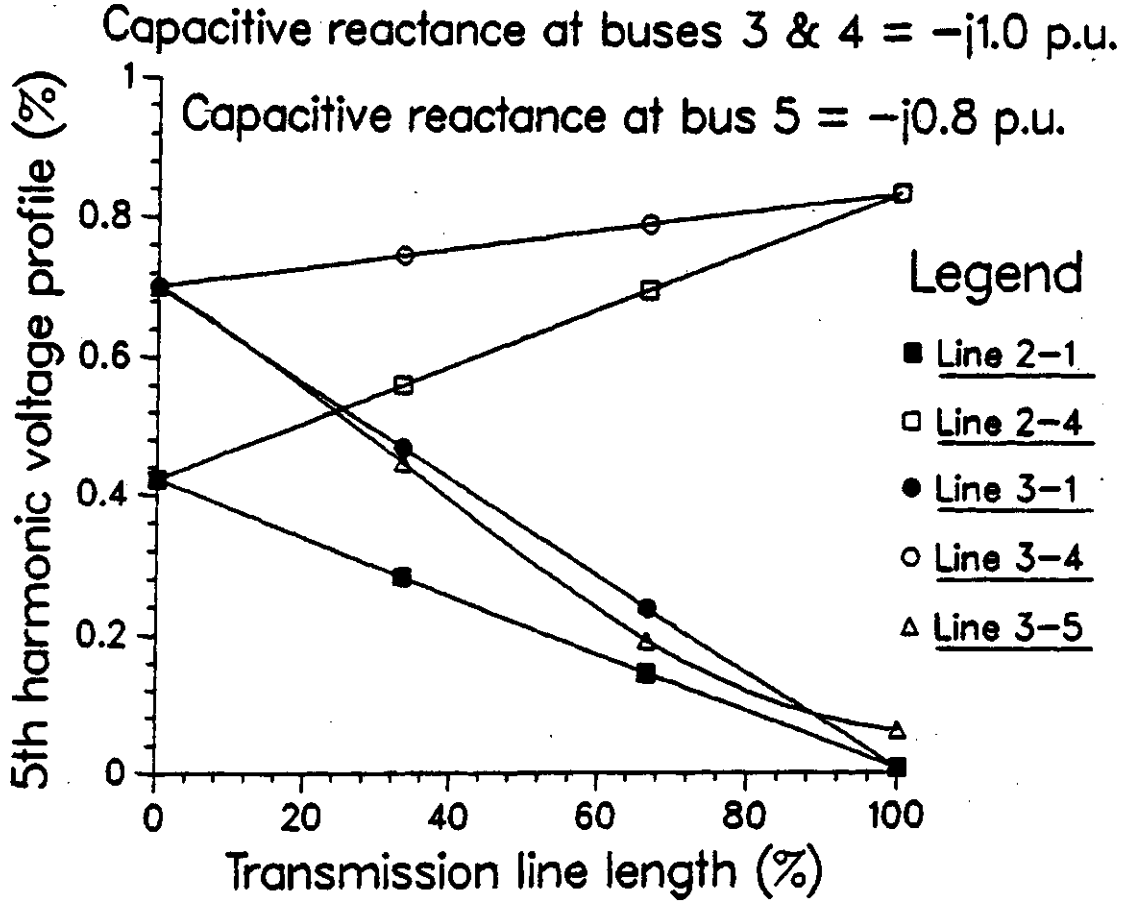

Figure 5.5: Harmonic voltage profile of transmission lines.

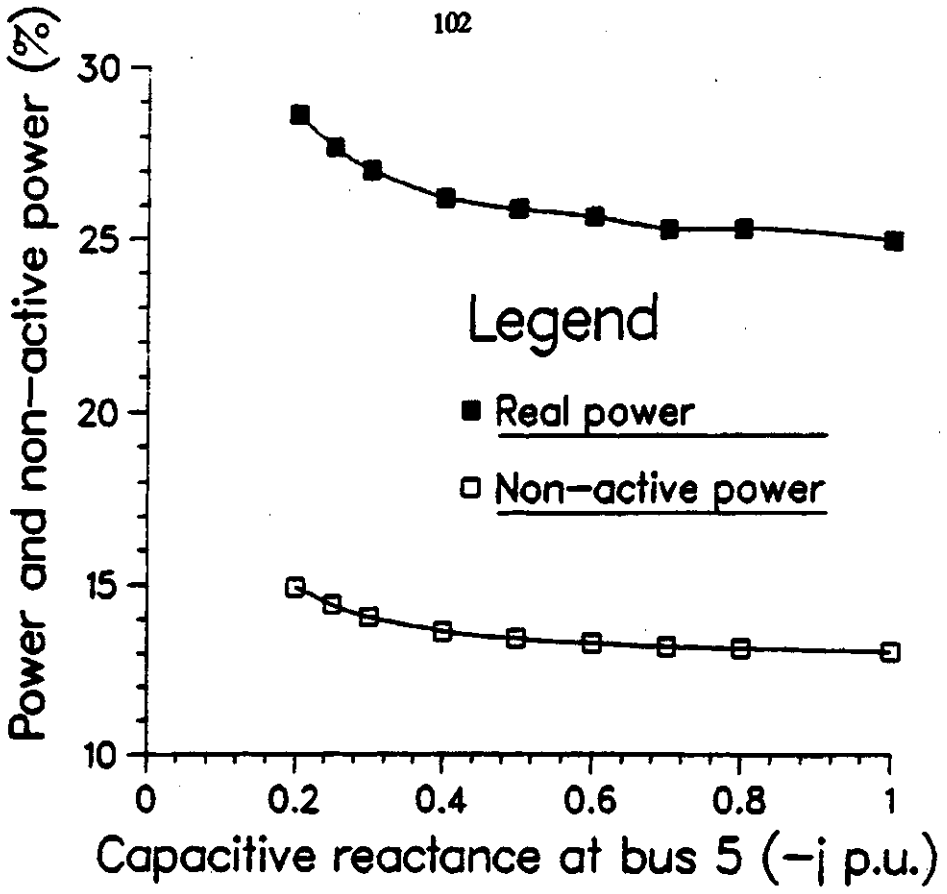

Figure 5.6: Power demand at the converter node.

voltages remain negligibly small as compared to the fifth harmonic voltages. The 11th and 13th harmonic voltages were very small and no resonance phenomena were observed.

Figures 5.9 and 5.10 illustrate the transmission line voltage profile for the resonance condition of fifth and seventh harmonic order respectively. The voltage profile is consistent with the expected results i.e. the voltage increases towards bus 3 with compensating capacitors responsible for the resonance condition. Under the resonance condition, the voltage at bus 3 is much larger than at bus 4 with the rectifier load, a case of self resonance condition.

In all diagrams, it is seen that the bus 5 voltage behaves in almost same manner as bus 3. Again no standing wave patterns were observed on any transmission line. The reason for this is the short length of the transmission lines.

The distortion factor, defined as the ratio of fundamental voltage to the total

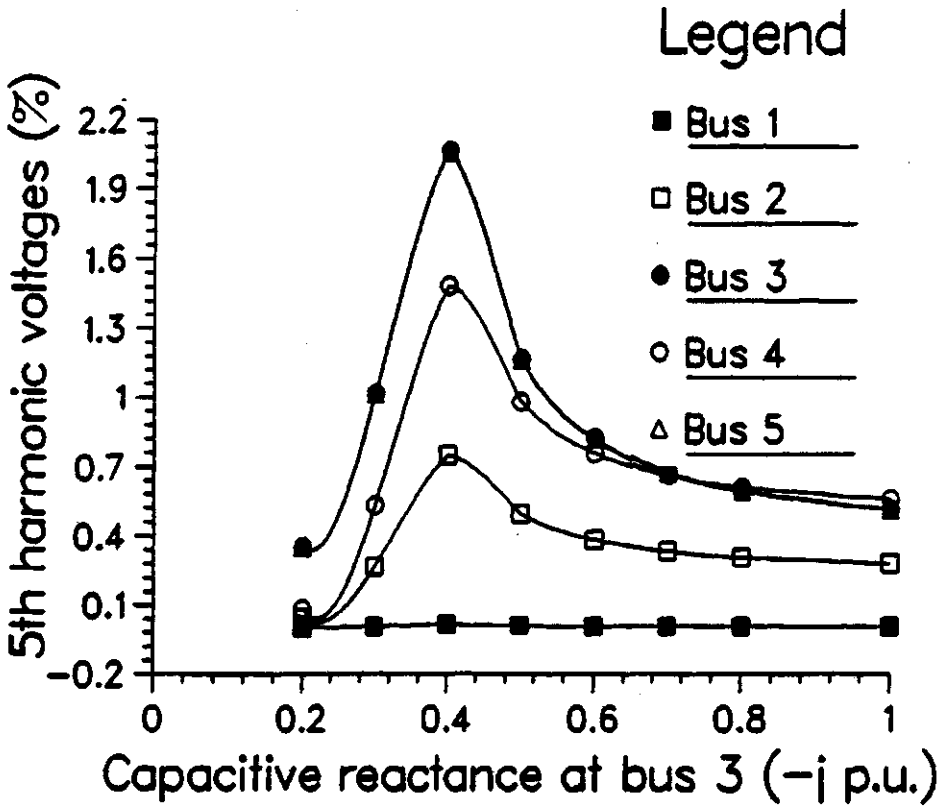

Figure 5.7: Effect of the capacitive reactance at bus 3 on fifth harmonic voltage magnitude(rms).

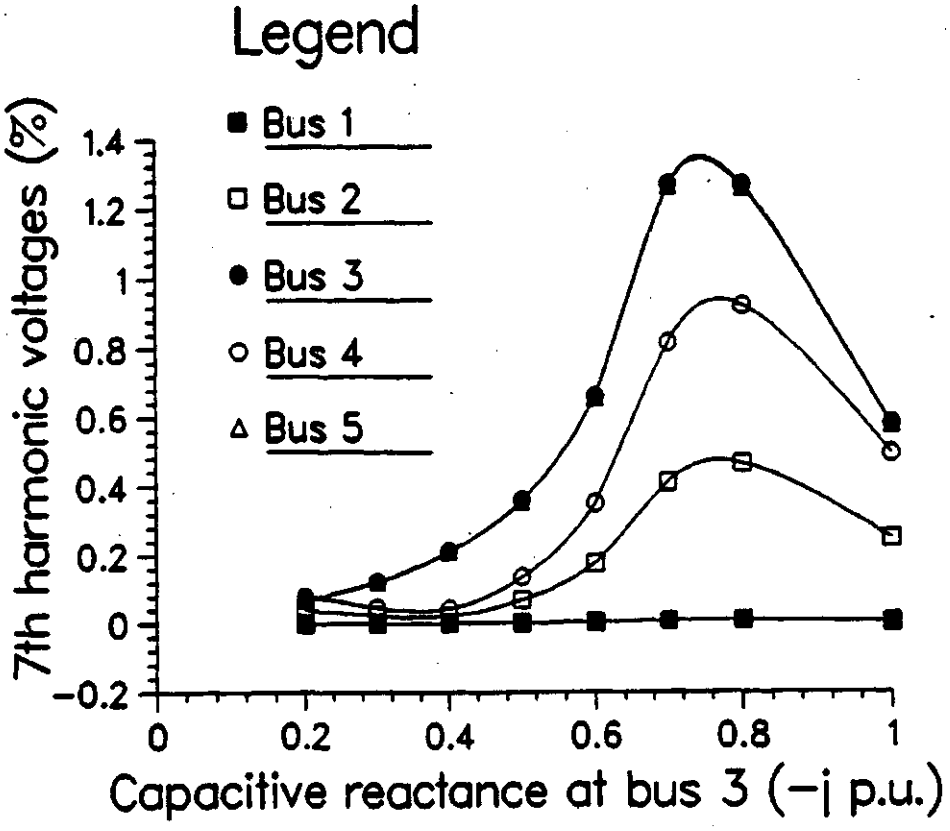

Figure 5.8: Effect of the capacitive reactance at bus 3 on 7th harmonic voltage magnitude(rms).

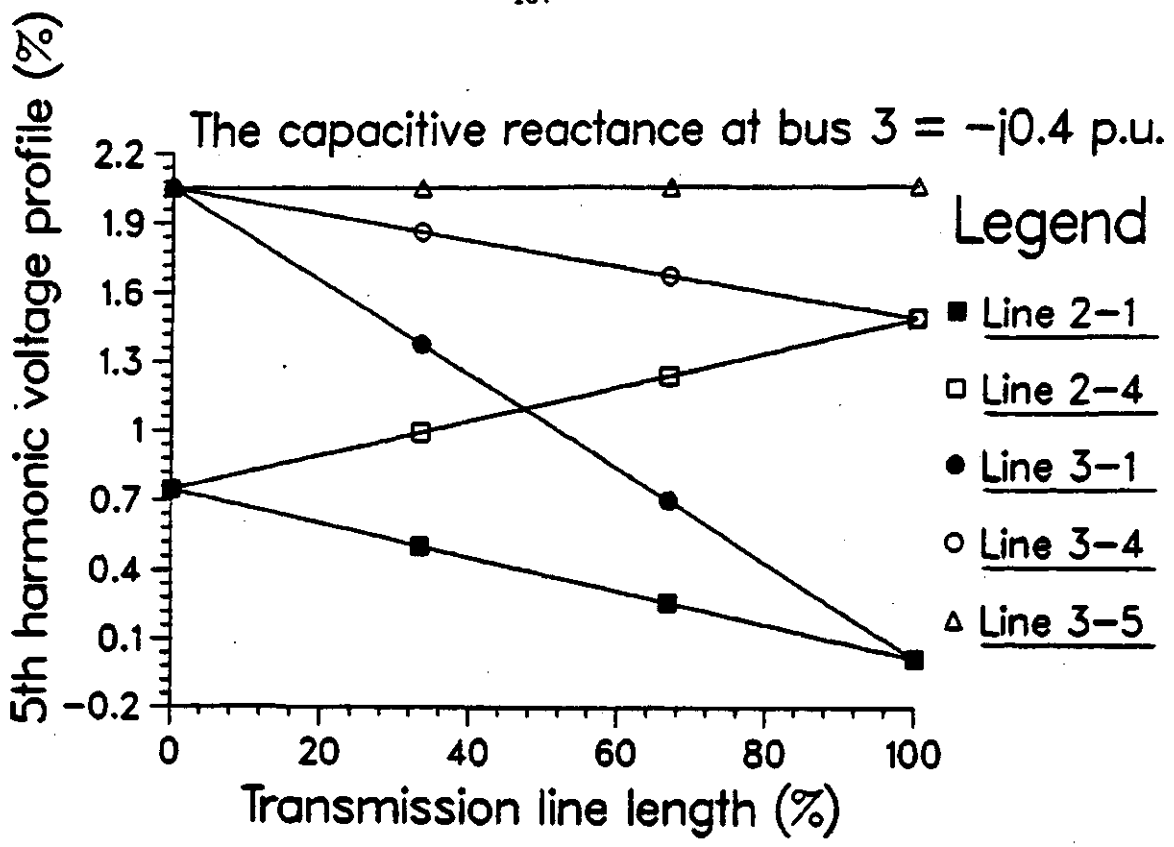

Figure 5.9: The fifth harmonic voltage profile of the transmission lines(compensation at bus 3).

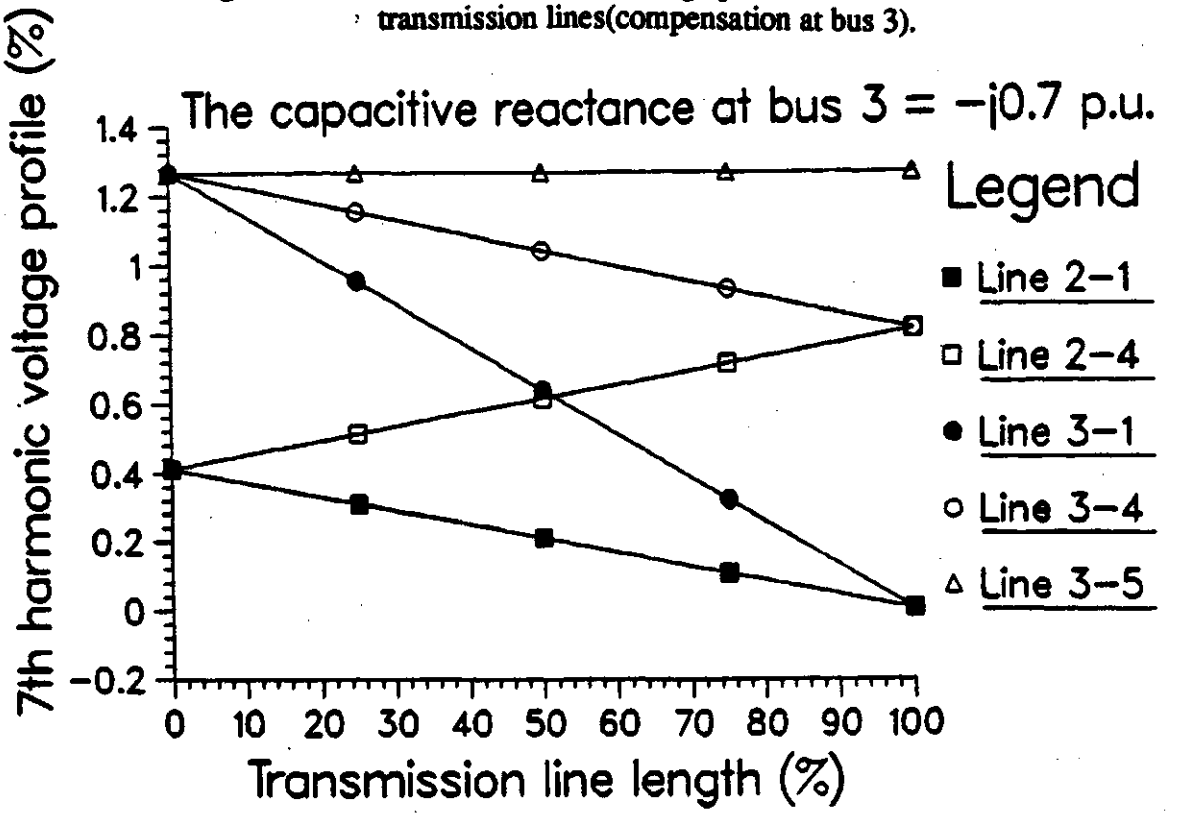

Figure 5.10: The seventh harmonic voltage profile of the transmission lines(compensation at bus 3).

rms voltage at a node, was calculated for various nodes. A distortion factor of 1 means the voltage is a single frequency sine wave. For a non-sinusoidal wave, it will always be smaller than 1. For the above example, the distortion factor was unity at bus 1 for all cases, whereas it was 0.999 at all other buses. The distortion factor for bus 3 goes down to 0.998 for the resonance condition.

The results presented above prove the validity of the program code and also illustrate the use of the algorithm in predicting resonance conditions. The voltage profile of the transmission lines is easily obtained. The results obtained illustrate the fact that the harmonic voltages and hence the voltage distortion will increase with the amount of non-linear load. A resonance condition also may exist for a particular amount of VAR compensation.

Although the compensation used in the above example is expressed in terms of the capacitive reactance, the compensation in terms of reactive power can also be handled by the program as is shown in the following examples. The voltages under the resonance condition illustrated for the fifth and the seventh harmonic orders are of small magnitude. Therefore it would not deteriorate the insulation capability. Nevertheless the harmonic voltages might interfere with instrumentation and the protection system equipment.

5.3. IEEE RBTS Test System

A small power transmission system, the RBTS(Roy Billinton Test System)[80], is a newly proposed power system for educational and research purposes. This system was chosen as an example, mainly due to its long transmission lines of approximately 250 km and 200 km. The system, shown in Figure 5.11, is comprised of six buses, nine lines, two generator buses and four load buses. The voltage level of the transmission system is 230 KV and the total installed capacity is 240 MW with 185 MW as the peak load.

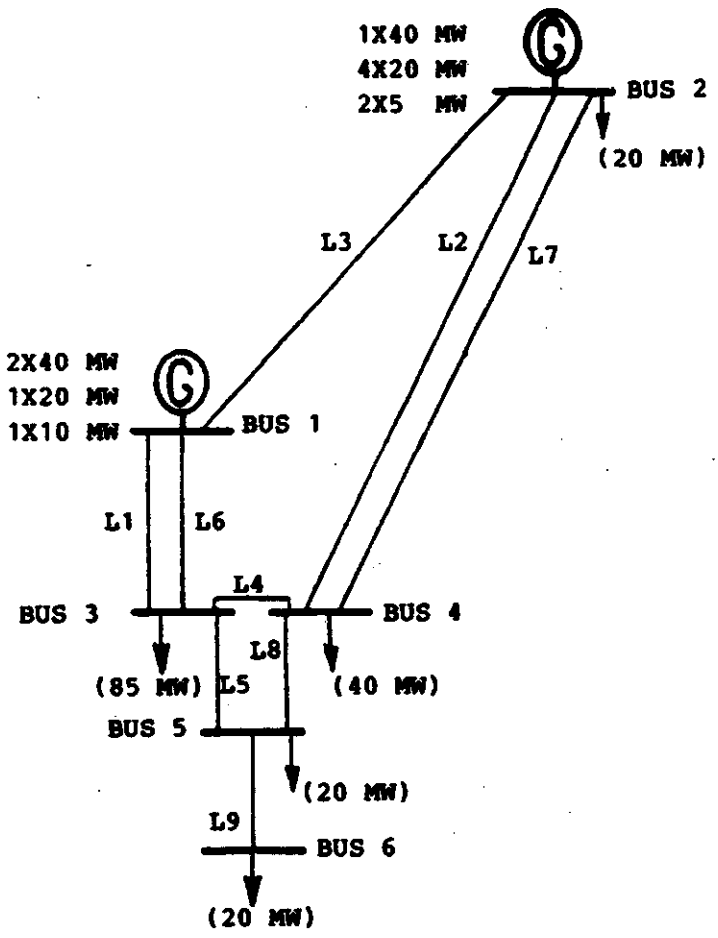

Figure 5.11: Single line diagram of IEEE test system.

The system load includes both linear load and the converter load. The converter load is installed at bus 4 and is a natural commutated rectifier in the 40 MVA, 13.2 KV class. The converter transformer is 230 KV/13.2 KV, 40 MVA, three phase, grounded wye to delta. The per unit reactances on a 100 MVA base are given in Table 5-3.

All the transmission lines are overhead, fully transposed, ACSR construction. Bus 1 is assumed to be the swing bus and bus 2 is a PV bus for the fundamental frequency load flow studies. Although there are various generating units at each of the generating buses, all generating units are replaced by a single negative sequence impedance representing a single unit of combined capacity for the purpose of

Table 5-3: Transmission line data for IEEE test system.

Line No.	Buses From	To	Line Length (km)	Positive Sequence Impedance (per unit) R	X	B
1, 6	1	3	75	0.0342	0.1800	0.0212
2, 7	2	4	250	0.1140	0.6000	0.0704
3	1	2	200	0.0912	0.4800	0.0564
4	3	4	50	0.0228	0.1200	0.0142
5	3	5	50	0.0228	0.1200	0.0142
8	4	5	50	0.0228	0.1200	0.0142
9	5	6	50	0.0228	0.1200	0.0142

harmonic analysis. Bus 1 is assumed to have a large equivalent negative sequence impedance of the generator and is considered to be open circuited for all harmonic frequencies. All the quantities in Table 5-3 are in per unit on a 230 KV, 100 MVA base. The quantities not available readily have been estimated.

The system described above using the line, load, and generation data comprises the base case used for a series of tests. Various tests were executed to illustrate the effects of variations in the system parameters. Table 5-1 describes these tests briefly. The detailed description of these tests is given in the following subsections.

5.3.1. Test A1: variation of rectifier load.

In the first test, the rectifier load(MW) was varied by changing the dc load impedance. The harmonic content of the current is affected by different load conditions in two ways. Firstly, the magnitude of the line current is directly dependent on the dc side load and secondly, the commutation angle is affected by the change in the dc current as was shown in Chapter 2.

In this test, the dc load impedance was varied and the resulting change in system harmonic voltages was studied. The results are shown in Figures 5.12 through

5.15. Figure 5.12 shows the fifth harmonic voltages, Figure 5.13 illustrates the seventh harmonic voltages, Figure 5.14 illustrates the distortion factor, and Figure 5.15 illustrates the transmission line voltage profile for fifth and seventh harmonic voltages for the rectifier load(P) demand of 36 MW.

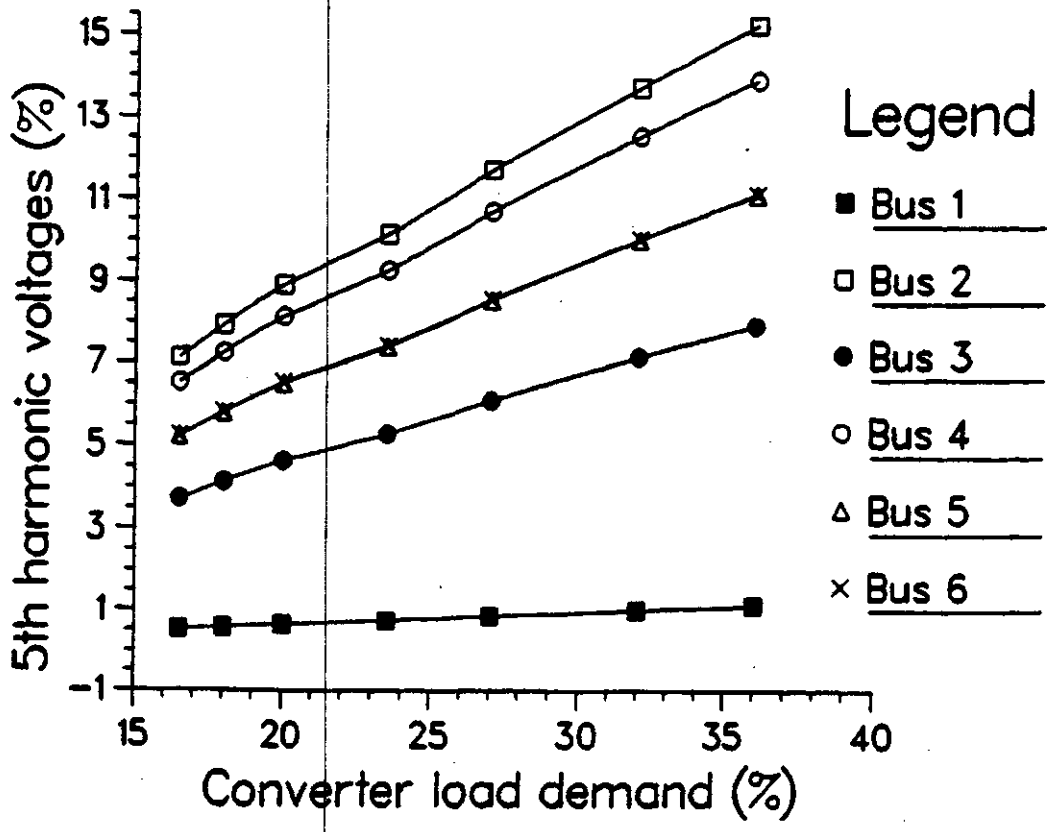

Figure 5.12: Effect of the converter load on the 5th harmonic voltages at system buses.

With the increase in load, the harmonic current injected also increases. This causes an increased harmonic voltage drop in the transmission system. As shown in Figure 5.12 the fifth harmonic voltage drop changes from about 7% to about 15 % at bus 2 when the load demand is increased from 16.5 MW to 36 MW. The similar response is observed for the seventh harmonic order as shown in Figure 5.13, but the magnitudes are smaller. The higher order harmonics, namely 11th and 13th were of smaller magnitude (about a maximum of 3 % at bus 2) and are not plotted.

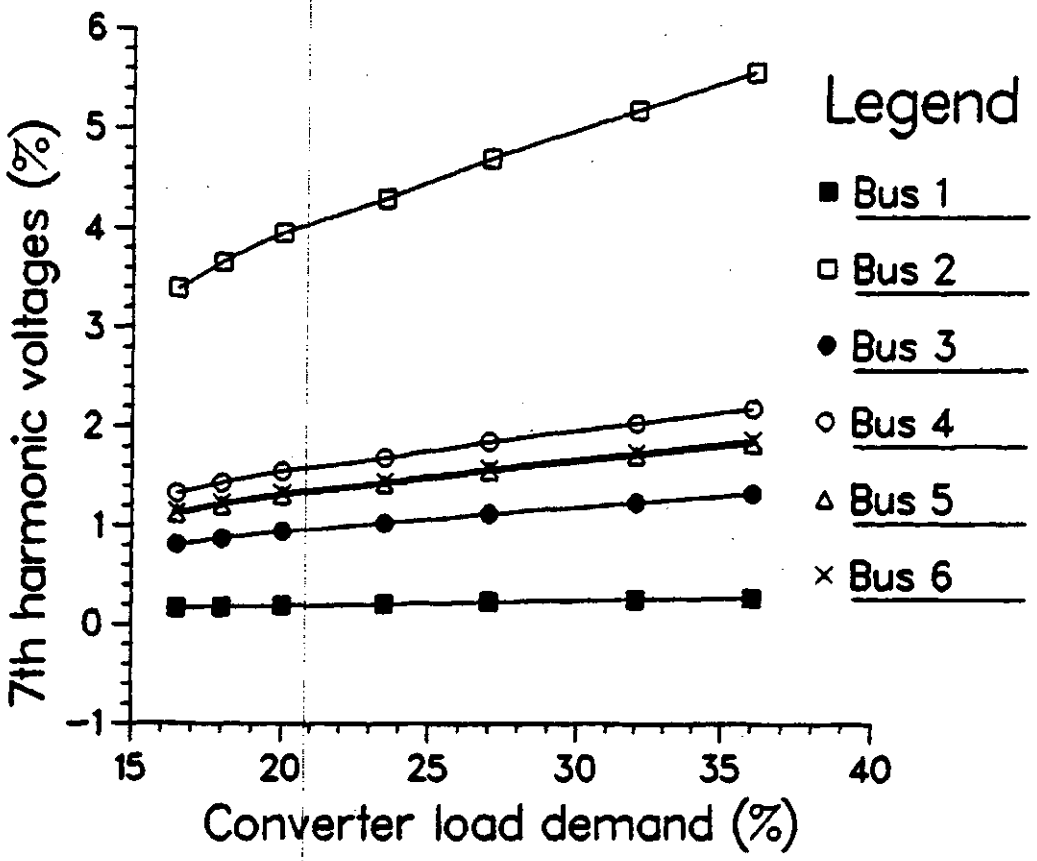

Figure 5.13: Effect of the converter load on the 7th harmonic voltages at system buses.

Figure 5.14 gives the voltage distortion factor for buses 2, 3, 4, and 5. The voltage distortion of bus 2 is poorest of all due to the fact that this bus suffers most from the harmonic voltages. The distortion factor at load buses 3, 4, and 5 is affected in two ways. Firstly, the magnitude of the fundamental voltage decreases as the load demand is increased and secondly, the harmonic voltage levels rise as the harmonic current injection is larger. A distortion factor of unity indicates a pure sine wave, as seen from Figure 5.14 where the maximum distortion factor reached is 0.9991 for bus 3.

Finally the transmission line harmonic voltage profiles for the fifth and the eleventh harmonic orders are given in Figures 5.15 and 5.16 respectively. The line between bus 2 and bus 4 exhibits a standing wave pattern for both 5th and 11th harmonics.

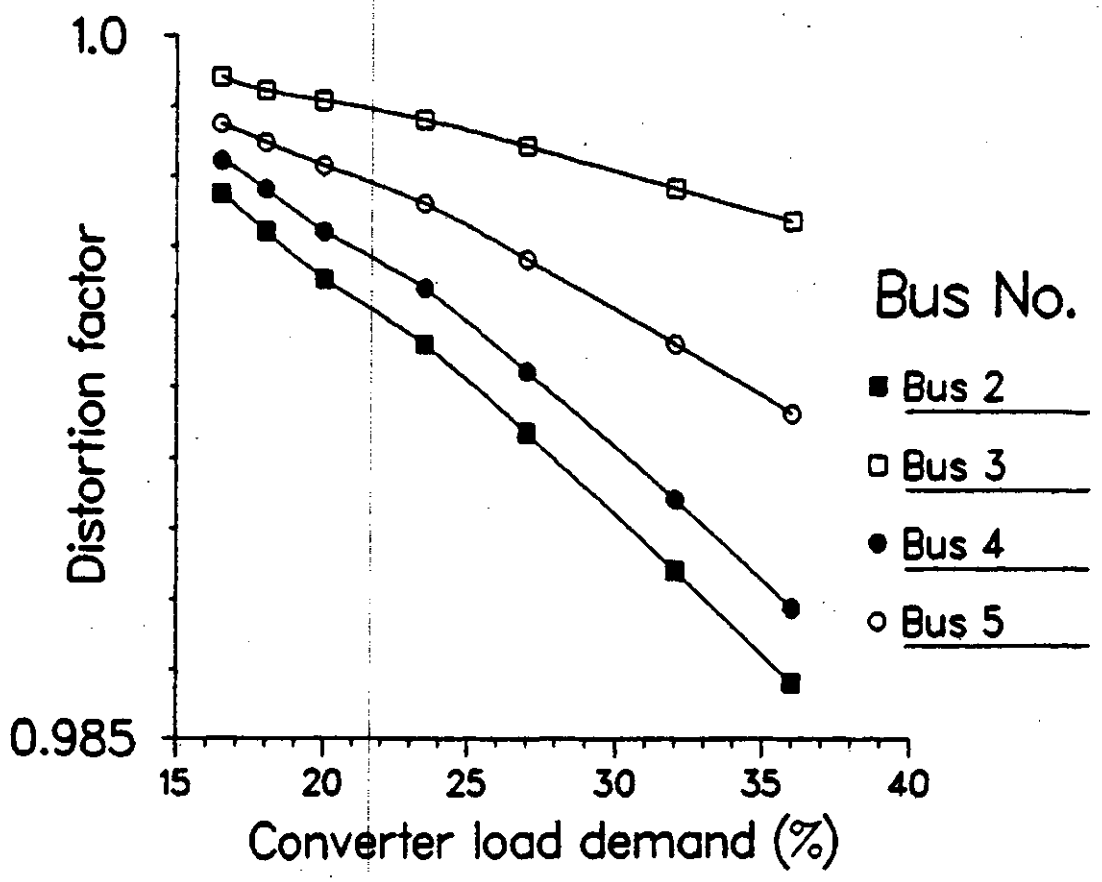

Figure 5.14: Effect of the converter load on the distortion factor.

The standing wave has a maximum of 16 percent voltage for fifth harmonic at about 60% of the line length from the bus 4. The standing wave for the 11th harmonic has a minimum of 0.5 percent voltage at about 35 percent of the line length from the bus 4. Total length of the line between buses 2 and 4 is 250 Kilometers. The next longest line between bus 1 and bus 2 also exhibits a slight standing wave for the 11th harmonic order. The line between buses 1 and 3 shows a more predictable result, i.e. the voltage monotonically increases toward a bus closer to the rectifier load. The voltage profile for the remaining lines, not shown here, is similar to that of the line 1-3.

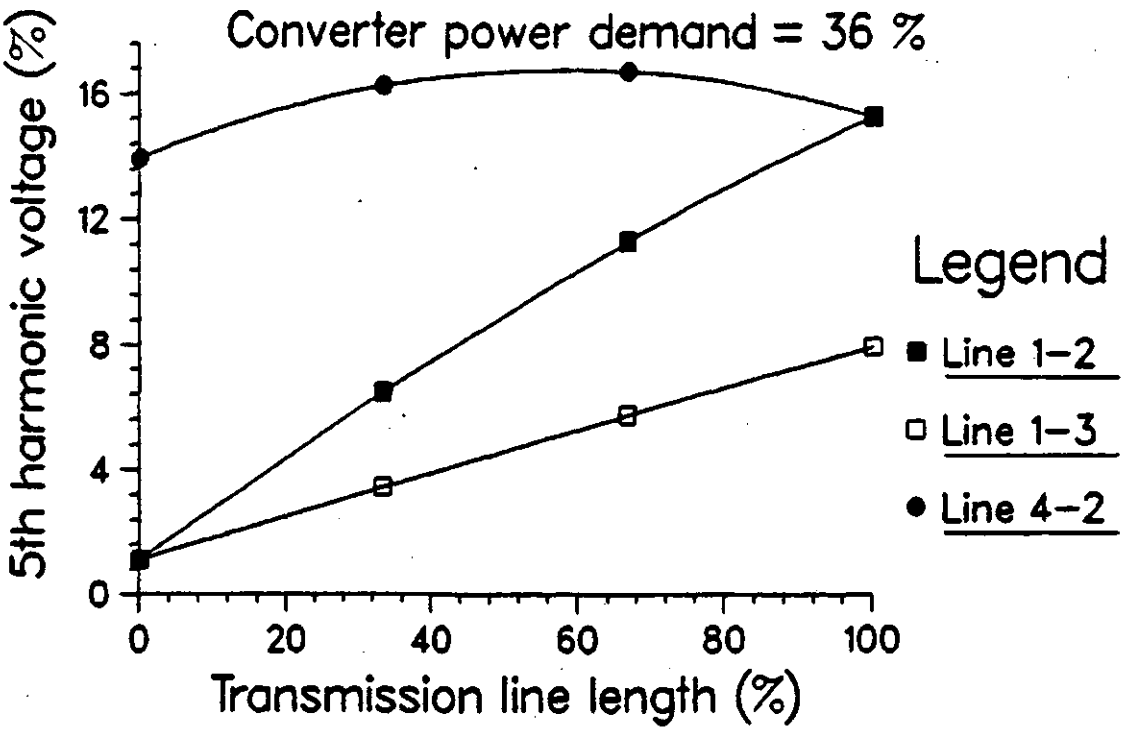

Figure 5.15: Transmission line harmonic voltage profiles for the 5th harmonic order.

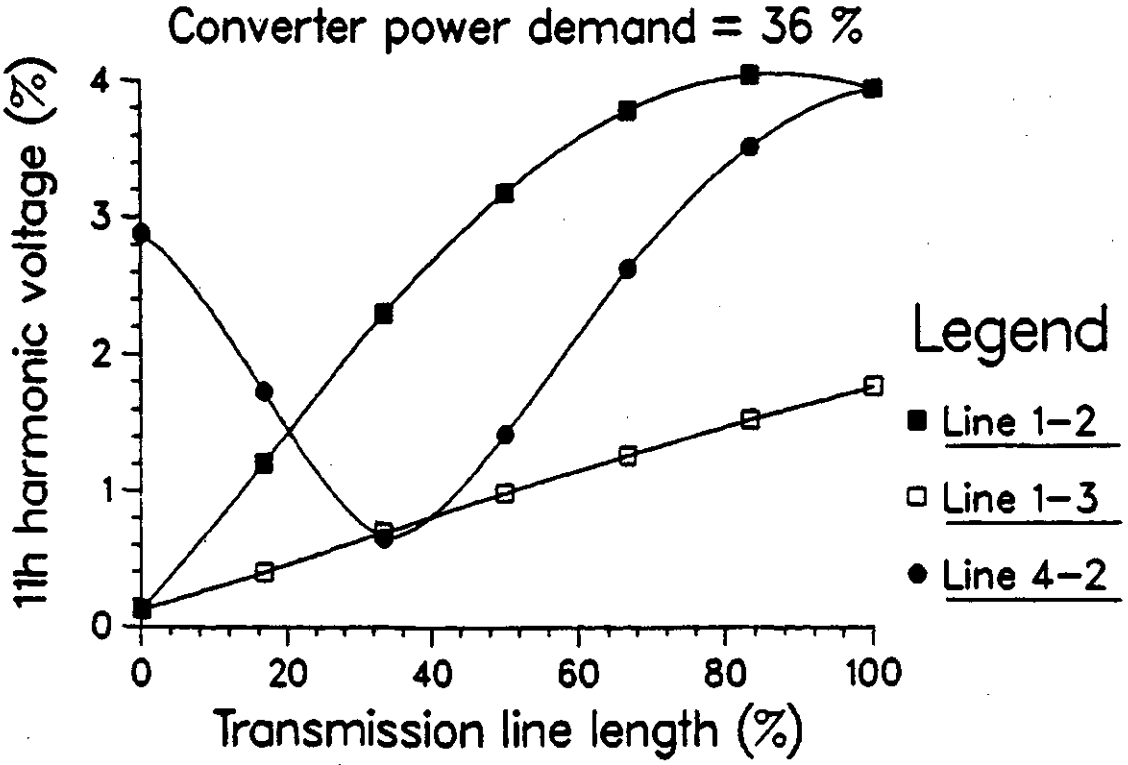

Figure 5.16: Transmission line harmonic voltage profiles for the 11th harmonic order.

5.3.2. Test A2: variation of delay angle of the converter

The output voltage of an ideal converter is directly proportional to the cosine of the delay angle of the converter. Therefore, the rectifier load and hence the rectifier line current harmonics injected into the power system also vary with the delay angle of the converter. In addition, there are secondary effects in an actual converter. These effects are due to the finite commutation delays involved and also because the magnitude of the harmonic current injected by the converter changes with the change in the operating point of the converter. In this test, the effects of the delay angle of the converter on the harmonic voltage profiles of the transmission lines were studied. The dc load side parameters were kept constant for this test.

The results found are similar to those of Test A1, since the change in delay angle of the converter indirectly changes the rectifier load. As an example, Figures 5.17 and 5.18 illustrate the fifth and thirteenth harmonic voltages. The levels of the harmonic voltages are larger for the smaller values of the delay angle and smaller for the larger values of the delay angle. The dc side voltage of the converter is proportional to the cosine of the delay angle less the voltage drop across the rectifying device and the commutation voltage loss. Therefore, a smaller value of firing angle results in greater power demand of the converter. A larger value of delay angle is synonymous with the less load demand, for the output voltage of the converter is reduced as the delay angle is increased.

The thirteenth harmonic voltages tend to go up again when the delay angle is larger than 55 degrees. This is due to the fact that commutation delay affects the magnitude of the harmonic currents in a non-linear manner and the thirteenth harmonic current is smaller at a delay angle of 55 degrees (about 0.88%) than at delay angle of 65 degrees (about 1.07 %). The commutation delay is different than the delay angle of the converter. The former refers to the finite amount of delay involved in commutation of the

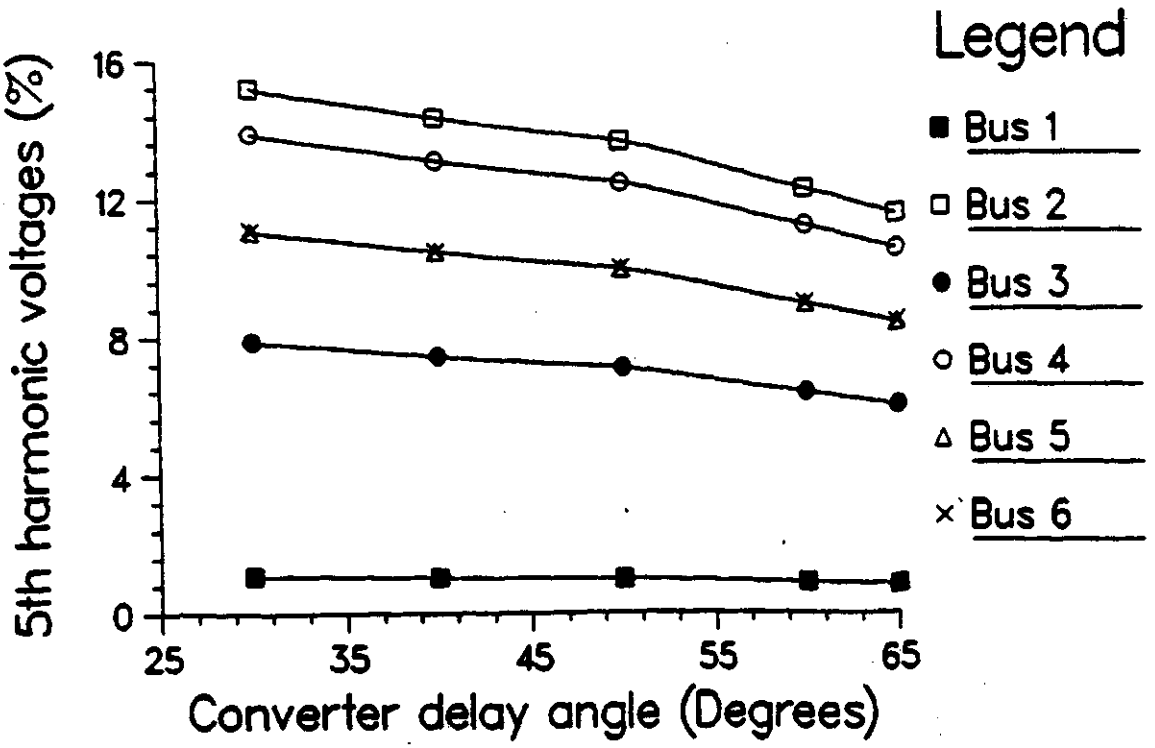

Figure 5.17: Effect of the delay angle of the converter on the fifth harmonic voltages.

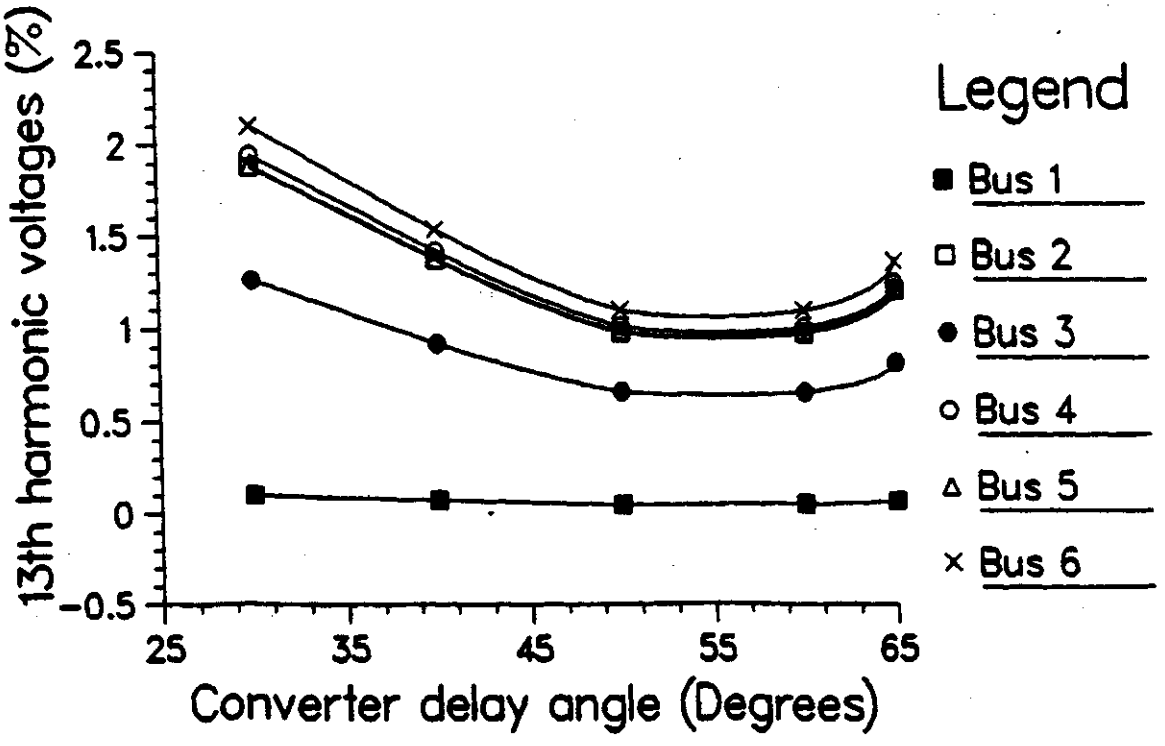

Figure 5.18: Effect of the delay angle of the converter on the thirteenth harmonic voltages.

conducting device by the on-coming device. Whereas the delay angle is the firing instant of the rectifier device measured with respect to the natural instant of conduction in each phase. The commutation delay decreases with the increase in delay angle of the converter as shown in Figure 5.19.

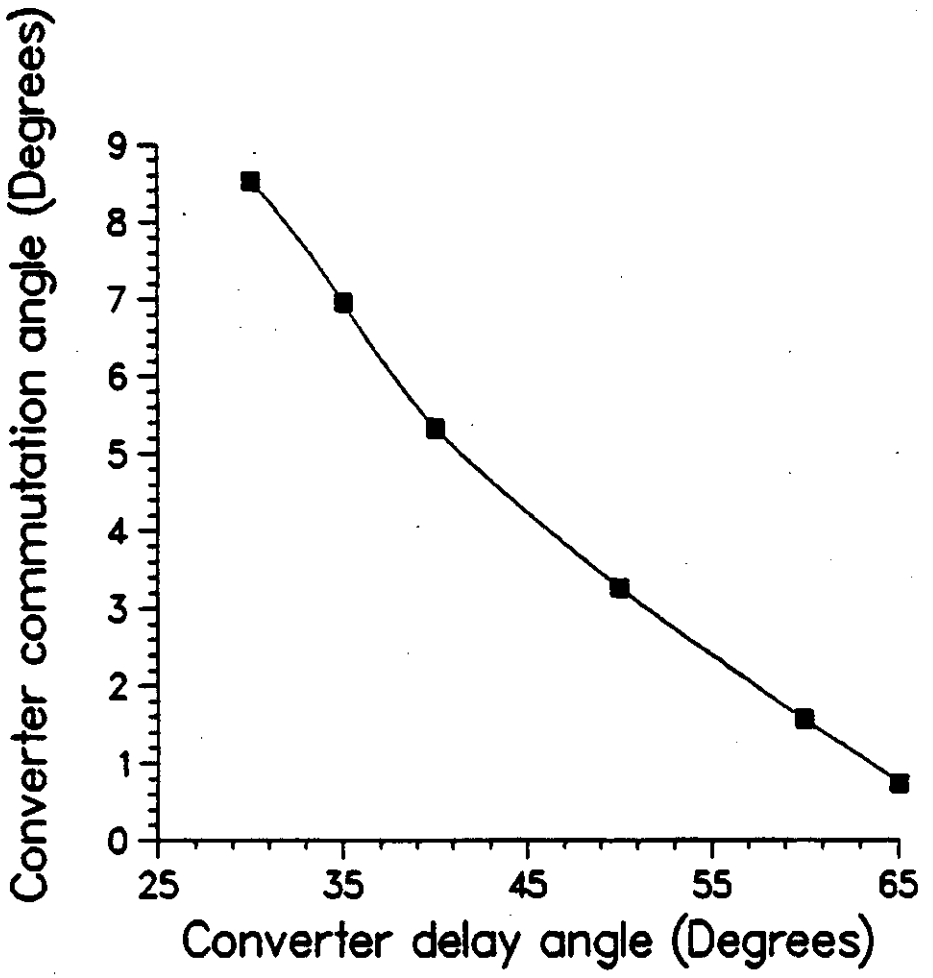

Figure 5.19: Effect of the delay angle of the converter on its commutation angle.

The transmission line L2 or L7 between buses 2 and 4 again exhibits a standing wave pattern for all values of the firing angle. As an example Figure 5.20 illustrates the line voltage profiles for the 11th harmonic order when the delay angle is 60 electrical degrees. The results are similar to those of Test A1 except that the magnitudes are smaller.

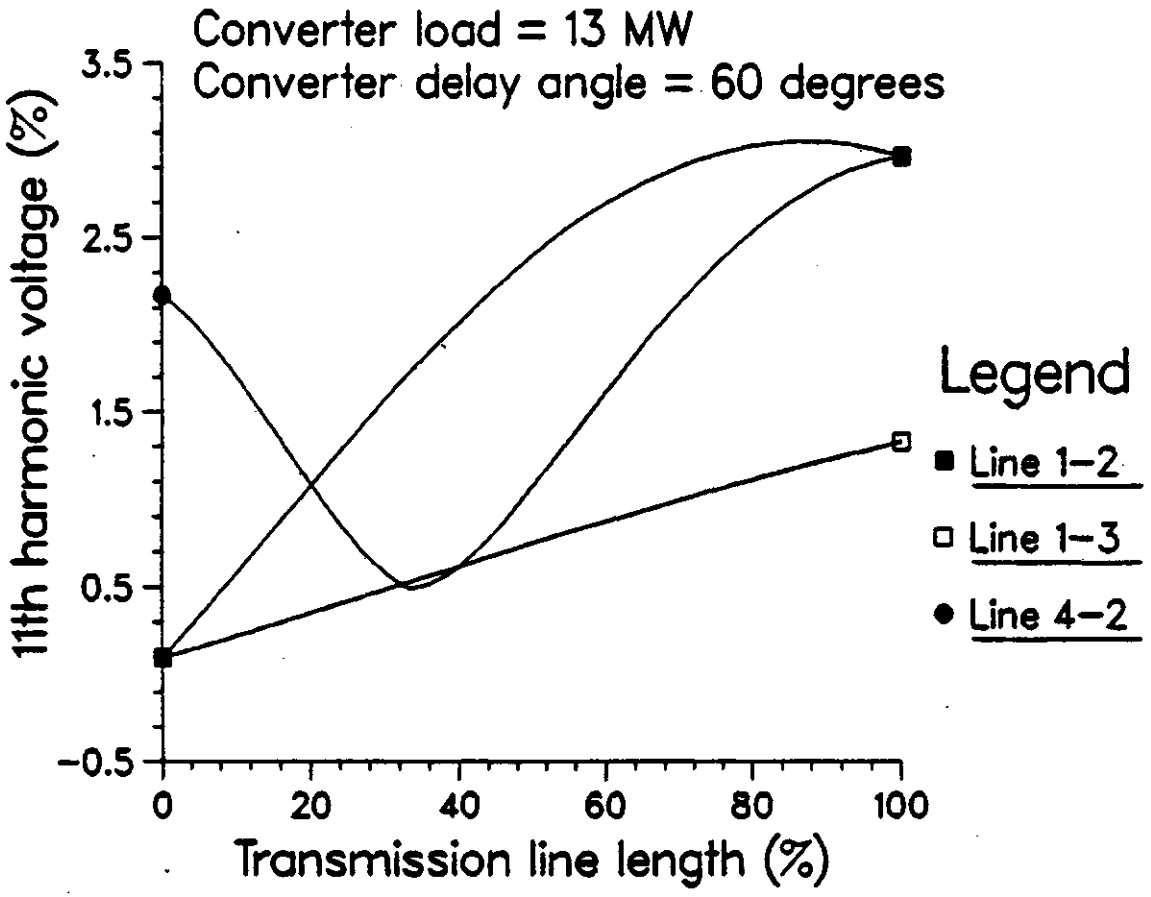

Figure 5.20: Transmission line voltage profiles for the 11th harmonic order(delay angle = 60°).

5.3.3. Test A3: variation of VAR compensation at buses 3 and 4

In this test, the resonance effect due to the variation of shunt reactive impedance was studied. The VAR compensation was applied at buses 3 and 4. The range of the compensation varied form 10 % through 50 % of the base value. The shunt capacitances were assumed to be connected in grounded wye configuration. Some highlights of the results are presented here. During this test the firing angle of the converter and the dc load parameters were kept constant. The delay angle and the dc load were chosen from the past tests such that the maximum harmonic current levels were injected.

Attention should be drawn to the fact that with the increased value of

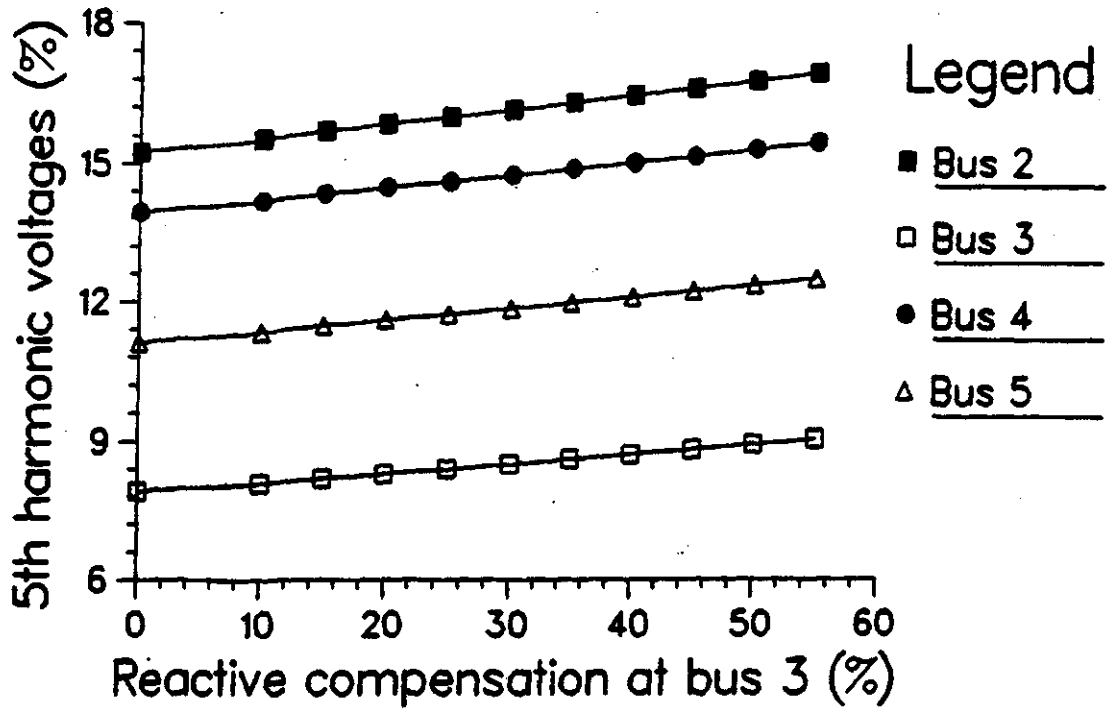

Figure 5.21: Effect of VAR compensation at bus 3 on the fifth harmonic voltages.

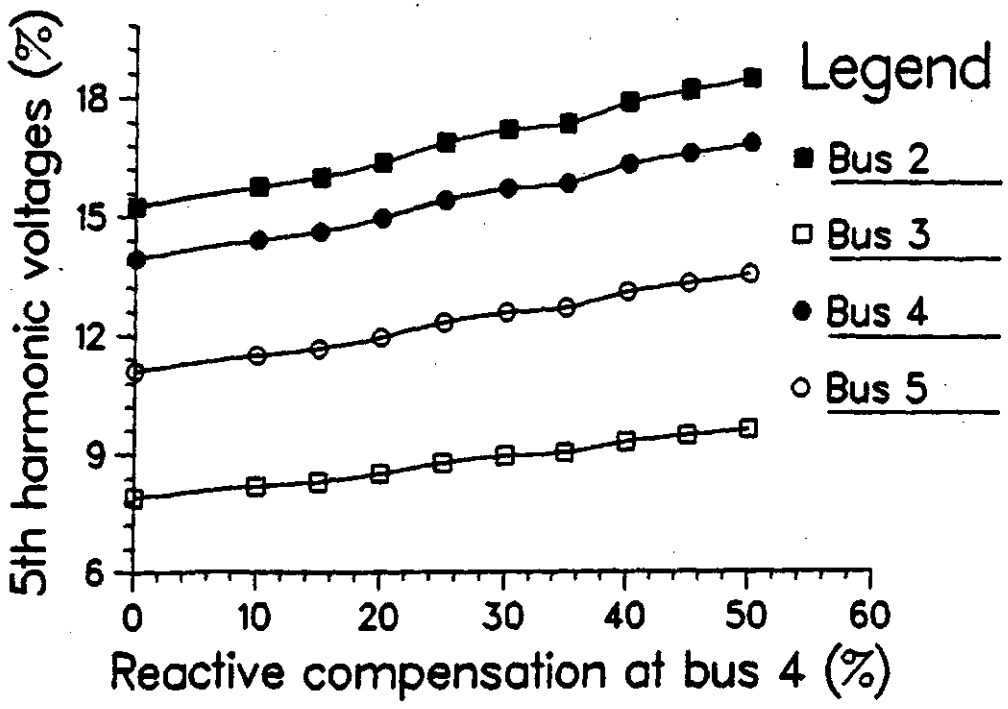

Figure 5.22: Effect of VAR compensation at bus 4 on the fifth harmonic voltages.

compensation, the voltage at the converter node is strengthened. As a result the power at the converter node, operating with same delay angle, increases. During some of the simulated tests the converter transformer was found to be in an over-loaded condition. The maximum over-load was 25 percent at the maximum VAR compensation of 50 percent.

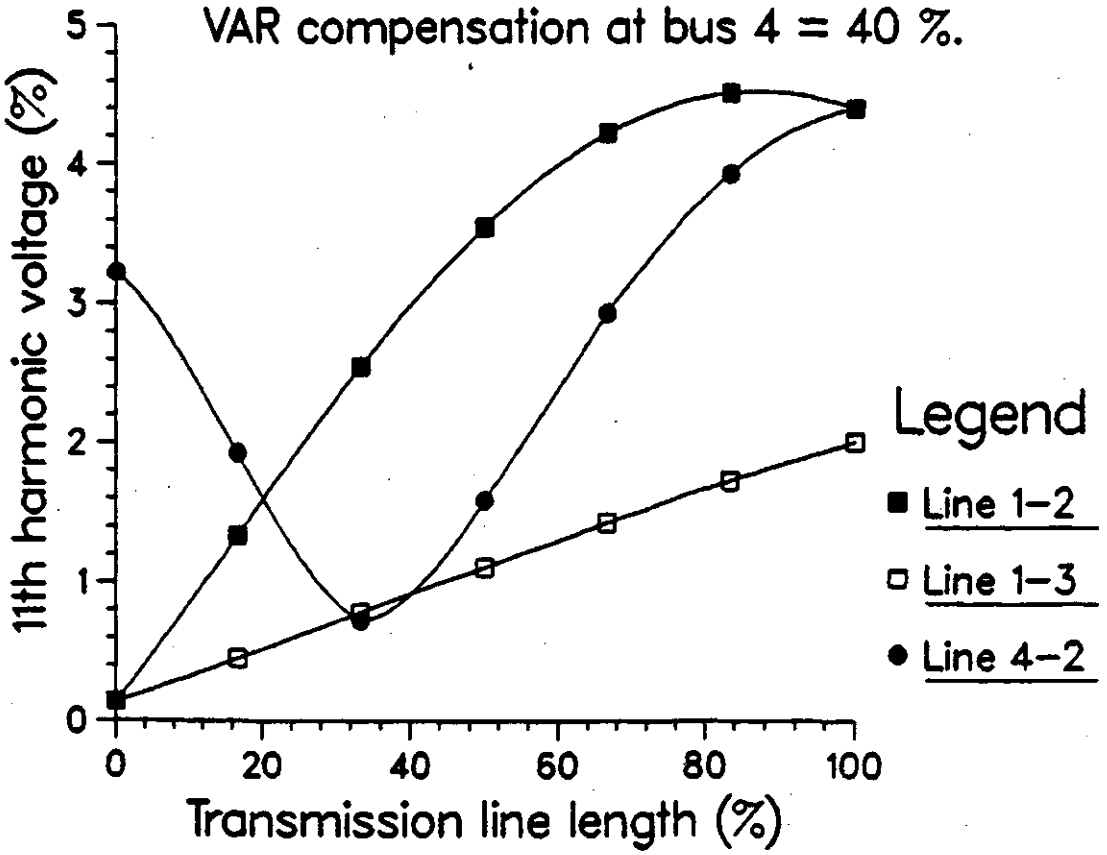

Figure 5.23: Transmission line voltage profiles for the eleventh harmonic order.

Figure 5.21 and 5.22 illustrate the 5th harmonic voltages at the system buses when the compensation was applied at bus 3 and bus 4 respectively. The harmonic voltages tend to go up due to the increased compensation. The base operating point of the converter was chosen such that the harmonic current injection was maximum when no compensation is applied. By applying the compensation, the power consumed at the converter was further increased. This caused an even higher harmonic current injection and the harmonic voltage tended to be larger. Nevertheless it is seen that no resonance

takes place within the range of the compensation. Similar conclusions were obtained for the higher order harmonics. The transmission line between bus 2 and bus 4 again exhibited a standing wave pattern due to its long length. Figure 5.23 demonstrates the example case of the eleventh harmonic for the compensation of 40% at bus 4.

5.4. SPC Test System

The next example was based on the Saskatchewan Power Corporation[81] transmission system. A six bus system, shown in Figure 5.24, comprises three generating stations namely Poplar River(PR), Boundary Dam(BD) and Queen Elizabeth(QE). The buses are numbered as shown in parentheses in Figure 5.24. Lumped loads were considered at all the substations and generating stations. The load at Regina (RG) substation (bus 6) includes both linear and non-linear loads. The non-linear load at Regina substation is a six-pulse converter load.

The transmission line data, the generator data and the load data for this system are given in Tables 5-4, 5-5, and 5-6 respectively. The data is represented on a base of 100 MVA. The converter load installed at bus RG(6) is a natural commutated rectifier in the 40 MVA, 25 KV class. The converter transformer is a 230 KV/25 KV, 40 MVA, three phase, grounded wye to delta and the per unit reactances on a 100 MVA base are shown in Figure 5.24. Two tests were carried out by varying the rectifier load and by varying the VAR compensation at Regina substation (bus 6).

5.4.1. Test B1: variation of rectifier load

This test was similar to Test A1 of the previous example. The rectifier load demand (MW) was varied by varying the dc load impedance. The harmonic content of the current was affected by different load condition and as a result harmonic voltage profile on the transmission system was affected.

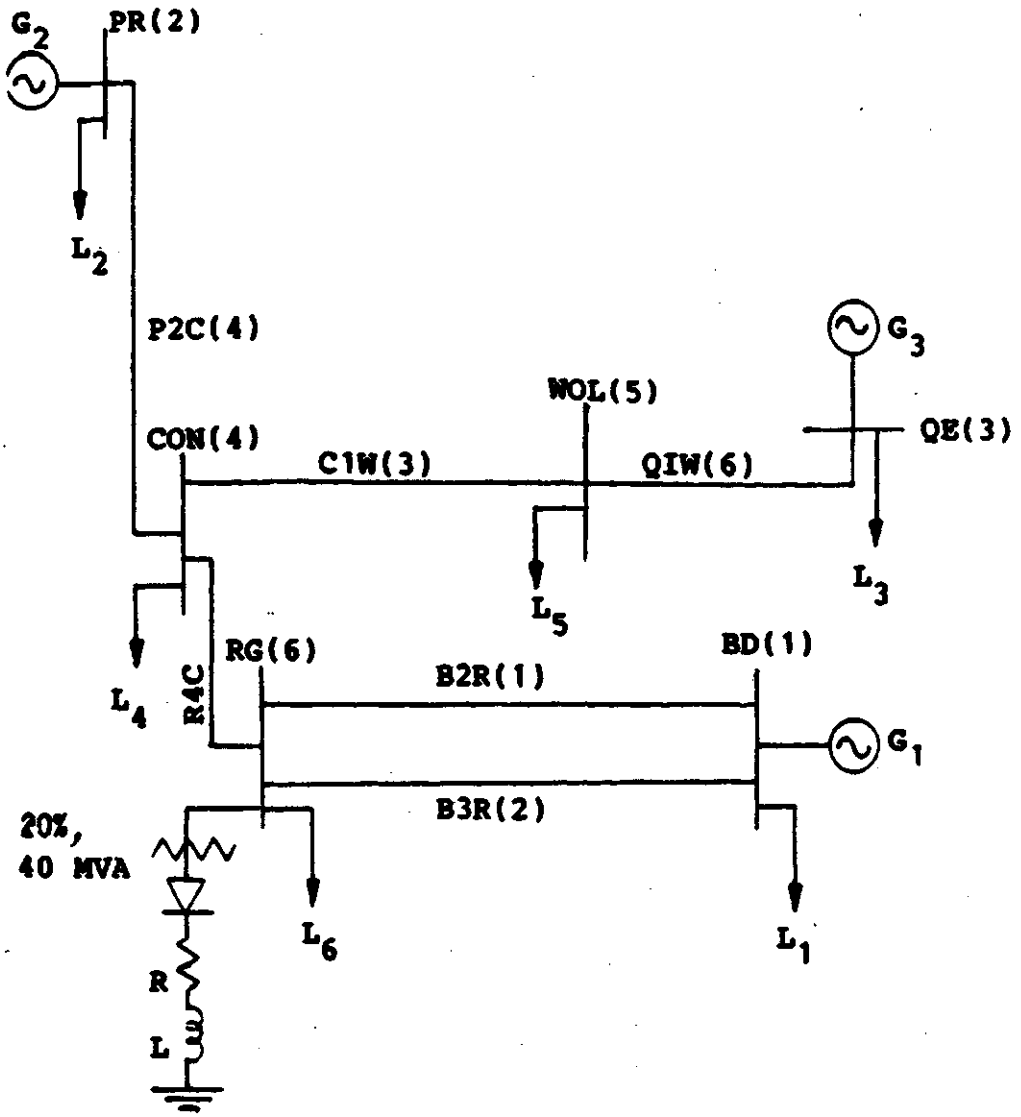

Figure 5.24: Single line diagram of the SPC system.

The results of this test are shown in Figures 5.25 through 5.27. Figure 5.25 shows the fifth harmonic voltages and Figure 5.26 illustrates the seventh harmonic voltages. Figure 5.27 demonstrates the transmission line harmonic voltage profile for the fifth harmonic order at a rectifier load demand of 28.5 MW. The results are more or less predictable except that Wolverine and Condie substations suffer the most distortion even though the harmonic generating load is at the Regina substation. Queen Elizabeth and Poplar generating stations, on the other hand, suffer least from the harmonic distortion. The harmonic voltages at all buses for both fifth and seventh harmonic orders increase with the increased load. The bus voltages for higher harmonic order are not plotted, for their magnitudes are smaller and their patterns are similar to those of the 5th harmonic.

Table 5-4: Transmission line data for SPC example.

Line No.	Line Name	Line Length (KM)	Positive Sequence Impedance (per unit) R	X	B
1	B2R	182.8	0.0210	0.1212	0.4506
2	B3R	182.8	0.0210	0.1212	0.4506
3	C1W	158.5	0.0172	0.1428	0.2909
4	P2C	174.4	0.0151	0.1134	0.437
5	R4C	21.4	0.0023	0.0181	0.0362
6	Q1W	104.6	0.0913	0.2651	0.0685

Table 5-5: Generator data for SPC example.

Generator No.	Connected Bus Name	Negative Sequence Impedance (per unit) R	X
1	BD	0.000603	0.037343
2	PR	0.000897	0.054236
3	QE	0.002160	0.096514

Table 5-6: Load data for SPC example.

Load No.	Connected Bus Name	Load in per unit Real	Reactive
1	BD	0.798	0.177
2	PR	0.250	0.100
3	QE	2.709	0.680
4	CON	0.608	0.0545
5	WOL	0.419	0.075
6	RG	2.65	0.54

The transmission network has two appreciably long lines namely the line between Boundary Dam (BD) and Regina (RG) substations and line between Condie (CON) and Wolverine (WOL) substations. The line between Wolverine and Condie

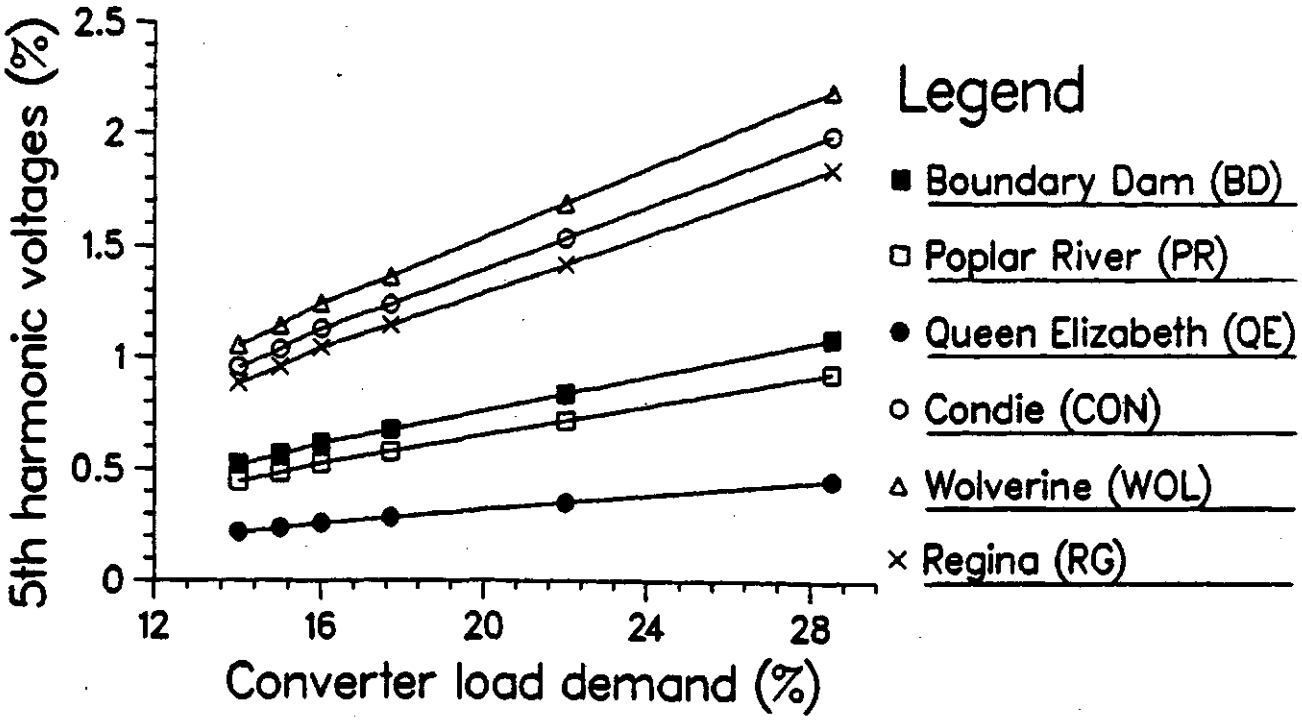

Figure 5.25: Effect of the converter load at bus RG (bus 6) on the 5th harmonic Voltages.

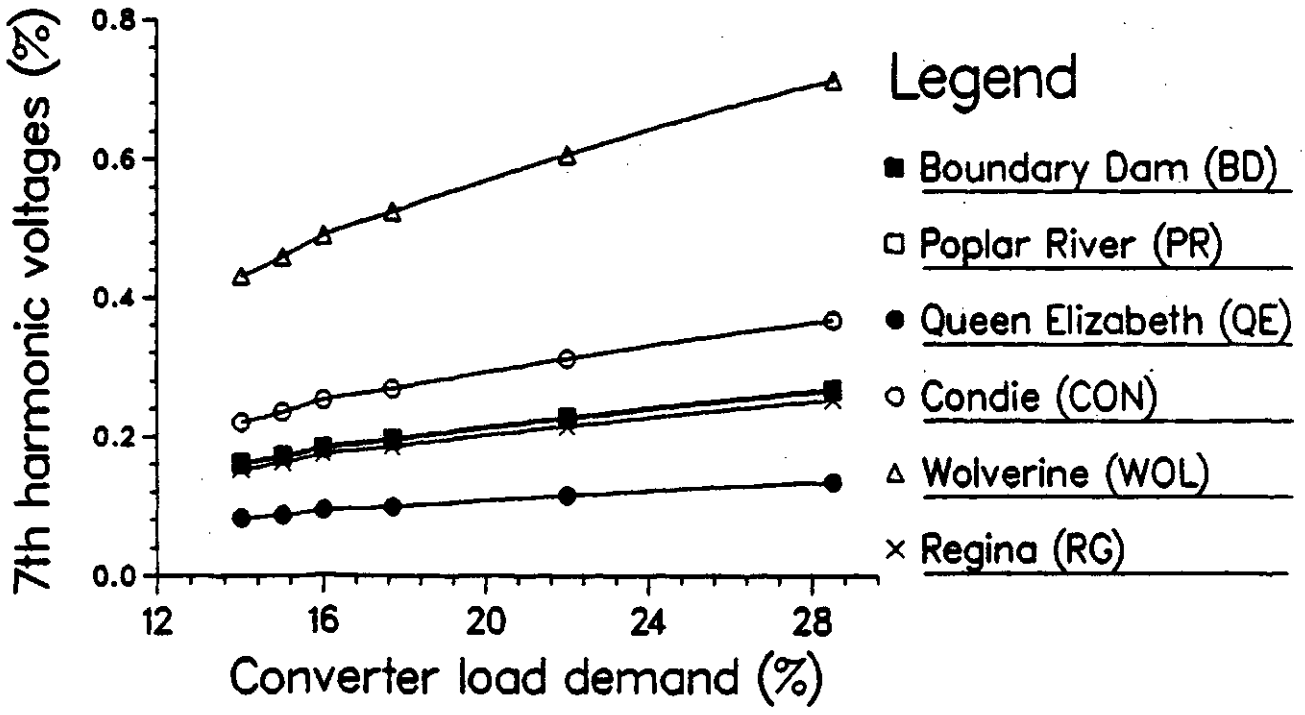

Figure 5.26: Effect of the converter load at bus RG (bus 6) on the 7th harmonic voltages.

substations has a slight standing wave as shown in Figure 5.27. The maximum of the fifth harmonic voltage profile occurs at about 60 percent of the line length from Condie (CON) substation. The remaining lines are short and do not exhibit any standing wave pattern.

5.4.2. Test B2: variation of VAR compensation at bus RG

The VAR compensation was applied at bus RG (6) by varying a shunt capacitive reactance. The shunt capacitive reactances are assumed to be connected in grounded wye configuration. This test was carried out to study the filtering or resonance effect of the shunt capacitive reactance. Due to local VAR compensation, the voltages at the system load buses tend to be higher. Since converter parameters, such as delay angle and the dc side load paramters, remain unchanged, the power consumption at the converter node tends to be higher.

Figure 5.28 shows the fifth harmonic bus voltages for this test. The magnitudes of the harmonic voltages increase by small amounts mainly due to the increased power consumption. Nevertheless the fifth harmonic voltage curves are much flatter indicating the filtering effect of the capacitive compensation. The magnitudes are larger as compared to those seen in Test B1. This is due to the fact that the rectifier load was chosen such that the maximum harmonic current injection took place when the compensation was absent.

Similar results are seen for the 7th harmonic voltages as shown in Figure 5.29. The filtering effect is more pronounced for the 7th harmonic order. The harmonic voltages remain relatively constant even though the power is increasing at the converter node due to the increased compensation. The transmission line voltage profile for the 7th harmonic order is shown in Figure 5.30. Except for two transmission lines between Queen Elizabeth and Wolverine substations and between Condie and Regina substations, all lines exhibit a slight standing wave pattern. The length of the lines which exhibited standing waves is greater than 158 km.

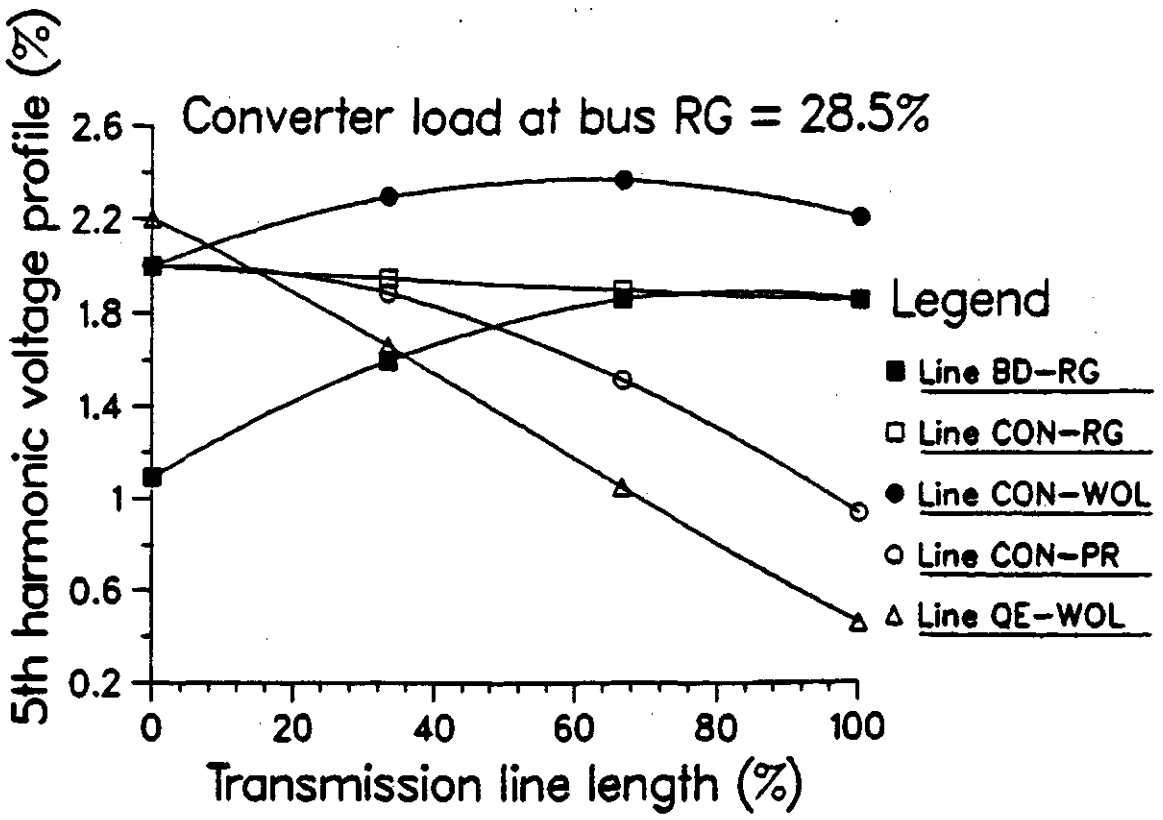

Figure 5.27: Transmission line voltage profile for the 5th harmonic order.

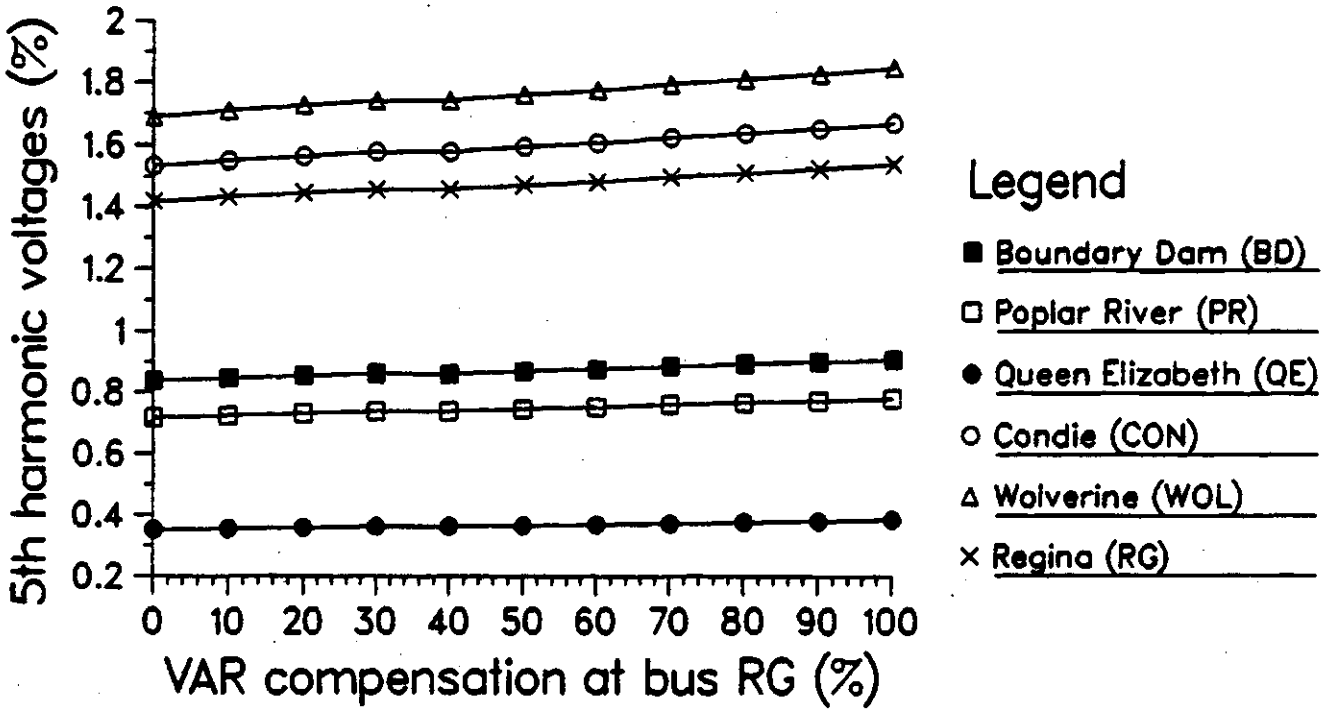

Figure 5.28: Effect of VAR compensation at bus RG on the fifth harmonic voltages.

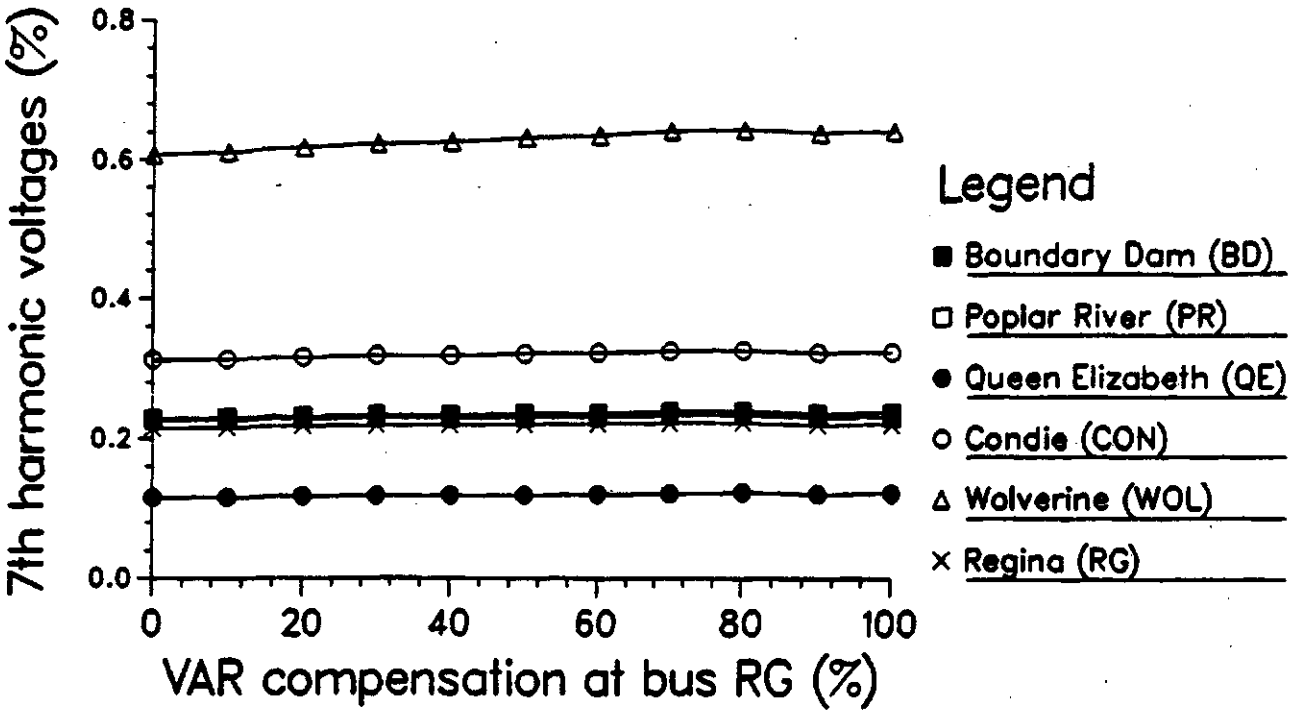

Figure 5.29: Effect of VAR compensation at bus RG on the seventh harmonic voltages.

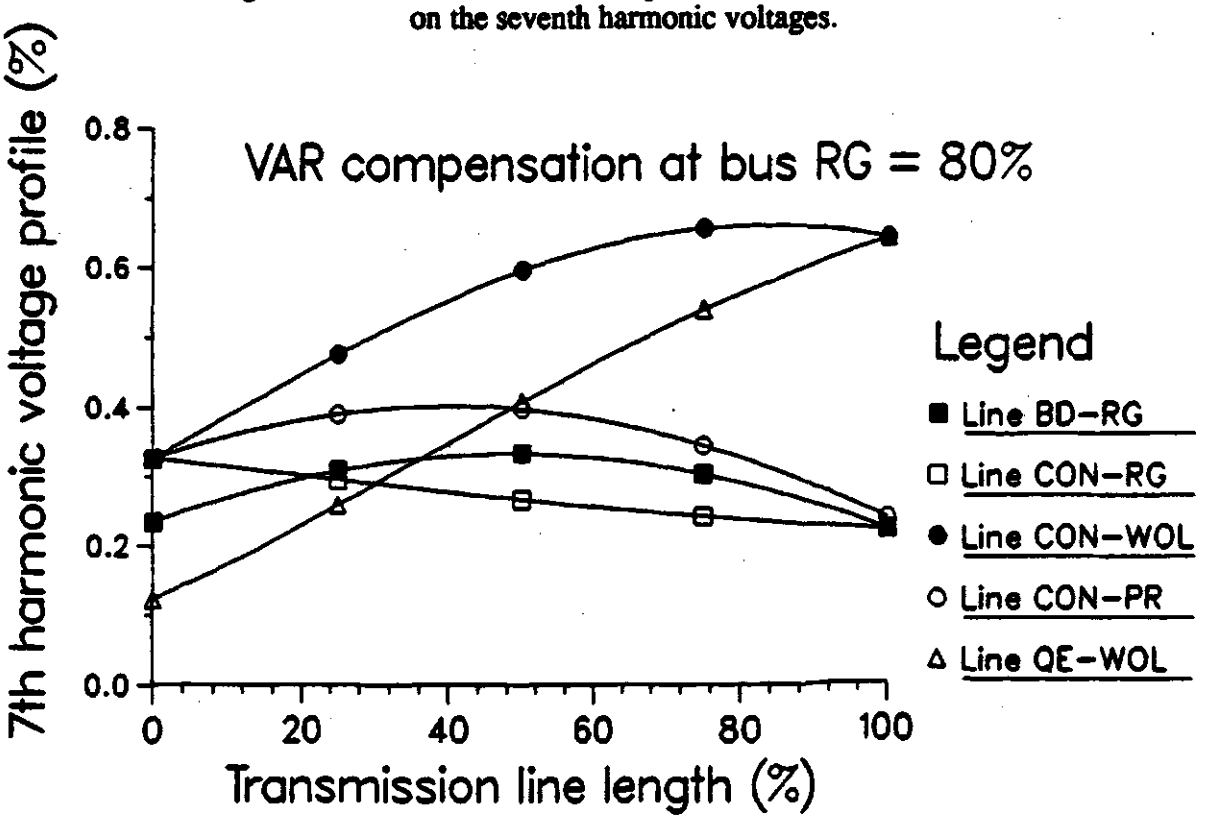

Figure 5.30: Transmission line harmonic voltage profiles.

5.5. Industrial Test System

Finally an industrial test system[34] comprised of 13 buses was chosen for the analysis. The system voltage was 69 KV and the load included both linear and non-linear types. As shown in Figure 5.31 there were three rectifier buses (nodes) energised through a short overhead 69 KV circuit. The substations PS1, PS2, and PS3 were energised through short lines from three supply buses ROC1, TAP, and CLT2. The transmission line between ROC230 and CLT230 is a short line of approximately 71 km. This circuit was energised at 230 KV. This system was taken from reference 34, where the complete description of the system can be found. The relevant data is given in Figure 5.31. All the values are in per unit on a 100 MVA base.

This example was chosen particularly to illustrate the use of the methodology to determine the harmonic voltages at various nodes in an industrial power system. The lines are short and hence the voltage profiles are not of much significance. Also there are three converters in the system and their interaction can also be studied simultaneously. All three converters are 30 MVA, 13.2 KV supplied by 30 MVA, 69 KV/13.2 KV transformers. The transformer configuration was grounded wye to delta as shown in the system diagram in Figure 5.31.

5.5.1. Test C1: variation of VAR compensation at bus CAP

There was capacitive VAR compensation installed at the bus CAP as shown in Figure 5.31. To illustrate the application of the methodology for this example, a test was carried out by varying the shunt capacitive compensation at bus CAP. The compensating capacitors were connected in the grounded wye configuration. The effect of varying compensation is shown in Figures 5.32 through 5.34. The seventh and eleventh harmonic bus voltages stay steady with the compensation and the distortion factor gets better with the compensation. The filtering effect of the compensation is pronounced. The

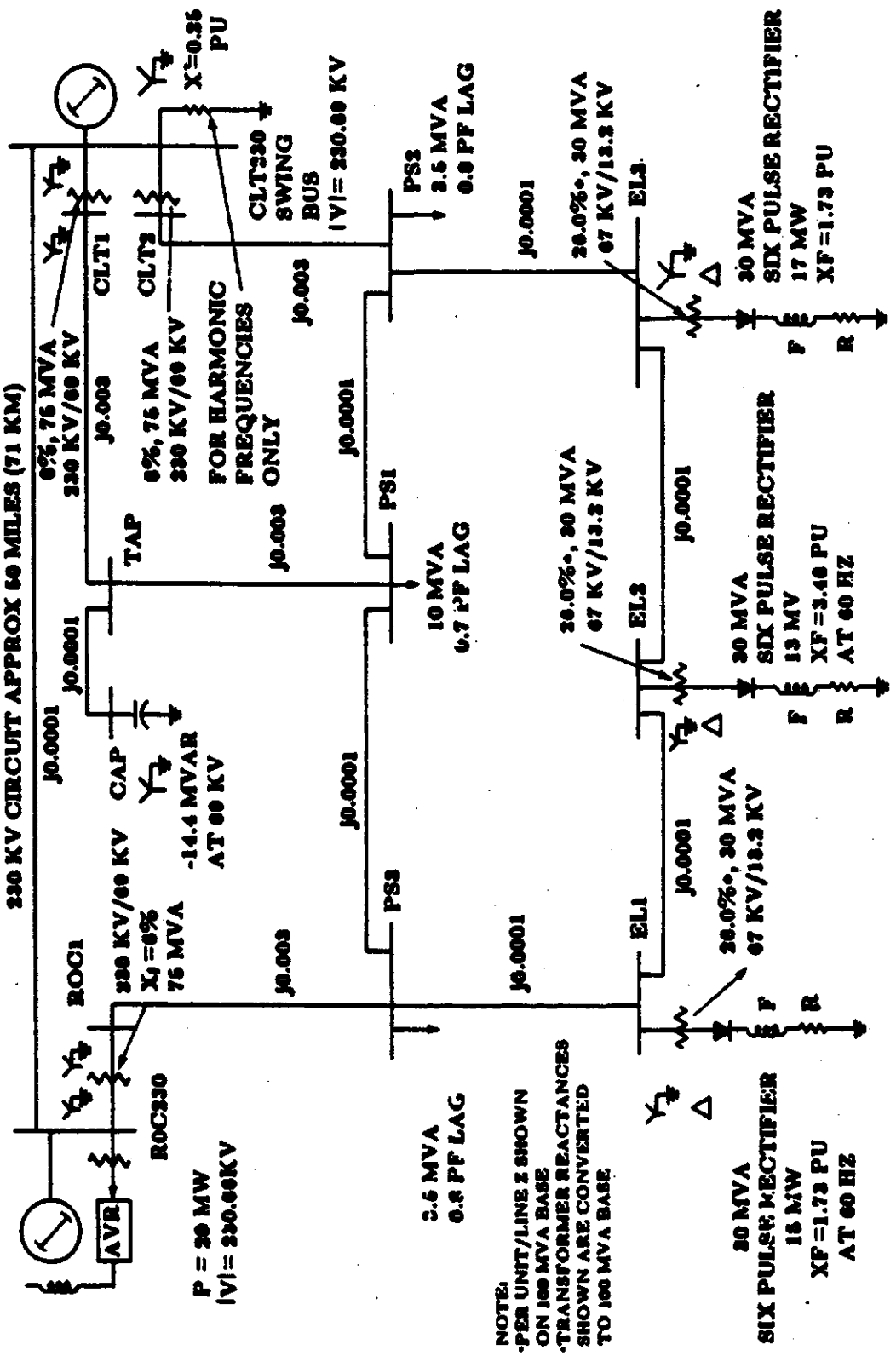

Figure 5.31: Single line diagram of the industrial power system.

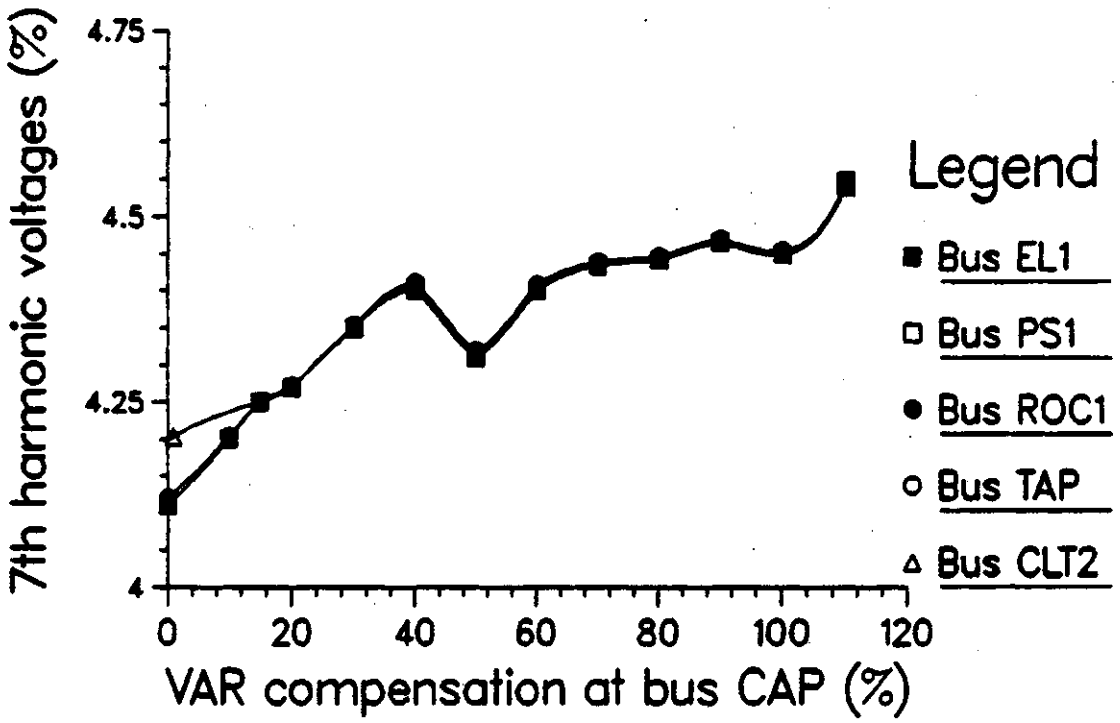

Figure 5.32: Effect of VAR compensation on the 7th harmonic voltages.

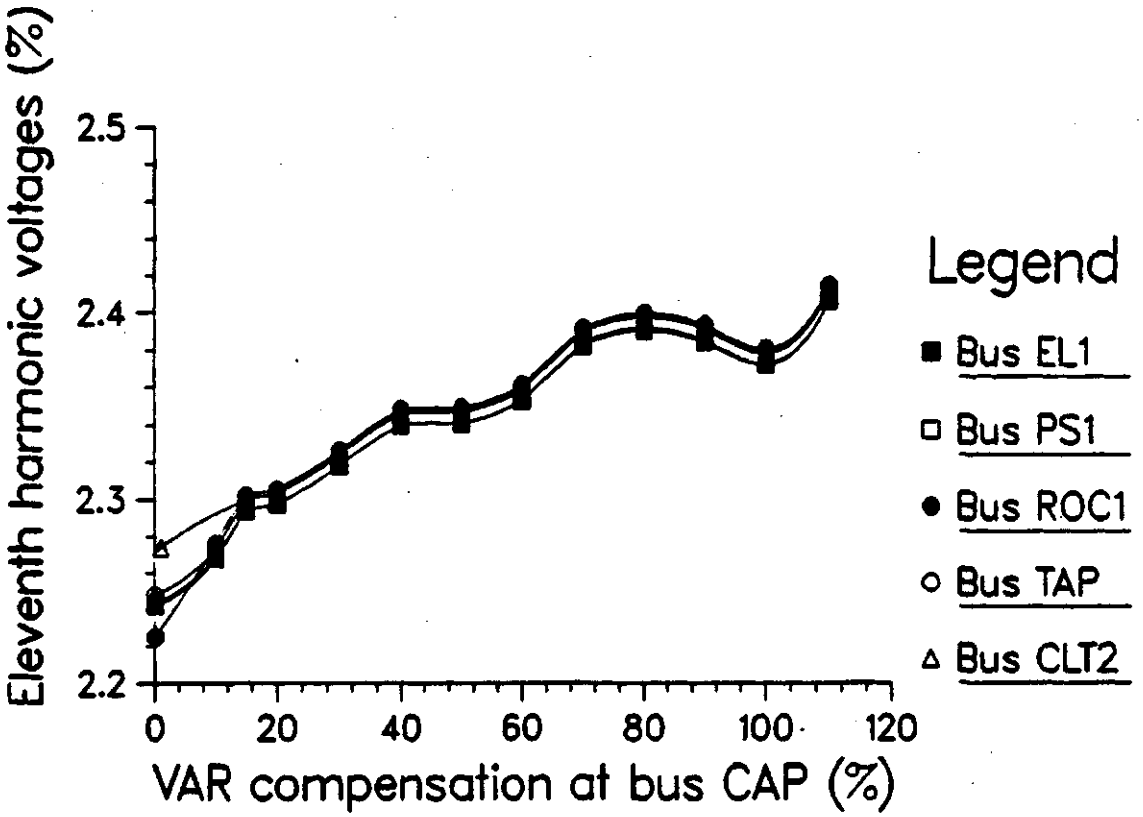

Figure 5.33: Effect of VAR compensation on the 11th harmonic voltages.

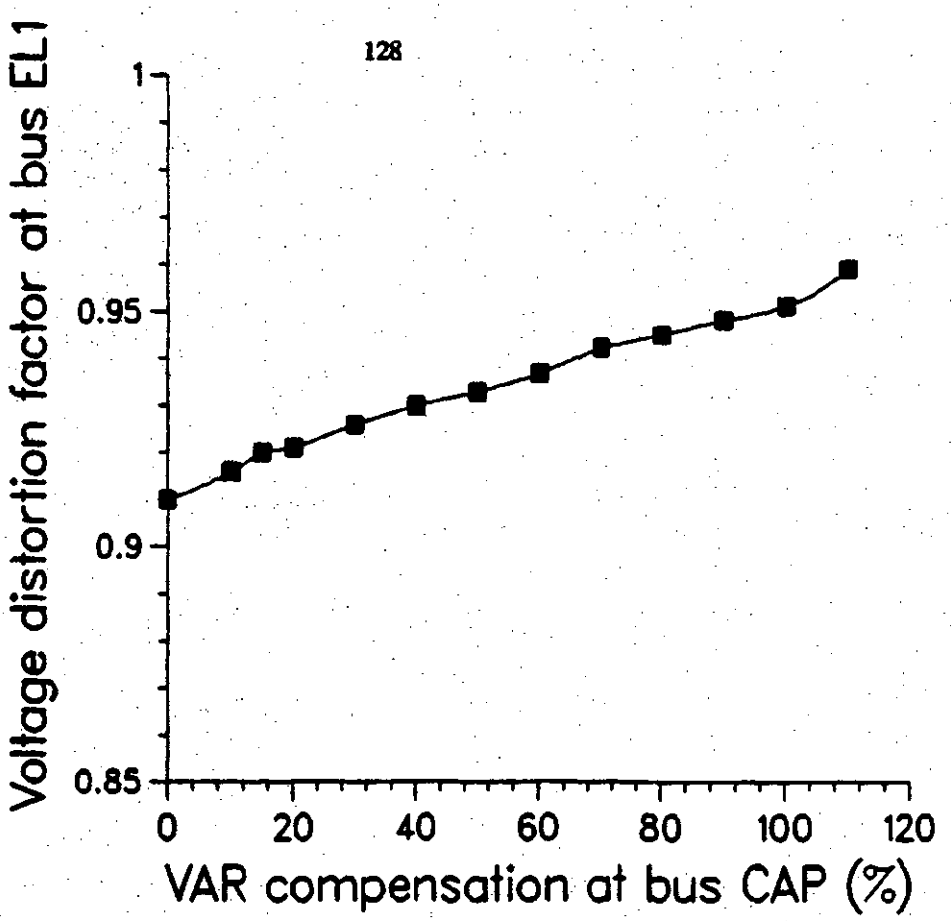

Figure 5.34: Effect of VAR compensation on voltage distortion factor at bus EL1.

slight increase in the harmonic voltages at buses is due to the increase in the harmonic current injection at larger value of VAR compensation.

The results are plotted for buses CLT2, ROC1, TAP, PS1, and EL1. Since the system is interconnected through short lines, voltages at all the buses follow the same pattern. Other buses not plotted here exhibit the same response as well.

5.6. Conclusion

In Chapter 5, various studies carried out on examples of power systems ranging from a network comprised of long transmission lines to a small industrial network are reported. The iterative methodology adopted to simulate the harmonic current penetration is shown to give satisfactory results. To prove the accuracy of the program, a simple five bus example system is taken from the literature. The results are shown to agree within 1% of the published results. The published results[32, 33, 34] were obtained through a

different methodology than the one proposed here. The close agreement between the results of two different methodologies provides credibility for the method used in this thesis.

It is also shown that the program is capable for the study of the filtering and resonance effects of shunt VAR compensation. Although the VAR compensation used is obtained through the use of the capacitors only, one can use a filter arrangement e.g. an inductance and capacitor filter. It is also shown that the program is capable of giving other relevant information about the operation of the converter such as its commutation angle.

The program makes use of the virtual buses in the system and as a result the transmission voltage profile is made available. As shown in this chapter such information can be used to investigate the standing wave pattern on transmission lines and to identify the points of maximum and minimum voltages on the transmission lines.

The distortion factor obtained gives the information as to the nature of the voltage waveform at a system node. Such information is of vital importance to a protection engineer in order to design an optimum protection system and avoid its malfunction due to harmonics. The distortion factor can also be used to monitor the pollution of the frequency of the power system. Distortion factor of 1 indicates single frequency of the power system. A lower value of distortion factor indicates a heavily polluted power system from the point of view of frequency.

The program is capable of giving many types of information about the harmonic character of the power system. Examples of several types information, available from the algorithm, are shown in this chapter. Different case studies are used to illustrate different example information that can be obtained. Other information that can be easily obtained is the bus impedance table for characteristic harmonic frequencies such as the one

shown in Table 5-7. The results shown in Table 5-7 are the impedance seen by the converter while looking into the power system for the first example of five bus system. The frequency and impedance table such as the one given here can also be used to determine the resonance and filtering effects. Smaller impedance signifies the filtering effect and a large impedance signify a resonance condition for that frequency. The seventh harmonic impedance is the largest for the case when the capacitive reactances at buses 3, 4, and 5 are -j1.0 p.u., -j1.0 p.u., and -j0.6 p.u. respectively. The bus 4 voltage exihibits the same behaviour as seen in Figure 5.2 and 5.4. As shown in Table 5-7 the system impedance is largest at fifth harmonic frequency when the capacitive reactance at bus 3 is -j0.4 per unit. The bus 4 voltage profile, shown in Figure 5.7, also exhibit a resonance condition at this value of the capacitive reactance.

Table 5-7: Bus impedance at harmonic frequency for five bus system.

Capacitive Reactances at Bus 3 = -j1.0 p.u., at Bus 4 = -j1.0 p.u., and at Bus 5 = -j0.6 p.u.

Frequency Hertz	Harmonic Order	Impedance of the System Seen from the Converter Bus Percent of Base Impedance	Degrees
240	5	11.88	71.79
420	7	57.71	-24.32
660	11	2.97	-66.65
780	13	3.84	50.08
1020	17	7.98	-21.66

Capacitive Reactances at Bus 3 = -j0.4 p.u.

Frequency Hertz	Harmonic Order	Impedance of the System Seen from the Converter Bus Percent of Base Impedance	Degrees
240	5	23.37	21.36
420	7	1.57	-22.85
660	11	4.47	-92.56
780	13	7.45	66.71
1020	17	10.21	84.88

6. CONCLUSIONS AND RECOMMENDATIONS

6.1. Introduction

In this chapter the concluding remarks are made pertaining to the investigation presented in this thesis. A summary of objectives achieved in this project is included. The present status of the program is highlighted. Some general and specific conclusions pertaining to the problem of harmonic signals present in the power system are given. Also included are difficulties associated with such investigations and the limitations of the program developed.

6.2. Summary

The overall objective of these studies was to develop an algorithm to compute the transmission line voltage profile for harmonic frequencies in the power system transmission network. Due to the complexities of different frequency planes, it was also the objective to get an accurate distortion factor on the power system buses and employ a simple methodology based upon the Fourier principles. In general these objectives have been met.

As described in Chapter 1, the harmonic signals have been present in power systems since their inception; however, the magnitudes were limited. As seen from the past literature, the investigations have mostly been from the point of view of impact of harmonics on communication networks. It is with the recent rapid increase in use of the solid state power conditioning equipment that the incident level of the harmonic signals has increased several fold. It has now become imperative to investigate their impacts on the quality of the voltage waveform and on the power system equipment. Most of the earlier investigations pertain to the measurement of the harmonic signals. Analysis techniques have been developed lately as described in the literature review in Chapter 1.

All the pieces of equipment used in the power system network are potential sources of harmonic generation. As shown in Chapter 2, the ac/dc power conditioning equipment such as a six-pulse fully controlled rectifier is largely responsible for most of the harmonic pollution of the power system. The impact of the current harmonics from the 12-pulse and higher order rectifiers is somewhat less due to the fact that the order of characteristic harmonics is higher. The impact is aggravated if there are large number of such devices installed on a power system.

There are other major sources of harmonics such as arc furnaces, power inverters, arc welding equipment, fluorescent lighting equipment. Arc furnaces give rise to varying harmonics and do not produce a stationary harmonic spectrum. Power inverters, used to integrate alternate energy sources onto the power grid, may cause extensive pollution of the frequency depending upon the control strategy. A square wave inverter system will give rise to lower order harmonics whereas a pulse width modulation method of inversion produces high frequency harmonics. A power inverter configuration is not used extensively these days, but it has the potential of being a viable system in future. Several other types of load mentioned in Chapter 2 are found extensively on a distribution network. Another noteworthy point is that the harmonics injected by rectifiers are of a stationary nature meaning that the harmonic spectrum does not vary with time whereas the harmonic spectrum of an arc furnace, on the other hand, is highly variable during various phases of operation of the furnace.

A discussion on the limitations of the fundamental load flow studies is also presented in Chapter 2. Due to the criterion of mismatch of power or voltage for the convergence of the solutions of the load flow equations, it is used at fundamental frequency only, since a source is capable of supplying power at the fundamental frequency only.

In Chapter 3, the concept of harmonic power flow is illustrated. Generators in a power system network are sources of all the power demand of the system, therefore it is obvious to ask how does the harmonic power arise. Harmonic power flow can be visualised as the power flowing to satisfy the demand of the current waveform at the converter load; i.e. the harmonic current flowing from source to load. This visualisation makes use of an erroneous assumption i.e. the source is capable of supplying harmonic current. In this thesis, this erroneous assumption is circumvented by considering the converter a source of energy. It is considered as a form of an energy conversion device which consumes energy from the source at the fundamental frequency and converts majority of that energy into useful energy on the dc load side and a fraction of that energy into harmonic energy that flows back into the ac network.

The knowledge of harmonic power is not known initially and hence no power flow algorithm can be used in the same manner as the implementation of the fundamental load flow. The initial information known to us is the current waveform or the current harmonic spectrum demand of the converter. This forms the first step of computation in the proposed non-linear frequency domain analysis. As described in Chapter 3, from the initial estimates the harmonic voltages at buses and the harmonic power flow are computed from the system admittance matrix. A new estimate of the converter current waveform is obtained from the newly obtained bus voltages, so on and so forth the process is iterated until the convergence is obtained.

In order to determine accurately the harmonic voltage distortion in the power system, an accurate model of the converter is desired. A detailed model of the converter, including the impact of the finite commutation delay, is given in Chapter 3. Since the performance of the converter is affected by the harmonic spectrum of the voltage at the converter bus, an iterative method is employed. The methodology presented takes

account of all the parameters of the system including the converter transformer resistance. In the case of a power transformer, a greater simplification can be achieved in the converter equations if the resistance of the transformer is neglected.

The voltage and current experience a phase shift in a three phase transformer. The amount of the phase shift is different for different harmonic frequency. An admittance matrix of a transformer is obtained by considering it as a phase shifting transformer. This necessitates the use of a virtual bus for each transformer in the system.

The transmission line models used are equivalent pi models obtained from the travelling wave equations. In order to obtain the voltage profile on a transmission line, it is subdivided into several equivalent pi's. The number of pi's included is arbitrarily chosen to be half as many as the harmonic order.

It is also shown through a laboratory experiment that the impedance of the synchronous generator for harmonic analysis is the negative sequence impedance appropriately scaled for the harmonic frequency of concern. Models of other power system equipment given in Chapter 3 are selected from the published literature. The application of the superposition theorem is reasoned out in the light of the fact that the delay angle of a rectifier is kept constant for an analysis. This argument is valid for off-line calculations used for the study of the worse impact of harmonics injected from rectifiers.

The conventional concept of energy flow in an electrical system denotes the notion of active power and reactive power. The active power or active energy follows the laws of conservation of energy and therefore its definition is valid under any circumstances. The definition of the reactive power, however, needs to be modified to accommodate the distortion power of the converter. As shown in Chapter 4, the distortion

power can not be easily separated from the net reactive power. Also the total volt-ampere demand of the converter, including reactive, distortion, and active power, is supplied by the source at the fundamental frequency. While active power gives an indication of the heating loss of the power system, the reactive and distortion power do not serve any purpose from the point of view of this thesis. Therefore both reactive and distortion powers are grouped together in one form of power called non-active power.

For a given operating point (given delay angle and dc load impedance) of the converter, the power demand is going to change with each iteration of the harmonic power flow calculations. Thus a true interaction of the power system network and the converter is obtained by including the load flow program in each iteration as shown in the modified algorithm given in Chapter 4. The criterion for convergence of the overall solution is modified to be the change in the successive power demand at the converter node. An example of convergence of the algorithm is shown in Figure 4.4 in Chapter 4 for a two bus example.

The sparsity of the system equations is exploited by applying the minimum degree algorithm to the Gaussian elimination process. The graphical approach and the linked data structure adopted for the implementation optimises the use of memory allocation.

Finally in Chapter 5 a number of case studies are presented. The examples of power system networks presented range from a transmission network of long lines to a complex industrial network. To show the accuracy of the program, a five bus example is studied. The results are compared with those published in the literature. It is found that for the same condition the results from this technique and the one used in the reported literature agree within 1%.

6.2.1. Present status of the algorithm

A computer program was written to implement the proposed algorithm for the harmonic analysis of a power transmission system. The program reported in this thesis have the following characteristics.

1. The program comprises several modules, namely the fundamental load flow module, the converter module, the Fourier transform module, and harmonic power flow module.

2. The final version of the program is written in the VAX PASCAL Version 3.7 computer language. Although care is taken to use standard PASCAL functions and routines, the use of some non-standard PASCAL functions was unavoidable. Also some in-house library routines are used. The program can be executed successfully on VAX/VMS computers.

3. There are several types of information that can be obtained from the program such as the harmonic bus voltages, the harmonic voltage profiles for the transmission lines, impact of the harmonic bus voltages on the converter performance, the impedance table.

4. The program employs a dynamic data structure rendering itself capable of handling any size of power system network. However it must be brought to the attention of the reader that while the harmonic power flow module employs a dynamic data structure, the other modules such as a load flow program employs a static declaration.

5. Accurate models of converter, transmission line, synchronous generator and phase shifting model of a transformer are implemented.

6. As per the objective of the thesis, the algorithm and the models of the power system equipment used are valid for characteristic harmonics.

7. The initial estimate of the power demand at a converter node should be made accurately by the equations given in Chapter 4(see step 1 of section 4.4), otherwise some convergence problem may be experienced.

6.3. Conclusion

The purpose of this investigation was to analyse a power system transmission network for harmonic voltage profile calculations. The algorithm and tools developed are simple, yet they give satisfactory results as shown in the thesis. The non-linear frequency domain analysis is shown to be an accurate way of investigating harmonic interaction between converters and the power system network. The algorithm is capable of providing information about the standing wave patterns, if any, on transmission lines. Experimental simulation studies were carried out to illustrate the results of the program. It is shown that the program is good for studying the effect of various parameters of the system such as the effect of the rectifier load, rectifier delay angle, and compensating capacitors. The resonance condition and filtering effects are also studied.

Among the information that can be obtained from the program, some of the more important are the voltage distortion factor, bus harmonic voltages, and the transmission line harmonic voltage profile. Other information can also be obtained from the program if so desired, such as the impedance versus frequency table.

In general the algorithm and methodology adopted have given satisfactory results. Some specific highlights of the investigation are as given below.

1. With any rectifier load, the assumption of the sinusoidal bus voltages in a power system is not valid. It is found in the case studies presented that the voltage distortion may be large if the power system is heavily loaded with rectifier load.

2. A simple one time calculation of the harmonic power flow does not give accurate harmonic interaction between the converter and the power system network. An iterative process, as the one given in this thesis, must be used in order to compute an accurate interaction between the power system and the converter.

3. It is not possible to study the interaction of the converter and the power system

by considering one frequency in isolation. The complete interaction can only be studied by including the impact of the compound voltage waveform at the converter bus.

4. The principle of superposition is applicable at the converter nodes as long as the delay angle of the converter is kept unchanged during a test.

5. The worst harmonic voltage distortion could occur somewhere in the middle of the transmission line resulting from a standing wave. This is particularly true if the line lengths are long, say more than 200 KM. The voltage profile is available from the algorithm.

6. The conventional definition of power cannot be used in analysing a power system for the harmonic frequencies. The definition must be modified to include the distortion volt-ampere power at the converter node.

7. It is determined from the investigation that a resonance condition may exist if the capacitors alone are used for VAR compensation. Also it is seen that the distortion volt-amperes cannot be corrected by capacitors alone[82], since a capacitor only provides reactive volt amperes. As a consequence of this, the power factor at a rectifier node can never be unity.

8. Major concerns that arise as a result of the presence of harmonic signals in a power system are (i) amount of the voltage distortion; (ii) the presence of standing waves on the transmission lines; and (iii) harmonic interaction with the protection and communication system. The proposed algorithm is found to give accurate information that can be used to answer these concerns.

6.4. Recommendations for Further Work

Although the present program and algorithm have been proven to give satisfactory results, there are ongoing improvements and further work that need to be done to further obtain a small increment in the accuracy of the results. Some of these recommendations resulting from the experience gained in this study are given below.

Since the power system network entails several types of equipment, it is difficult to include the impact of each of these. It is essentially a process of evolution of a

study and the principal recommendations centre on the development of accurate models of the equipment whose approximate models have been used in this thesis. One of the means to investigate such equipment would be to study them as two port networks excited by controlled harmonic power supplies of desired frequency and voltage.

Another recommendation for future work is to investigate the impact of other harmonic sources such as arc furnaces and arc welding equipment. The incident level of the harmonics on a distribution network is several times more than on the transmission network. In order to study such systems, accurate models of all possible non-linear loads should be included.

The recommendations pertaining to the study presented herein mainly centres on the experience with the program and actual field experimentation and measurement of the harmonic bus voltages. Specifically the following steps should be carried out to gain experience with the program.

1. Measurement of harmonic current spectrum of the converter operating at a known operating point i.e. the known delay angle and the dc load parameters.

2. Measurement of the bus harmonic voltages at or near the converter node and measurement of harmonic voltages at certain discrete points of the transmission line.

3. Measurement of power flow into the converter using digital techniques. The induction watt hour meter is not a valid device for such measurement, because the harmonic orders of 5, 11, 19 give rise to a negative torque[4].

4. The example system used for field tests should be simulated under the same conditions and the results should be compared with the field results.

5. Although the program can handle other harmonic sources if the harmonic current spectrum of such sources were known, however, no efforts have been made to study the dynamic interaction of such devices with the power system network. An example of such a device is a dynamic VAR compensator[83]. Due to the electronic switching involved, they also inject harmonics and at the

same time they act as filters. It is strongly recommended to investigate the validation of the model of dynamic VAR compensators and study their interaction with the power system network.

6. The impact of noncharacteristic harmonics generated[84, 85] from the converter should be studied.

7. Finally the three phase models of the power system network should be investigated for the purpose of studying unbalanced systems. The proposed algorithm assumes a balanced power system network. It is also assumed that the transmission lines are fully transposed and are symmetric. The length of the line between two consecutive transposed ends should be smaller than the wavelength of the frequency of concern.

References

1. Norman, F., Snejdar, C., and Wilkinson, J.R., "Variable Speed Drives in Utility Application", Tech. report, Canadian Electrical Association, Research & Development, Suite 580, One Westmount Square, Montreal, Quebec, Canada, 1983.

2. Mahmoud. A.A., and Grady, W.M., "Power System Harmonics", Tech. report, IEEE Tutrial Course, Course Text, 84 EH0221-2-PWR, February 1984.

3. Stratford, R.P., "Harmonic Pollution on Power System - A change in Philosophy", *IEEE Transaction on Industry Application*, Vol. IA-16, No. 5, Sept./Oct. 1980.

4. Fuchs, F.F., Roesler, D.J., and Alashhab, F.S., "Sensitivity of Electrical Appliances to Harmonic and Fractional Harmonics of the Power System Voltage. Part I: Transformer and Induction Motors". 86 WM 170-5, A paper presented at the Winter Power Meeting, New York, February 2-7, 1986

5. Fuchs, F.F., Roesler, D.J., and Kovacs K.P., "Sensitivity of Electrical Appliances to Harmonic and Fractional Harmonics of the Power System Voltage. Part II: T.V. Sets, Induction Watthour Meters and Universal Machines". 86 WM 171-3, A paper presented at the Winter Power Meeting, New York, February 2-7, 1986

6. Power System Relay Committee, "Sine Wave Distortion on Power Systems and the Impact on Protective Relaying", Tech. report, IEEE Power Engineering Soceity, March 1984.

7. George, A. and Liu, J.W.H., "A Fast Implementation of the Minimum Degree Algorithm Using Quotient Graphs", *ACM Transaction on Mathematical Software*, Vol. 6, No. 3, September 1980, pp. 337-357.

8. Sato, N. and Tinney, W.F., "Technique for Exploiting the Sparsity of the Network Admittance Matrix", *IEEE Transaction on Power Apparatus and Systems*, Vol. PAS-82, December 1963, pp. 944-950.

9. Clinker, C.R., "Harmonic Voltages and Currents in Wye and Delta Connected Transformers", *AIEE Transaction*, Vol. 33, 1914, pp. 723-33.

10. Joint Committee on Inductive Interference, "Report to the Railroad Commission on the State of California", *AIEE Transaction*, Vol. 33, 1914, pp. 1441-1508.

11. Peters, J., "Harmonic in Transformer Magnetizing Currents", *AIEE Transaction*, Vol. 34, 1915, pp. 2157-2195.

12. Read, J.C, "The Calculation of Rectifier and Inverter Performance Characteristics", *Journal of IEE*, Vol. 92 Pt II, 1945, pp. 495.

13. Kloss, Albert, *A Basic Guide to Power Electronics*, John Wiley & Sons, New York, 1985.

14. Kimbark, E.W., *Direct Current Transmission, Vol - I*, Wiley - Interscience, New York, 1971.

15. Osborne, H., "Discussion of harmonics in Transformer Magnetising Current", *AIEE Transaction*, Vol. 34, 1915.

16. Morgan, T., Bairos, C., Kimball, G., "The Triple Harmonic Equivalent Circuit - Three Phase Power Transformer Banks", *AIEE Transaction*, 1933, pp. 64-74.

17. IEEE Power System Harmoinics Working Group, "Bibliography of Power System Harmonics, Part I", *IEEE Transaction on Power Appratus and System*, Vol. PAS-103, No. 9, September 1984, pp. 2460-2469.

18. IEEE Power System Harmoinics Working Group, "Bibliography of Power System Harmonics, Part II", *IEEE Transaction on Power Appratus and System*, Vol. PAS-103, No. 9, September 1984, pp. 2470-2478.

19. CEA, "Interference to Telecommunication Systems from Power Systems", Tech. report, Canadian Electric Association, June 1984, CEA report 84-168TD32

20. IEEE Committee, *Guide for Harmonic-Control and Reactive Compensation of Static Converters*, 1981, IEEE Standard No. 519-1981

21. Halley, B.R., "Calculating AC Harmonics Generated by Non-Linear Power Converter", Master's thesis, Electrical Engineering, Purdue University, August 1982, M.Sc. Thesis

22. Emanuel, A. E., "Harmonic Generators Modeling and Harmonic Power Flow in Power Systems", *Second International Conference on Harmonics in power Systems Proceedings, Winnipeg, Manitoba, Canada*, October 6-8 1986.

23. Dewan, S. B., and Kankam, D. A., "Method for Harmonic Analysis of Cycloconverters", *IEEE Transaction on Industry and General Application*, Vol. IGA - 6, Sept. 1970, pp. 455-62.

24. Barton, T.H., *Pulse Width Modulation Waveforms - The Bessel Approximation*, 1982, Class Notes, University of Calgary, Calgary, Canada

25. Arrillaga, J., Bradley, D.A., and Bodger, P.S., *Power System Harmonics*, John Wiley & Sons, New York, 1985.

26. Mahmoud, A.A., and Shultz, R.D, "A Method for Analyzing Harmonic Distribution in A.C. Power Systems", *IEEE Transaction on Power Apparatus and System*, Vol. PAS-101, No. 6, June 1982, pp. 1815 - 1824.

27. McGraw_Edison Company, United Technologies Corporation, and system Control Inc., "Study of Distribution System Surge and Harmonic Charactreristics", Tech. report, Electric Power Research Institute, November 1980, EPRI EL-1627, Project 1024-1, Final Report

28. Hingorani, N.G., "Simulation of AC System Impedance in HVDC System Studies", *IEEE Transaction on Power Apparatus and System*, Vol. PAS-89, No. 5/6, May/June 1970, pp. 820-826.

29. Stratford, R.P., "Analysis and control of Harmonic Current in Systems with Static Power Converters", *IEEE Transaction on Industry Application*, Vol. IA-17, No. 1, January/February 1981.

30. Ortmeyer, T.H., "Harmonic Analysis Methodology", *IEEE PES Tutorial Course*, February 1984, pp. 74-84, Course Text 84 EH0221-2-PWR

31. Coi, B.T., "Fast Steady-State Solution for HVDC Analysis", *IEEE Transaction on*

Power Apparatus and System, Vol. PAS - 99, No. 6, November 1980, pp. 2453-2460.

32. Xia, D., Heydt, G.T., "Harmonic Power Flow Studies Part I- Formulation and Solution", *IEEE Transaction on Power Apparatus and System*, Vol. PAS-101, No. 6, June 1982, pp. 1252-1265.

33. Xia, D., Heydt, G.T., "Harmonic Power Flow Studies Part II- Practical Application", *IEEE Transaction on Power Apparatus and System*, Vol. PAS-101, No. 6, June 1982, pp. 1266-1270.

34. Heydt, G.T., Grady, W.M., Xia, D., "Harmonic Power Flow Studies Volume 1: Theoretical Basis", Tech. report, Electric Power Research Institute, November 1983, EPRI EL-3300, Project 1764-7, Final Report

35. Pilleggi, D.J., Chandra, N.H., Emanuel, A.E., "Prediction of Harmonic Voltages in Distribution Systems", *IEEE Transaction on Power Apparatus and System*, Vol. PAS-100, No. 3, March 1981, pp. 1307-1313.

36. Stevenson, W.D., *Elements of Power System Analysis*, McGraw Hill Book Co. New York, 1968.

37. Anderson, Paul, *Analysis of Faulted Power Systems*, Iowa State Uiversity Press, Ames, Iowa, 1973.

38. Shepherd, W., and Zand, P., *Energy Flow and Power Factor in Nonsinusoidal Circuits*, Cambridge University Press, Cambridge, U.K., 1979.

39. Rashid, M.H., *Power Electronics Circuits, Devices, and Application*, Prentice Hall, Englewood Cliffs, New Jersey, 1988.

40. Hoft, R.G., *Semiconductor Power Electronics*, Van Nostrand Reinhold Co. New York, 1986.

41. Dewan , S.B., and Straughen, A., *Power Semiconductor Circuits*, John Wiley and Sons, New York, 1975.

42. Finney, David, *The Power Thyristor and its Applications*, McGraw Hill Book Co. New York, 1980.

43. Pelly, B. R., *Thyristor Phase-Controlled Converters and Cycloconverters*, John Wiley and Sons, New York, 1971.

44. Dubey, Gopal K., *Power Semiconductor Controlled Drives*, Prentice Hall Inc. Englewood Cliffs, New Jersey, 1989.

45. Williams , J.K., *Power Thyristor and its Applications*, John Wiley and Sons, New York, 1989.

46. Bowles, J.P., "Alternative Techniques and Optimisation of Voltage and Reactive Power Control at H.V.D.C. Converter Stations", *IEEE Transaction on Power Apparatus and System*, Vol. PAS-100, No. 3, March 1980, pp. 1307-1313.

47. Jahn, H.H., and Kauferle, J., "Measuring and Evaluating Current Fluctuations of Arc-furnaces", *IEE Conference on Sources and Effect of Power System Disturbances*, April 1974, pp. 1307-1313, Conference Publication Number 110

48. Say, M.G., *The Performance and Design of ac Machines; Transformers, Three-phase Induction Machines and Synchronous Machines*, Pitman Paperbacks, London, 1968.

49. Wallace, A.K., Ward, E.S., and Wright, A., "Sources of harmonic currents in slip-ring induction motor", *IEE Proceeding*, Vol. 121, April 1974, pp. 1495-1500.

50. Pilleggi, D.J. and Emanuel, A.E., "Field Experience with Harmonic Injecting Equipment in Distribution Networks", *IEEE Transaction on Power Apparatus and System*, Vol. PAS-101, No. 8, August 1982, pp. 2790-2797.

51. Tschappu, F, "Problems of the exact measurement of electrical energy in networks having harmonic content in the current", *Landis and Gur Review*, Vol. 28, No. 2, 1981, pp. 8-15.

52. Szabados, B., and Lee, J., "Harmonic Impedance Measurements on Transformers", *IEEE Transaction on Power Apparatus and Systems*, Vol. PAS-100, No. 12, December 1981, pp. 5020-5026.

53. Szabados, B., and Hill, E., "On Line Measurements of Power System Harmonics", *IEEE Transaction on Industry Application*, Vol. IA-26, No. 2, July 1977, pp. 170-175.

54. Stagg, G.W., and El-Abiad, A.H., *Computer Methods in Power System Analysis*, McGraw-Hill Book Company, New York, 1968.

55. Goldberg, Saul and Horton, W. F., "The Effects of Harmonics and The Skin Effect on Conductor Losses", *International Power Conference Proceedings*, July 1986.

56. Horton, W.F. and Goldberg, Saul, "Propagation of Harmonics in the Electric Distribution System", *International Power Conference Proceedings*, July 1986.

57. Kennelly, A.E., Laws, F.A., and Pierce, P.H., "Experimental researches on skin effect in condcutors", *AIEE Transaction*, Vol. 34, 1915, pp. 1953-2018.

58. Sharma V.K., and Fleming R.J., "Harmonic Analysis of Power Transmission Network in the Frequency Domain", *Second International Conference on Harmonics in power Systems Proceedings, Winnipeg, Manitoba, Canada*, October 1986.

59. Kimbark, E.W., *Electrical Transmission of Power and Signals*, Wiley & Sons, Inc. New York, 1950.

60. Dommel, H.W., and Marti, J.R., "Overhead Transmission Line Models for Steady State and Transient Analysis", *Presented to Power System Planning & Operation Section, Canadian Electrical Association, Montreal, Quebec*, March 1985.

61. Gardinet, G.E., "Discussion on High Voltage D.C. Transmission", *IEE Conference Publication No. 22, part 2*, September 1966, Conference on High Voltage D.C. Transmission, University of Manchester

62. Arseneau, R. and Szabados, B., "Synchronous Motor Impedances Measured at Harmonic Frequencies", *A Paper Presented at the IEEE PES Summer Meeting, Vancouver, British Columbia, Canada*, July 1979.

63. IEEE Committee, *Test Procedures for Synchronous Machines*, 1983, IEEE Guide: Test Procedure Std 115-1983

64. CIGRE Working Group, "Harmonics, Characteristic Parameters, Methods of Study, Estimating of Existing Values in the Network", *Electra*, 1977, pp. 35-54.

65. McGranaghan, M.F., Dugan, R.C., and Sponsler, W.L., "Digital Simulation of Distribution system Frequency-Repsonse Characteristics", *IEEE Transaction on Power Apparatus and Systems*, Vol. PAS-100, No. 3, March 1981.

66. Berg, G.J., and Hakim, M.M.A., "Dynamic Single Unit Representation of Induction Motor Groups", *IEEE Transaction on Power Apparatus and Systems*, Vol. PAS-95, No. 3, January/February 1976, pp. 155-165.

67. Murotani, K., "Discussion on A Method of Analysing Harmonic Distribution in AC Power System", *IEEE Transaction on Power Apparatus and Systems*, Vol. PAS-101, No. 6, June 1982, pp. 1823-1824.

68. Markgraf, B., Lanrenz, F., and Tyll, H., "Harmonic Characteristics of Static VAR Compensators", *Presented to Power System Planning & Operation Section, Canadian Electrical Association, Montreal, Quebec*, March 1985.

69. Shepherd, W., and Zakikhani, P., "Suggested Definition of Reactive Power for Nonsinusoidal Systems", *IEE Proceedings*, Vol. 119, No. 9, Sept. 1972, pp. 1361-1362, Correspondence

70. Budeanu, C., "The Different Opinions and Conception Regarding Reactive Power in Nonsinusoidal Systems", Tech. report, Rumanian National Institute, Bucharest, 1927.

71. Sachdev, M.S., *Analysis of Composite A-C and D-C Systems*, PhD dissertation, Electrical Engineering, University of Saskatchewan, March 1969, Ph.D. Dissertation

72. Erisman, A.M., "Sparse Matrix Problems in Electric Power System Analysis", *Sparse Matrices and their Uses, a book edited by Iain S. Duff, Academic Press, New York*, 1981, pp. 30-56.

73. George, A., "Direct Solution of Sparse Positive Definite Systems: Some Basic Ideas and Open Problem", *Sparse Matrices and their Uses, a book edited by Iain S. Duff, Academic Press, New York*, 1981, pp. 283-301.

74. Markowitz, H.M., "The Elimination form of the Inverse and its Application to linear programming", *Management Science*, No. 3, 1957, pp. 255-269.

75. Gustavson, F.G., "Some Basic Tehcniques for Solving Sparse Systems of Linear Equations", *Sparse Matrices and their Applications*, Plenum Press, New York, 1972, pp. 41-52.

76. Duff, I.S., "A Sparse Future", *Sparse Matrices and their Uses, a book edited by Iain S. Duff, Academic Press, New York*, 1981, pp. 30-56.

77. George, A. and Liu, J.W.H., "A Minimal Storage Implementaion of the Minimum Degree Algorithm", *SIAM Journal of Numerical Analysis*, Vol. 17, No. 3, April 1980, pp. 282-299.

78. Tremblay, Jean-Paul, and Sorenson, P.G., *An Introduction to Data Structures with Applications*, McGraw Hill Book Co. New York, 1984.

79. Horowitz, E. and Sahni, S., *Fundamentals of Data Strucutres in Pascal*, Computer Science Press, Rockville, MD, 1984.

80. Billinton, R. et. al., "A Reliability Test System for Educational Purposes - Basic Data". 89 WM 035-7, A paper presented at the Winter Power Meeting of IEEE Power Engineering Soceity, New York, January 29 - February 3, 1989

81. Kolla, S.R., "Application of Modal Trnasformation for Fault Analysis and Digital Distance Relaying", Master's thesis, Electrical Engineering, University of Saskatchewan, August 1985, M.Sc. Thesis

82. Garche, Martin, "Correction in Supply System with Harmonic Content", *Energy and Automation*, Vol. VIII, August 1988.

83. Gyugyi, L. and Taylor, E.R., "Characteristics of Static, Thyristor-Controlled Shunt Compensators for Power Transmission System Applications", *IEEE Transaction on Power Apparatus and Systems*, Vol. PAS-99, No. 5, Sept/Oct 1980.

84. Phadke, A.G., and Harlow, J.H., "Generation of Abnormal Harmonics in High Voltage AC-DC Power Systems", *IEEE Transaction on Power Apparatus and Systems*, Vol. PAS-87, No. 3, March 1968.

85. Fengreng, H., and Zhang, J., "Analysis on the Influence of Non-Characteristics Harmonics on the 500 KV SVC Thryistors", *Second International Conference on Harmonics in power Systems Proceedings, Winnipeg, Manitoba, Canada*, October 1986.

86. Parter, S.V., "The Use of Linear Graphs in Gaussian Elimination", *SIAM Review*, No. 3, 1961, pp. 364-369.

87. Rose, D.J., "A Graph Theoretic Study of the Numerical Solution of Sparse Positive Definite Systema", *Graph Theory and Computing*, Academic Press, New York, 1972.

88. Smith, R.L. and Stratford, R.P., "Application Considerations in Handling Effects of SCR Generated Harmonics in Cement Plants", *IEEE Transaction on Industry Application*, Vol. IA-17, No. 1, January/February 1981.

89. Linders, J. R., "Electric Wave Distortions: Their Hidden costs and Containment", *IEEE Transaction on Industry Application*, Vol. IA-15, No. 5, Sept./Oct. 1979.

90. Cuthill, E., and McKee, J., "Reducing the Bandwidth of Sparse System Matrices", *Proceedings of 24th National Congress, Association of Computing Machine*, Brandon System Press, New York, 1969, pp. 157-172.

91. Eisenstat, S.C., Gursky, M.C., Schultz M.H., and Sherman, A. H., "Yale Sparse Matrix Package", Tech. report, Lawrence Livermore Laboratory, California, August 1975, Report # 112

92. Ibrahim, S.A. and Sachdev, M.S., *Newton Raphson Load Flow Technique Using Polar Coordinates*, October 1979, Department of Electrical Engineering, University of Saskatchewan, Saskatchewan, S7N 0W0 Canada

93. Olejnicsak, K. and Heydt, G.T., "Basic Measurement of Generation and Flow of Harmonic Signals in Balanced and Unbalanced Three-Phase Power Systems", *A*

Paper Presented at the IEEE PES Winter Meeting, New York, New York, January 1989.

94. Shutner, T.C., Vollkommer, Jr., Kirkpatrick, T.L, "Survey of Harmonic Levels on the American Electric Power Distribution System", *A Paper Presented at the IEEE PES Winter Meeting, New York, New York*, January 1989.

A. Mathematical Model of the Converter

A.1. Introduction

A mathematical model of a six pulse converter is presented. A step by step solution of the differential equation given in Chapter 3 is presented. The description of the six pulse converter is given in Chapter 3 and Chapter 2 and can also be found in the texts by Rashid[39], Dewan[41], Finney[42] etc. For the purpose of illustrating steps of solution of differential equation, the commutation interval $[-\pi/3+\alpha,\ -\pi/3+\alpha+\mu]$, during which the line C (SCR3) is commutated by the on coming SCR1 in line A, is considered. Figure 3.4 in Chapter 3 represents the circuit configuration during this interval. This diagram is reproduced in Figure A.1. The governing differential equations, obtained by applying Kirchhoff's Current Law, are given by equations (A.1), (A.2), and (A.3).

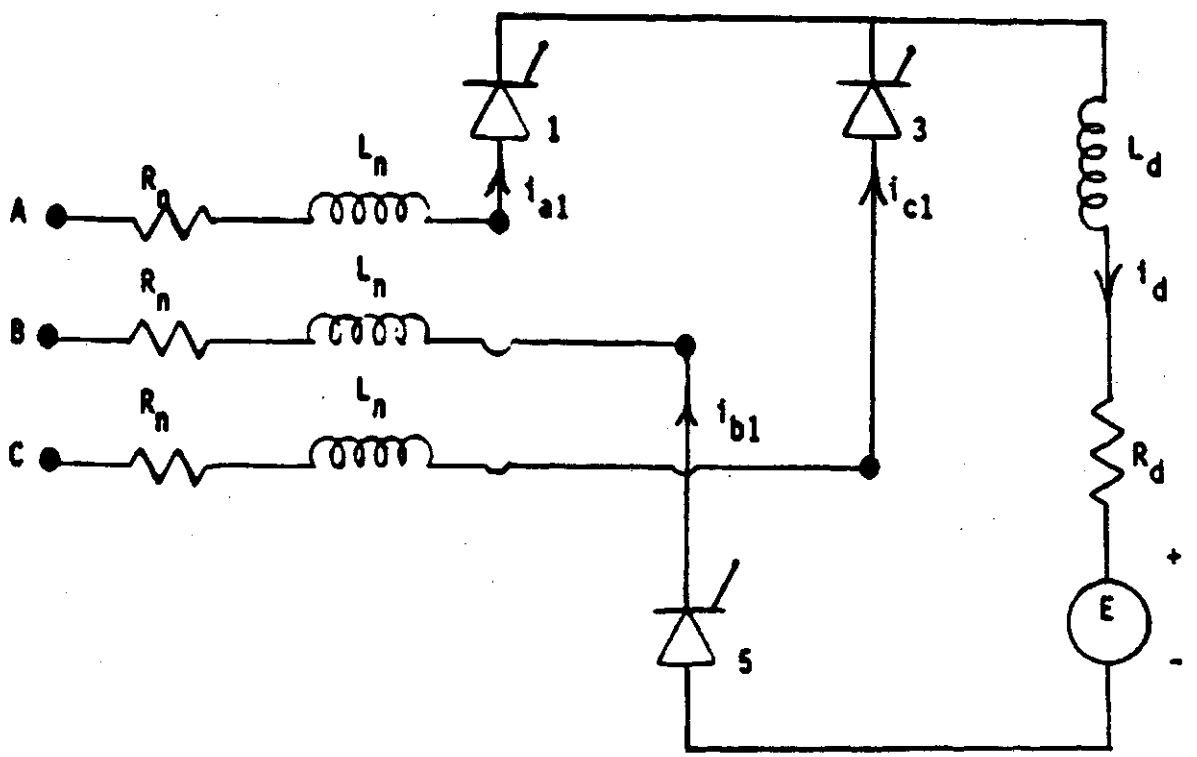

Figure A.1: Bridge Converter during Commutation

$$v_{ac} = [R_n + L_nD][i_{a1} - i_{c1}], \tag{A.1}$$

$$v_{ab}-E = (R_n+L_nD)i_{a1} + [R_n+R_d+(L_n+L_d)D]i_d, \tag{A.2}$$

$$and\ i_{a1} + i_{c1} = i_{b1} = i_d. \tag{A.3}$$

A.2. Miscellaneous Variables

In order to simplify the notation, the various variables defined on the page 38 of Chapter 3 are used in the following analysis. Definitions of these variables are also given here as below.

$$f_{a1}(\omega t) = \sum_{k=1,3,5,\ldots} \frac{V_{Lk}}{Z_{12k}} cos(k\omega t + \delta_k\pi/6 - \phi_{12k}) - \sum_{k=1,3,5,\ldots} Z_{Tk}V_{Lk} cos(k\omega t+\delta_k\frac{5\pi}{6}+\phi_{Tk}),$$

$$f_{c1}(\omega t) = f_{a1}(\omega t) + \sum_{k=1,3,5,\ldots} \frac{V_{Lk}}{Z_{nk}} cos(k\omega t + \delta_k 5\pi/6 - \phi_{nk}),$$

$$f_{a2}(\omega t) = \sum_{k=1,3,5,\ldots} \frac{V_{Lk}}{Z_{22k}} cos(k\omega t + \delta_k\pi/6 - \phi_{22k}),$$

$|Z_{nk}|$ Angle $\phi_{nk} = R_n + k\omega L_n$,

$|Z_{12k}|$ Angle $\phi_{12k} = 3R_n + 2R_d + k\omega(3L_n + 2L_d)$,

$|Z_{22k}|$ Angle $\phi_{22k} = 2R_n + R_d + k\omega(2L_n + L_d)$,

$|Z_{11k}|$ Angle $\phi_{11k} = R_n + R_d + k\omega(L_n + L_d)$,

$$Z_{Tk} = \frac{Z_{11k}}{Z_{nk}Z_{12k}},$$

$$\tau_{12} = \frac{3L_n + 2L_d}{3R_n + 2R_d},$$

$$\tau_n = \frac{L_n}{R_n}, \quad and$$

$$\tau_{22} = \frac{2L_n + L_d}{2R_n + R_d}.$$

A.3. Solution of Currents during Commutation Interval

The equations governing the conduction pattern of the converter circuit are first order set of differential equations. The solution is obtained by method of substitution. From equation (A.1), the following solution is obtained.

$$i_{a1} - i_{c1} = A_{11}e^{-R_n t/L_n} - \sum_{k=1,3,5,\ldots} \frac{V_{Lk}}{Z_{nk}} \cos\left(k\omega t + \frac{5\pi\delta_k}{6} - \phi_{nk}\right)$$

or

$$i_{c1} = i_{a1} - A_{11}e^{-R_n t/L_n} + \sum_{k=1,3,5,\ldots} I_{nk} \cos\left(k\omega t + \frac{5\pi\delta_k}{6} - \phi_{nk}\right).$$

From the above equation and the equation (A.1), the equation (A.4) is obtained.

$$i_d = 2i_{a1} - A_{11}e^{-R_n t/L_n} + \sum_{k=1,3,5,\ldots} I_{nk} \cos\left(k\omega t + \frac{5\pi\delta_k}{6} - \phi_{nk}\right). \qquad (A.4)$$

Substituting i_d form equation (A.4) into equation (A.2), the following differential equation is obtained.

$$(R_n+L_nD)i_{a1} + 2[R_n+R_d+(L_n+L_d)D]i_{a1}$$

$$-(R_n+R_d)A_{11}e^{-\theta/\omega\tau_n} - \frac{R_n}{L_n}(L_n+L_d)A_{11}e^{-\theta/\omega\tau_n}$$

$$+ \sum_{k=1,3,5,\ldots} (R_n+R_d)I_{nk} \cos(k\omega t + \frac{5\pi\delta_k}{6} - \phi_{nk})$$

$$- \sum_{k=1,3,5,\ldots} k\omega(L_n+L_d)I_{nk} \sin(k\omega t + \frac{5\pi\delta_k}{6} - \phi_{nk})$$

$$= v_{ab} - E$$

Rearranging the above equation, the equation (A.5) is obtained.

$$(3R_n+2R_d)i_{a1}+(3L_n+2L_d)Di_{a1}$$

$$= \frac{R_dL_n+R_nL_d}{L_n} A_{11}e^{-\theta/\omega\tau_n}$$

$$- \sum_{k=1,3,5,\ldots} \frac{V_{Lk}Z_{11k}}{Z_{nk}} \cos(k\omega t + \frac{5\pi\delta_k}{6} - \phi_{nk}+\phi_{11k})$$

$$+ \sum_{k=1,3,5,\ldots} V_{Lk}\cos(k\omega t + \frac{\pi\delta_k}{6}) - E. \qquad (A.5)$$

The homogeneous solution and four particular solutions of i_{a1} are as given in equations (A.6), (A.7), (A.8), (A.9), and (A.10).

The homogeneous solution of i_{a1} *is*

$$A_{12}e^{\frac{\theta}{\omega\tau_{12}}}. \tag{A.6}$$

The particular integral No. 1 *is*

$$-\sum_{k=1,3,5,\ldots}\frac{V_{Lk}Z_{11k}}{Z_{nk}Z_{12k}}\cos(k\omega t + \frac{5\pi\delta_k}{6} - \phi_{nk} - \phi_{12k} + \phi_{11k}). \tag{A.7}$$

The particular integral No. 2 *is*

$$\sum_{k=1,3,5,\ldots}\frac{V_{Lk}}{Z_{12k}}\cos(k\omega t + \frac{\pi\delta_k}{6} - \phi_{12k}). \tag{A.8}$$

The particular integral No. 3 *is*

$$\frac{E}{3R_n + 2R_d}. \tag{A.9}$$

The particular integral No. 4 *is*

$$\frac{R_dL_n - R_nL_d}{L_n}A_{11}e^{-\theta/\omega\tau_n} \;/\; L_{12}[\frac{1}{\tau_{12}} - \frac{1}{\tau_n}]$$

or

$$\frac{R_dL_n - R_nL_d}{L_nL_{12}}\frac{L_nL_{12}}{R_{12}L_n - R_nL_{12}}A_{11}e^{-\theta/\omega\tau_n}$$

or

$$\frac{R_dL_n - R_nL_d}{(3R_n+2R_d)L_n - R_n(3L_n+2L_d)}A_{11}e^{-\theta/\omega\tau_n}$$

or

$$\frac{1}{2}A_{11}e^{-\theta/\omega\tau_n}. \tag{A.10}$$

Therefore the complete solution of i_{a1} is given by equation (A.11).

$$i_{a1} = A_{12}e^{-\theta/\omega\tau_{12}} + A_{11}e^{-\theta/\omega\tau_n} + f_{a1}(\omega t) - E/(3R_n+2R_d). \tag{A.11}$$

The solution for i_{c1} is obtained by the addition of i_{a1} to the solution of the

equation (A.1). The equation (A.12) gives the solution of i_{c1}. Similarly the solution of i_{b1} is obtained from the equation (A.3) and is given by equation (A.13). Various constants and functions used are defined in Section (A.2).

$$i_{c1} = A_{12}e^{-\theta/\omega\tau_{12}} - A_{11}e^{-\theta/\omega\tau_{n}} + f_{c1}(\omega t) - E/(3R_n+2R_d) \quad (A.12)$$

$$i_{b1} = 2A_{12}e^{-\theta/\omega\tau_{12}} + f_{a1}(\omega t) + f_{c1}(\omega t) - 2E/(3R_n+2R_d) \quad (A.13)$$

A.4. Solution of Currents following the Commutation Interval

Following the commutation interval, the operation of the converter reverts back to normal. This conduction pattern is defined by the interval $[-\pi/3+\alpha+\mu, \alpha]$, when lines A and B are conducting and the differential equations given by (A.14), (A.15), and (A.16) govern the conduction.

$$i_{a2} = -i_{b2} = i_d, \quad (A.14)$$

$$v_{ab}-E = [R_n + L_nD]i_{a2}+[R_n+R_d+(L_nD+L_d)D]i_d, \quad (A.15)$$

$$and \; i_{c2} = 0. \quad (A.16)$$

The equation (A.15) is a first order simple differential equation and its solution yields the value of i_{a2}. Using the concept of homogeneous and particular solution of the equation (A.15), the complete solution of i_{a1} is obtained and is given by the equation (A.17). The solution of i_{b2} is then obtained from equations (A.3) and (A.17) and is given by equation (A.18).

$$i_{a2} = A_{22}e^{-\theta/\omega\tau_{22}} \frac{E}{2R_n+R_d} + \sum_{k=1,3,5,\ldots} \frac{V_{Lk}}{Z_{22k}} \cos\left(k\omega t + \frac{\pi\delta_k}{6} - \phi_{22k}\right)$$

or

$$i_{a2} = A_{22}e^{-\theta/\omega\tau_{22}} + f_{a2}(\omega t) - E/(2R_n+R_d). \quad (A.17)$$

$$i_{b2} = -A_{22}e^{-\theta/\omega\tau_{22}} - f_{a2}(\omega t) + E/(2R_n+R_d). \quad (A.18)$$

From equations (A.11), (A.12), (A.13), (A.17), and (A.18) a complete solution of current in the ac line of the converter is determined as described in Chapter 3.

B. Definitions Pertaining to Graph Theory

B.1. Introduction

The application of graph theory in studying the effect of sparseness of a matrix in Gauss elimination process was discussed in Chapter 4. In order ot optimize the computation and storage required in solving a linear system of equations, it is important to determine the optimal order of the matrix A. The application of graph theory in determining the optimal order is a well proven technique[73, 76, 77]. Since it enables one to choose an optimal elimination schemes. In this chapter, the definitions of terminology are given and their meaning explained.

Consider a system of N equations in N unknowns, i.e. $A\underline{x} = \underline{y}$, where A is an N by N matrix and $\underline{x}$ and $\underline{y}$ are column vectors of dimension N. The structure of the matrix plays significant role in determining the efficiency of the Gauss elimination process and further factoring[77, 86]. The structure of the matrix A can be easily represented by a graph of nodes and edges.

A node P_i is associated with each index i and an arc is connected between two nodes P_i and P_j for i = j, if either a_{ij} or a_{ji} os not zero. This configuration of 'nodes' and 'arcs' is called a graph G of A or simply G(A). An example is shown in Figure B.1 where matrix A is a 5 by 5 matrix with only 13 non zero elements. G(A) is the associated graph.

B.2. Definitions

A **graph** is defined as a set of nodes and edges that connect the nodes. For the above example, G(A) = (P, E) where P = [1,2,3,4,5] and E = [{1,2}, {1,3}, {1,4}, {1,5}].

$$A = \begin{bmatrix} a_{11} & a_{12} & a_{13} & a_{14} & a_{15} \\ a_{21} & a_{22} & 0 & 0 & 0 \\ a_{31} & 0 & a_{33} & 0 & 0 \\ a_{41} & 0 & 0 & a_{44} & 0 \\ a_{51} & 0 & 0 & 0 & a_{55} \end{bmatrix}$$

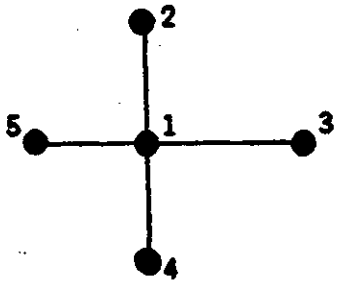

Figure B.1: The Matrix A and the Associated Graph G(A)

A graph is **connected** if there is a path connecting each pair of distinct nodes and is **disconnected** if there are two or more subgraphs. In this chapter only connected graphs are considered.

A **neighbour** of a node x is defined as the node adjacent to the node x, e.g. nodes 2, 3, 4, and 5 are neighbour of node 1 in Figure B.1. Neighbour of node 2 is node 1, so on and so forth.

An **adjacent** set of x is defined as the set of all neighbours of the node x and is denoted by Adj(x), e.g. in Figure B.1 Adj(1) = {2,3,4,5}, Adj(2) = {1}, Adj(3) = {1}, Adj(4) = {1}, and Adj(5) = {1}.

A **degree** of a node x is defined as the number of elements in its adjacent set, i.e. |Adj(x)|. The degree is denoted by Deg(x). For the example shown in Figure B.1, Deg(1) = 4, Deg(2) = Deg(3) = Deg(4) = Deg(5) = 1.

A **path of length l** between two nodes is an ordered set of distinct nodes

$(p_0,p_1,...,p_l)$. For example the path between nodes 2 and 5 in Figure B.1 is (2,1,5) of length 2.

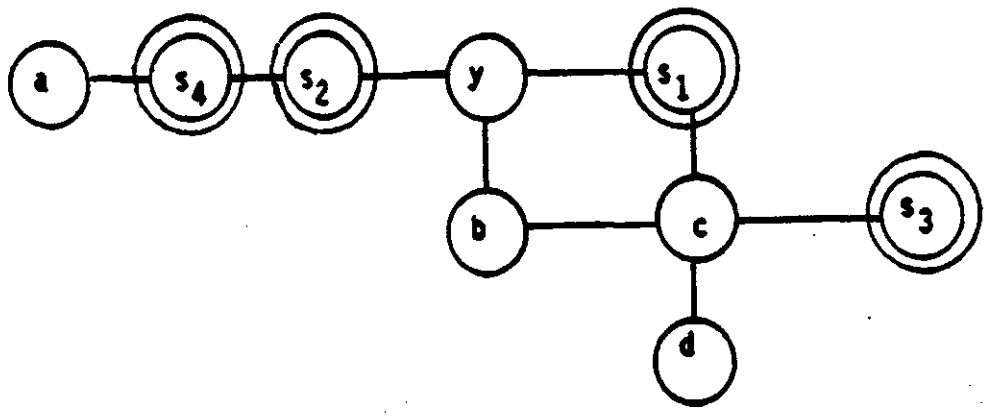

Figure B.2: An example of A Graph with Eliminated Nodes

Reachability of a node x from node y through a subgraph S exist if there is a path from node y to node x through S. All the adjacent nodes of a node y are said to be reachable from y through S. The set of nodes reachable from node y is denoted by Reach(y). For example, consider a graph shown in Figure B.2 where double circled nodes belong to a subgraph called S. Then Reach(y), where y is not in S, defined as the set of nodes reachable from y through S is given by

Reach(y) = {a,b,c,}

since the following paths can be found through S:

(y,s_2,s_4,a), (y,b), and (y,s_1,c).

The node d does not belong to Reach(y,S), since no path can reach d without going through the node c.

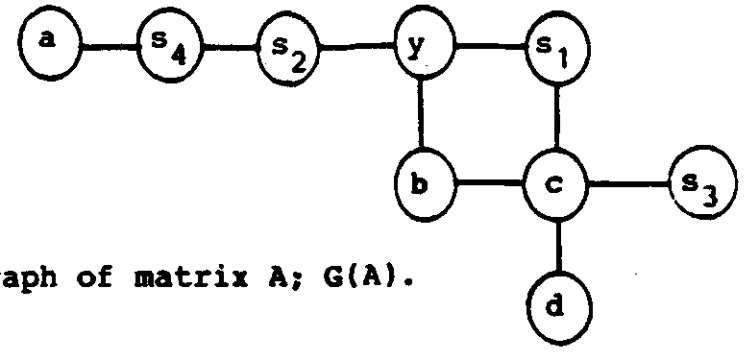

(a) Graph of matrix A; G(A).

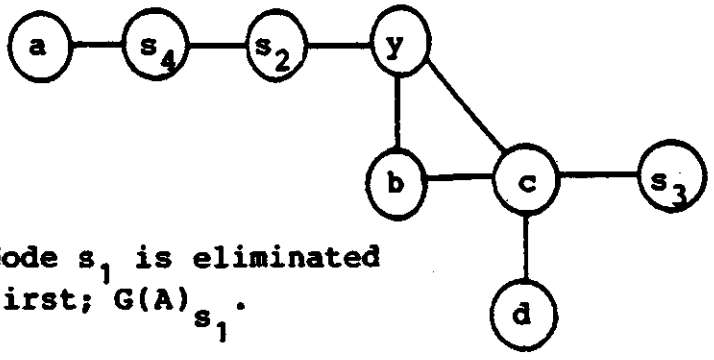

(b) Node s_1 is eliminated first; $G(A)_{s_1}$.

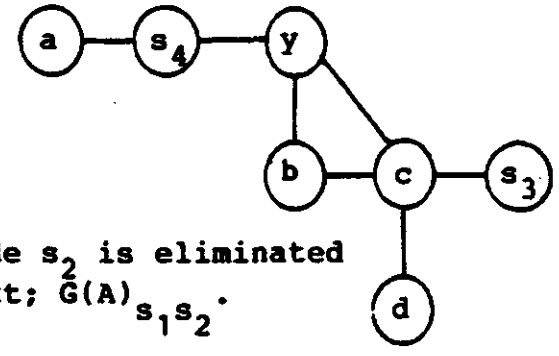

(c) Node s_2 is eliminated next; $G(A)_{s_1 s_2}$.

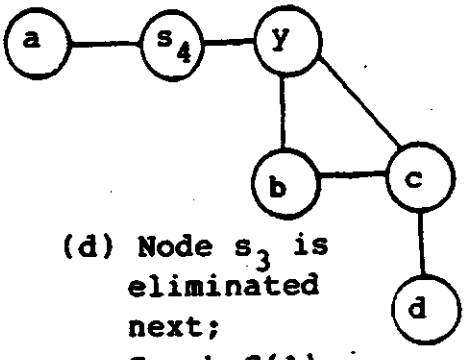

(d) Node s_3 is eliminated next; Graph $G(A)_{s_1 s_2 s_3}$.

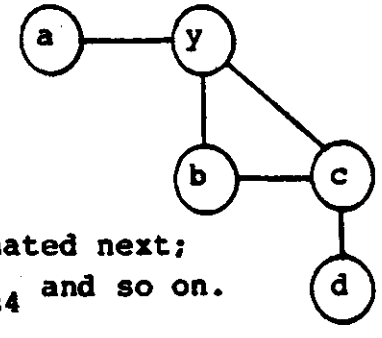

(e) Node s_4 is eliminated next; Graph $G(A)_{s_1 s_2 s_3 s4}$ and so on.

Figure B.3: Gaussian Elimination Process in terms of Elimination Graph

B.3. Gaussian Elimination Process in terms of Graphs

Symmetric Matrix A of order N by N can be represented by a graph G(A). The Gaussian elimination process is used to factor the matrix A in U^TU. The elimination process applied to A can be viewed as a sequence of graph transformations on G(A)[87]. An elimination graph of G(A) by y, where y is the eliminated node, is denoted by $G(A)_y$. The elimination graph $G(A)_y$ comprises all set of nodes of G(A) less the node y and set of edges less the edges associated with node y plus the new edges required to connect the adjacent nodes of y, i.e.

$$G(A)_y = (X-\{y\},\ E(X-\{y\}) \cup \{\{u,v\} | u,v \in Adj(y)\})$$

With this definition, the process of Gaussian elimination on a matrix A can be viewed as a sequence of elimination graph as shown in Figure B.3.

B.4. Gaussian Elimination Process in terms of Reachable Sets

As seen in the previous example, the process of elimination graph results in new edges being created and hence the memory required to do such a transformation is unpredictable. The use of reachable sets results in the elimination process being modelled on the original G(A), thus preventing the creation of new edges. For example, the elimination graph $G(A)_4$ shown in Figure B.3 corresponds to the graph shown in Figure B.2. Where nodes s_1, s_2, s_3, and s_4 have been eliminated and belong to a subgraph S. In the elimination graph $G(A)_4$ (Figure B.3), the adjacent sets of all the nodes are defined as below.

Adj(a) = {y}

Adj(b) = {y, c}

Adj(c) = {b, d, y}

Adj(d) = {c}

Adj(y) = {a, b, c}

From the corresponding graph shown in Figure B.2 and Figure B.4(e) the reach sets of nodes that are yet to be eliminated through S are obtained as below.

Reach(a,S) = {y} since the path is (a,s_4,s_2,y).

Reach(b,S) = {y, c} since paths are (b,y) and (b,c).

Reach(c,S) = {b, d, y} since paths are (c,b), (c,d), and (c,s_1,y).

Reach(d,S) = {c} since the path is (d,c).

Reach(y,S) = {a, b, c} since paths are (y,s_4,s_2,a), (y,b), and (y,s_1,c).

These reachable sets are precisely the adjacent sets in the elimination graph $G(A)_4$. Thus the explicit representation of the elimination graph can be avoided and the whole process of Gaussian elimination can be carried out on the original graph using the definition of reach sets. The correspondence between each of the elimination graph of Figure B.3 is given in Figure B.4.

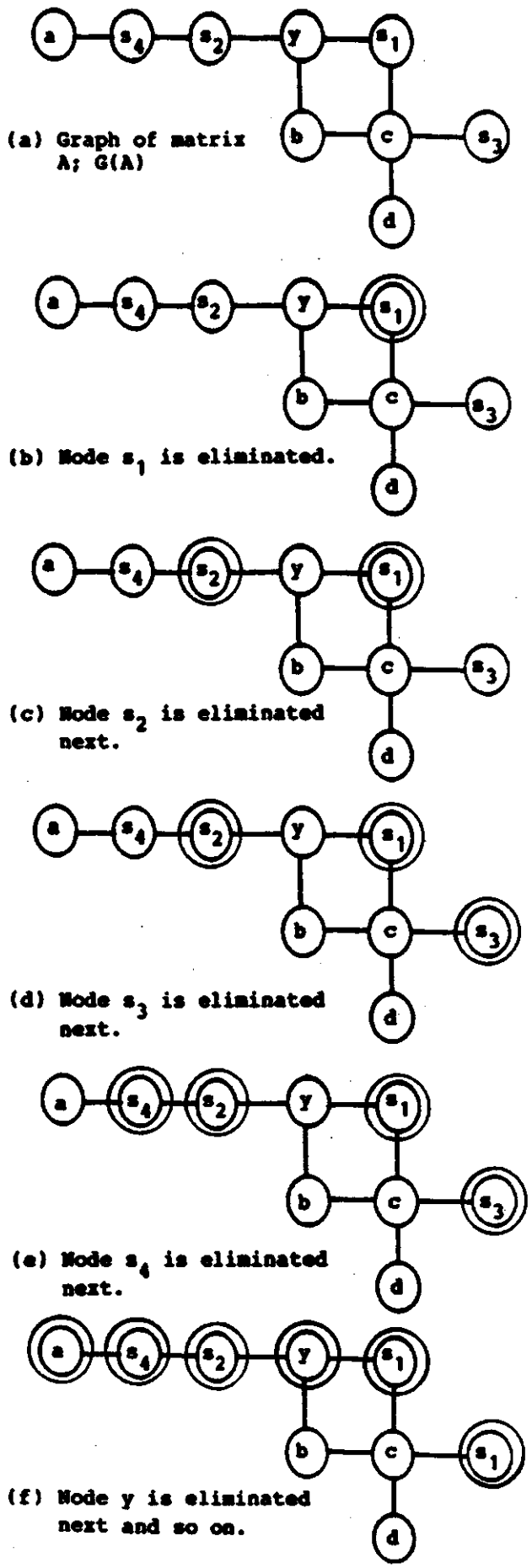

Figure B.4: Example of Gaussian Elimination Process in terms of Reachable Sets

C. Harmonic Definitions

C.1. Definitions

The following definitions are used in the thesis for harmonic frequency analysis. The definition of power, reactive power and distortion power are given in this appendix. Several standard definitions for distortion factor are described below. The IEEE standard[20] definition of the voltage and current distortion factor is used in the thesis.

1. Distorted Voltage Waveform.

$$v(t)=\sum_{k=1}^{\infty}\sqrt{2}V_k Cos(k\omega t+\theta_k)$$

2. Distorted Current Waveform.

$$i(t)t)=\sum_{k=1}^{\infty}\sqrt{2}I_k Cos(k\omega t+\phi_k)$$

3. Apparent Volt Ampere.

$$S^2=\sum_{k=1}^{\infty}V_k^2\sum_{j=1}^{\infty}I_j^2$$

4. Real Power (Watts).

$$P=\sum_{k=1}^{\infty}V_k I_k Cos(\phi_k)$$

5. Non Active Power including both reactive and distortion power.

$$QD^2=S^2-P^2$$

6. Voltage Distortion Factor(IEEE standard[20]).

$$DF_v=\frac{V_1}{[V_1^2+V_2^2+V_3^2+...+V_n 2/^2]^{1/2}}$$

7. Current Distortion Factor (IEEE Standard[20]).

$$DF_i=\frac{I_1}{[I_1^2+I_2^2+I_3^2+...+I_n^2]^{1/2}}$$

8. Voltage Distortion Factor(IEC standard).

$$DF_v = 100.\frac{[V_2^2+V_3^2+...+V_n^2]^{1/2}}{[V_1^2+V_2^2+...+V_n^2]^{1/2}}$$

9. Current Distortion Factor (IEC Standard).

$$DF_i = 100.\frac{[I_2^2+I_3^2+...+I_n^2]^{1/2}}{[I_1^2+I_2^2+...+I_n^2]^{1/2}}$$